Electrical and Optical Investigations of the Condensed Matter Physics of Junction Diodes under Charge Carrier Injection

A thesis

submitted in partial fulfillment of the

requirements for the degree of

Doctor of Philosophy

by

Kanika Bansal

20083008

Indian Institute of Science Education and Research - Pune

June, 2014

Dedicated to my parents.

CERTIFICATE

Certified that the work incorporated in this thesis entitled **Electrical and Optical Investigations of the Condensed Matter Physics of Junction Diodes under Charge Carrier Injection** submitted by **Kanika Bansal** was carried out by the candidate, under my supervision. The work presented here or any part of it has not been included in any other thesis submitted previously for the award of any degree or diploma from any other university or institution.

Date: **Dr. Shouvik Datta**

Supervisor

DECLARATION

I declare that this written submission represents my ideas in my own words and where others' ideas have been included, I have adequately cited and referenced the original sources. I also declare that I have adhered to all principles of academic honesty and integrity and have not misrepresented or fabricated or falsified any idea/ data/ fact/ source in my submission. I understand that violation of the above will be cause for disciplinary action by the Institute and can also evoke penal action from the sources which have thus not been properly cited or from whom proper permission has not been taken when needed.

Date: **Kanika Bansal**

Roll No. 20083008

Acknowledgements

Words cannot express my gratitude for everyone I have crossed paths with in my journey from a hesitant college graduate to a learner of science. I can only say that my true acknowledgements are ampler than these few pages.

First and foremost I would like to thank my supervisor, Dr. Shouvik Datta for providing an encouraging and independent work environment. His persistence has helped me gradually develop a critical approach towards experimental science. His enthusiasm for physics is always inspiring and his high ethical values are the standard for me to attempt to live up to.

I wish to thank my RAC members Dr. G. V. Pavan Kumar, Dr. Shivaprasad Patil, Dr. Pankaj Poddar and Dr. Surjeet Singh for providing encouraging and constructive feedback on my work. I am grateful to my teachers, my TA mentors - Prof. Mukhi, Prof. Gangal, Dr. Athalye and Dr. Santhanam - and all the other faculty members of the Dept. of Physics at IISER-Pune for solidifying my basic understanding of physics. I would also like to mention the mentorship I received from Dr. Ambika during my initial days at IISER, be it the small hostel issues or all the help with administrative procedures.

I would like to express my gratitude to Prof. Ganesh, Director IISER Pune and Prof. Mukhi, Chair Physics Program, for providing funding for attending conferences which gave me a good exposure and huge opportunities for learning. I would also like to thank CSIR and DST for providing me research scholarship and travel funding.

I must mention the daunting challenge of building a new lab, twice - at Sai Trinity and h cross - which appeared seamless due to the soothing presence of my lab members Arthur and Padmashri. I am thankful to Amit and Kaustav for maintaining the spirit of the lab. I also wish to thank Prof. M. Henini (Nottingham University, UK) for providing me quantum dot samples I have used in a part of my work.

A big vote of thanks goes to all my physics batch mates - Arthur, Arun, Mayur, Murthy, Padmashri, Resmi and Somu - for the fun filled initial years at IISER. Solving tutorials in the common room, discussing complex physical phenomena, bickering over the political state of affairs and IISER cricket league were made even more fun activities due to their presence. Shukla ji, Ramya, Anupam, Vimal, Snehal, Sunil, Danveer and all

the other student members of IISER physics department deserve a special mention for intriguing discussions.

I would like to take this opportunity to thank Prof. Rao for his help whenever required. I am thankful to Neelesh sir and Prashant for sorting out various lab issues. Assistance of Prabhakar and Tushar was instrumental in getting all the paper work in order.

I wish to thank Exciting Science Group and Dr. Guruswamy, Dr. Anirban and Shraddha for providing me the opportunity to interact with enthusiastic school kids through their outreach programs. It was indeed a pleasure.

Working in the lab was always complemented by a light and lively environment in the cafeteria and hostel. A big thanks to Mayur, Snehal, Ameya, Shradhdha, Mitali and many more who shared their tasty, homemade food with me. When it comes to campus food, it would be unacceptable to not mention Tamil mess which provided awesome food and a great platform to discuss campus developments, Indian politics and world peace.

My friends made the long and tiresome journey bearable through their upbeat nature. The transitions from Bhavani Ajala to HR2 to New Hostel with these friends gave me countless moments to cherish. I am thankful to all my biology friends - Abhishek, Aniruddh, Harsha, Jay Pee, Mithila, Payal, Reshma and Rini - for teaching me the biology jargons I now know. I acquired a great deal of wisdom through their repeatedly failing IPs. I hope some of our path breaking research ideas mixing physics and biology breathe some real air one day. When not discussing potentially Nobel winning ideas, Abhishek has been a great badminton teacher. Curiosity and knowledge of Harsha has always made me realize how ignorant I had been and how far I still have to go. Poems of Jay Pee increased the amplitude of every celebration. Mithila always added a pleasant touch of creativity to the proceedings. Rini was a complete package filled with entertainment, righteousness, particularity and, sometimes, glitches. I am thankful to her for all the ‘Rinika moments’ we shared. Payal was a very good roommate, her caring attitude never let me feel far from home. Her determination and sincerity have been inspiring for me.

I want to extend my gratitude to Mayur and Vimal for the countless favors I received from them. They helped me in every possible way during my stay at Pune.

Mayur has been a teacher, a brother, a friend and even a cook, when needed. Vimal has been my mentor, especially when I used to feel low. His never ending preaching sessions with little context and multiple interruptions rarely helped in bringing me out of my local minima! I am especially thankful to Vandana, who never hesitated to offer her help to me.

I cannot express in words the profound sense of gratitude I have for my family. My father, although not with us anymore, was the person who motivated and stimulated me to pursue research as a career. My mother has always encouraged me in all endeavors I have ever taken up. Without her help and guidance, it would not have been possible for me to accomplish this important goal. I also want to thank my brother Naman and my father-in-law for their support during the business end of this work.

Last but not the least, I would like to mention Vaibhav, my husband whom I cannot thank enough, in fact, I refuse to do so. He has been a friend with infinite patience since the beginning. His presence simply makes everything I have worth having and everything I do worth doing.

June, 2014 **Kanika Bansal**

Contents

Abstract

In this thesis we present our studies of the dielectric properties of junction based diode structures under charge carrier injection. This regime remains less explored even after decades of research in the field of semiconductors. However, it is a necessary working condition for a set of diodes like electroluminescent diodes, producing light emission and hence important from the fundamental and application points of view. Nevertheless, the presence of a large number of free charge carriers in this regime, giving rise to different time scale processes and possibility of carrier interactions imposes experimental challenges and complexities. In such a scenario, conventional characterization techniques and understanding of junction diodes based on depletion approximation and electrostatics break down. Hence, we modified the existing techniques and developed new techniques and analyses to probe electroluminescent diode structures under charge injection. We observed counter intuitive response beyond the available understanding of these structures. We probed the connection between electrical and optical properties and its manifestations to understand carrier transport in these active devices.

We used impedance spectroscopy and developed voltage modulated electroluminescence spectroscopy to study mainly AlGaInP based multi quantum well electroluminescent diodes (ELDs) for relatively low frequencies. We observed that under high injection, reactance of the diodes acquires inductive like behavior, which is perceived as negative capacitance (NC). Occurrence of NC was found to be accompanied by the onset of modulated light emission. Magnitudes of both increase in a correlated fashion with decreasing modulation frequencies. These observations are technologically important but are beyond the conventional diffusion capacitance model of the diode under forward bias. We explained that this interdependence of electrical and optical properties in case of ELDs is due to the participation of slow non-radiative defect channels in the fast radiative recombination dynamics.

We theoretically demonstrated how NC can appear in the admittance response of a diode in general. We identified that the positive valued and increasing current transient

after the application of a forward bias step is the signature of NC. During the temperature scan of these devices, we observed that the quantum confinement affects the response under modulation in a way that is not apparent from room temperature studies. For low temperature regime, low frequency defect response causes a counterintuitive increase in modulated light emission with increasing temperature. At higher temperatures, thermally activated escape of charge carriers from the quantum well starts to affect the device response. As a result, modulated light output maximizes in a certain temperature range below room temperature. We suggest that for better efficiency of devices in high frequency (~GHz) direct modulation applications, it is desirable to reduce low frequency response which prevents charge carriers from following the fast modulation. Nevertheless, quantum well parameters should be tuned to get maximum modulated light output around working temperature of the device.

We further observed that the frequency domain steady state electrical impedance response of electronic rate processes activated with dc bias reveals an intricate picture of the carrier dynamics. We demonstrated that the sudden change in frequency dependence of this bias activated response, after the onset of light emission, points towards the presence of an excitonic state. This response vanishes with increasing bias indicating Mott transition. Hence for the first time, we electrically identified the possible signatures of the formation of excitonic states and their subsequent Mott transition to electron hole plasma.

We further applied our techniques and analyses to different ELDs and functionally different Silicon-based diodes. We demonstrated that our understanding can be generalized to explain the dissimilar frequency dependent reactance in these functionally different junction diodes under charge carrier injection.

Chapter 1

Introduction

1.1 Motivation

Charge injection is an essential condition for the working of light emitting diodes and lasers which make the lion's share of our technology dependent daily life. Applications of these diodes are so high that a great deal of effort in this field is directed towards constructing better and more efficient devices with lower cost using newly available technologies for growth and characterization. However, the basic physics of these devices, even as a simplistic system of p-n junction diodes under high carrier injection, is not fully understood. It is important from the point of view of basic physics and applied technology to comprehend the condensed matter physics of these devices under their operating conditions. This is a regime where conventional understanding of diodes based on depletion approximation and electrostatics may not work due to the presence of large number of charge carriers and their interactions. One needs to understand the dielectric changes a material undergoes, when light emission starts or when lasing starts. With the use of quantum structures, effect of quantum confinement on these properties also becomes important.

Moreover, the mechanism of light emission is interesting in itself to be probed using electrical techniques in a full device configuration. Usually only optical techniques are used to detect the presence of exciton state and its Mott transition to free electron-hole plasma state through recombination dynamics. The studies or predictions for their electrical signatures are few and far between.

We therefore present a study on the various electrical and optical aspects of active electroluminescent diodes. We used small signal sinusoidal modulation to perturb the system for frequencies below 2 MHz and observed the electrical and optical response of the system. Most of the results presented in this thesis are for multi quantum well based electroluminescent diodes. However, we have shown that our understanding and results are well applicable to quantum dot laser diodes and functionally different Si based diodes and hence can be generalized to other diode based devices under charge injection in appropriate parameter range.

In this chapter, we are presenting a brief overview of the semiconductor and diode physics concepts which we have used or are useful to understand the work presented in the following chapters.

1.2 Semiconductor background

In solids, coexistence of similar electronic states from constituent atoms gives rise to a broader structure of closely spaced energy levels called bands[1-3]. In presence of the periodic potential of lattice, these bands form a structure in energy (E) and momentum (k) space maintaining E and k conservation. This results in forbidden energy regions for selected k values called energy band gaps. At 0 K, the highest energy band which is completely occupied is called the valence band and the lowest energy band which is completely empty is called the conduction band. Forbidden energy gap between valence and conduction band is the fundamental band gap (commonly known as the band gap) of the material[4]. Semiconductors are the materials which have band gaps between ~ 0.1 eV to ~3 eV. When conduction band minimum and valence band maximum coincide in k space, band gap is direct and if k value differs for both it is indirect[3]. Figure 1.1 shows the band structures of two most common semiconductor materials (Si and GaAs). Fundamental band gaps of Si and GaAs are 1.12 eV and 1.42 eV respectively. However, the biggest difference between these materials is that the GaAs, having direct band gap shows efficient radiative recombination (light emission) which is not possible in case of bulk Si which has an indirect band gap. It is interesting to mention here that Si does have

a second direct band gap around 3.4 eV[5]. Also, in case of porous and nano-crystalline Si, light emission has been observed[6, 7].

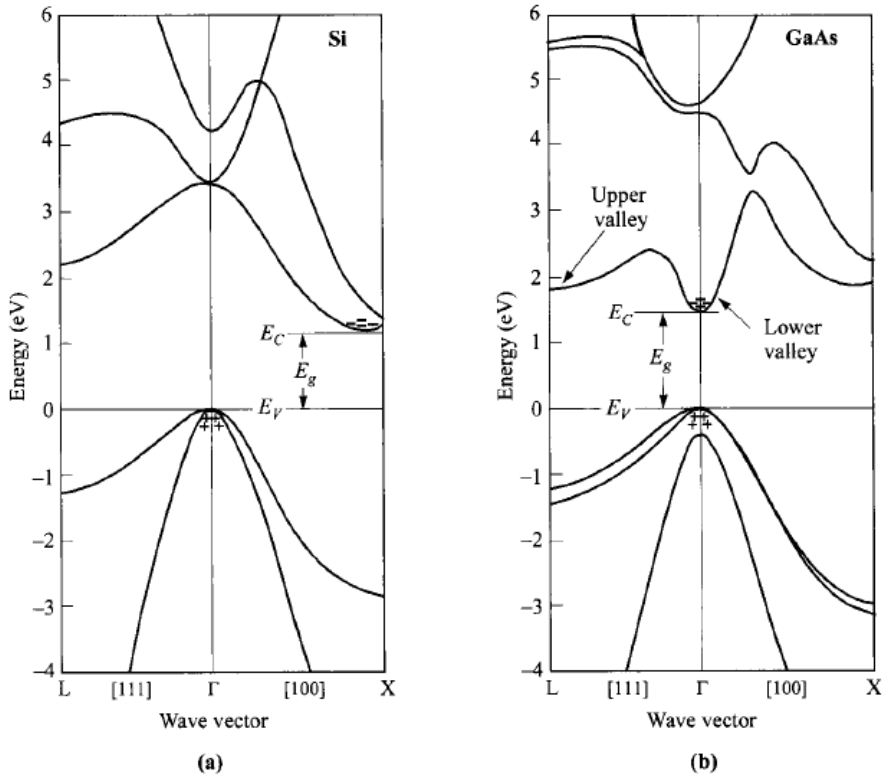

Figure 1.1: Energy band diagram of (a) Si and (b) GaAs (from reference 4 based on reference 8). E_g denotes band gap and Γ denotes k=0. E_V and E_C denote valence and conduction band extremum points respectively. (+) and (-) signs denote holes and electrons respectively in corresponding bands. Indirect nature of Si band gap and direct nature of GaAs band gap can be seen.

Depending upon the structure of the material, band gap can vary vastly as mentioned in table 1.1.

Table 1.1: Band gaps and structures of some bulk semiconductors (at 300 K)[9, 10]

Material	Si	GaAs	GaP	GaN	CdTe
Band gap (eV)	1.12 Indirect	1.42 Direct	2.26 Indirect	3.4 Direct	1.44 Direct
Structure	Diamond cubic	Zinc-blende	Zinc-blende	Wurtzite	Zinc-blende
Group	IV	III-V	III-V	III-V	II-VI

At 0 K, due to the unavailability of free electrons in conduction band, semiconductors are insulators. With increase in temperature, thermal fluctuations provide sufficient thermal energy to electrons to jump to conduction band leaving behind an empty space in valance band with net positive charge known as 'hole'. When empty energy states are available, free electrons in conduction band and free holes in valence band can move under the influence of external field and conduct electricity. Typical conductivity of semiconductors lies between that of metals and insulators (10^{2}-10^{-8} S/cm).

Effective dynamics of these charge carriers in the bands and their interaction with each other or different objects in the solid (impurities, lattice vibration, external field etc.) give rise to a variety of interesting and useful physical phenomena in semiconductors. For simplicity, dynamics of these quantum particles (electrons and holes) bound with the potential of lattice can be approximated to their motion as free classical particles in respective bands, when their respective free masses are replaced by their 'effective mass' (m^{*})[11]. It represents the mass these particles seem to have under the presence of external force. Effective mass is given by the relation $m^{*} = \hbar^{2}[d^{2}E(k)/dk^{2}]^{-1}$ where $\hbar$ is reduced Planck's constant[3]. Effective masses of electrons and holes vary in different materials and generally are anisotropic in the crystal[1].

In an intrinsic (pure) semiconductor, concentration of free electrons and holes remains same maintaining the neutrality condition. This concentration is on the order of ~10^{11} cm^{-3} which is too low for any technological use[12]. However, properties of semiconductors are very sensitive to any impurities or irregularities in the intrinsic lattice structure. For example, in ideal case, charge carrier concentration increases with increasing temperature and therefore, resistivity should go down; but practically, the decrease in resistivity with temperature can deviate from its monotonicity due to the presence of defects or/and impurities[4, 13]. Introduction of impurities in the material alters its band structure which can be exploited to induce properties varying from one extreme (highly conducing or metallic) to the other (insulating).

To alter the properties of semiconductors for various applications, they can be doped externally, to be made either electron rich (n-type) or hole rich (p-type). Apart

from doping, making alloys of two semiconductors or producing strain in the lattice by epitaxial growth of two lattice-mismatched structures can also modify the band structure[12] ultimately altering the physical properties of the material system. In real devices based on semiconductors, some/all of above are used in combination to produce different physical properties.

We understand that for electrons to take part in transport in the presence of an external field, they have to be promoted to the conduction band where empty energy states are available for their movement. So it would be important to know the concentration of free electron to understand the dynamics of the material or device. The number of electrons *n* in the conduction band is given by[4]:

$$n = \int_{E_C}^{\infty} N(E)F(E)dE \tag{1.1}$$

Where E_C is the conduction band edge, *N(E)* is the total number of states (the density of states (DOS) which describes the total number of available electronic states per unit volume and energy) and *F(E)* is the Fermi-Dirac distribution function governing the occupation probability of available states, given as[4]:

$$F(E) = \frac{1}{1+\exp\left[(E-E_F)/k_B T\right]} \tag{1.2}$$

where k_B is Boltzmann constant and E_F is the Fermi level and is determined by the charge neutrality condition. E_F describes the maximum energy an electron can have and exists in the middle of the band for an ideal intrinsic semiconductor at 0 K. This also explains why semiconductors are insulators at 0 K. A similar expression can be written for holes. For doped semiconductors due to the presence of donor atoms (n-type) or acceptor atoms (p-type) impurity energy levels get introduced in between the band gap and Fermi level position also gets altered. For low levels of doping (or injection as will be described later) Fermi level remains several k_BT below E_C and Fermi-Dirac distribution can be approximated to a Boltzmann distribution function. In this configuration semiconductor is called *Non-degenerate*. For a non-degenerate semiconductor *n* is proportional to a Boltzmann like factor as given by[3, 4]:

$$n \propto \exp\left(-\frac{E_C - E_F}{k_B T}\right) \tag{1.3}$$

For Degenerate semiconductors, one has to use Fermi-Dirac statistics for calculations. In this work we will deal with the semiconductor systems and states described mainly by the non-degenerate properties.

1.2.1 Different recombination processes in semiconductors

Presence of any external field (temperature variation, electric field, magnetic field, mechanical stress, electromagnetic radiation etc.) influences the dynamics of charge carriers inside the semiconductors[12, 14]. These external perturbations can excite electrons into conduction band (also generating a hole in valence band), can modify the intrinsic band structure or/and alter the effective mass of the charge carriers. For example, in the presence of electromagnetic radiation of energy above band gap, photon absorption can take place transferring electrons to the conduction band. Electrons and holes can also be injected in their respective bands by high forward bias. In such situation, presence of extra electrons in conduction band (and holes in valence band) disturbs the equilibrium concentration of free charge carriers. To achieve the equilibrium, electrons can release their energy to recombine with holes in the valence band via different processes. When electron and hole recombine releasing energy as a photon, it is called radiative recombination which makes the basis of electroluminescent devices. In case of direct band gap semiconductors, radiative recombination can happen directly between bands (also between excitonic levels, as will be discussed later). For such transitions, recombination rate (R) is proportional to the electron (n) and hole (p) concentration:

$$R = npR_c \tag{1.4}$$

where R_c is the recombination coefficient[4]. In case of indirect band gap materials, the transition cannot happen directly between bands to maintain the momentum conservation. Then recombination can occur via electronic defect (traps) states (which exist within the band gap due to the presence of defects or impurities) following Shockley-Read-Hole statistics[15-17]. In this case, recombination is non-radiative, with a rate given by[4]:

$$R_{SRH} = \frac{\sigma_n \sigma_p v_{Th} N_t (pn - n_i^2)}{\sigma_n \left(n + n_i \exp \frac{E_t - E_F}{k_B T} \right) + \sigma_p \left(p + n_i \exp \frac{E_F - E_t}{k_B T} \right)} \quad (1.5)$$

where σ_n and σ_p are electron and hole capture cross sections by the trap states, v_{Th} is the thermal velocity of electrons, n_i represents equilibrium intrinsic electron concentration. E_t and E_F represent defect energy level and intrinsic Fermi level respectively. N_t is the density of defects. Energy of excited electron can also be transferred to another electron-hole system (Auger process) and/or phonons (heat) which is also a non-radiative process. We do not intend to go into the details of these processes which, by itself, is a field with very rich physics (for an overview reference 14 and 18 can be consulted). However, we intend to mention here that depending upon the structure of semiconductors and their response to applied field they can exhibit different physical phenomena and can be used for different device functionalities. For example, radiative recombination after the injection of charge carriers is the key process inside a light emitting diode[19]. In case of solar cells free charge carriers should be collected at different electrical contacts without undergoing any recombination[20]. Generally, materials can undergo different processes but it is the dominance of one which makes them useful for certain applications. Probability of the desired process inside the constituent materials dictates the efficiency of the device based on it. In the context of this thesis, we are interested in radiative recombination process and related device structures.

In bulk semiconductors rate of radiative transition R is given by equation (1.4). In general, efficiency of radiative recombination (η) is given by the ratio of the rate of radiative recombination (R) and the rate of total recombination (R') (including radiative and non-radiative). Presence of any other recombination path way which is non-radiative competes against radiative recombination and reduces its efficiency. Effective recombination time of the carriers due to the presence of all the possible recombination path ways is given by (considering two mutually exclusive path ways one being radiative and one being non-radiative):

$$\frac{1}{\tau_{eff}} = \frac{1}{\tau_{radiative}} + \frac{1}{\tau_{nonradiative}} \quad (1.6)$$

We will discuss in chapter 2 how defect response (non-radiative) can couple with radiative recombination when device characteristics are measured under sinusoidal modulation of low frequencies (significantly lower than the rate of raidative recombination), and the behavior can deviate from equation (1.6).

1.2.2 Excitons in semiconductors

An electron in conduction band and a hole in valence band are bound with mutual Coulomb attraction. Such a bound pair of electron and hole is called an 'exciton'[12, 18]. In materials with small dielectric constants, Coulomb attraction between an electron and a hole is very strong and exciton sizes are small with high binding energy (0.1 to 1 eV). These excitons are called Frenkel excitons[21] and exist in organic semiconductors. On the other hand, in the materials with high dielectric constant (like inorganic semiconductors), Coulomb potential gets screened and excitons have large radii and small binding energies (on the order of few meV). This class of excitons is called Wannier-Mott excitons[22] and is relevant in present case. Wannier-Mott excitons can be viewed like a hydrogen atom with discrete energy levels (E_j) given by[22]: $E_j = \mu e^4 / 2\varepsilon^2 h^2 j^2$ where j=1, 2, 3…, e is the electronic charge, ε is the dielectric constant of the material, and μ is the reduced mass of electron and hole system inside the material. Excitons can make ion or molecule like complexes by combining two or more electron-hole pairs[23]. Apart from these free excitons, bound excitons also exist where charge carriers are bound to impurity states or excitonic ions[14]. Excitons states are short lived at room temperature and they dissociate by emitting photons (and phonons in case of indirect band gap materials). This is the reason why excitons are studied at low temperature and in pure samples where the probability of their breakdown is lowered[14]. However, in case of quantum wells (and other lower dimension structures) significant exciton population can exist even at room temperature due to the stationary nature of the resonant excitonic state as a result of quantum confinement effect[24-26]. We will further discus this in section 1.4.1.

Only under low densities, bosonic excitons can be understood by the hydrogen atom model. Under high density excitons interact with each other to form electron-hole liquid. Bose-Einstein condensate (BEC) like state had also been predicted theoretically

for excitons[27, 28] with relatively higher (~1 K) condensation temperatures due to low effective masses. They had also been predicted to show cooper pair like formation with high densities at low temperature[27, 29]. Main experimental challenge for the observation of such condensed phases of excitons is their low binding energies and very short life time. Auger recombination[30], which is a competing fast non-radiative process, is also a challenge. At sub-Kelvin temperatures, BEC of excitons has been observed recently[31, 32]. Excitons can couple with different quasi particles in the crystal and make bosonic complexes. Due to the strong dipole interaction between excitons and photons in a cavity, polaritons are formed. These are called exciton-polariton and are a good candidate to observe BEC[33, 34].

Excitons are the basis of the next generation of many devices like exciton-polariton based ultralow threshold lasers, solar cells etc. and believed to play a major role in lasing mechanism of quantum wires. However, their studies are dominated by optical spectroscopy based techniques. These techniques require very careful interpretation of the observed light emission spectra with a lot of different parameters affecting spectral features. To our knowledge, there are no electrical methods to probe the delicate condensed phases of excitons. In chapter 5, we will discuss the electrical technique we have proposed to probe excitons and their transition to free electron-hole plasma in the semiconductor.

1.3 Semiconductor p-n junction

p-n junctions (junctions of p and n type materials) are the basic building blocks of almost every semiconductor device and an integral part of the current electronic systems. Physics of p-n junctions which followed slowly after their invention can be considered as the basic physics of devices based on them. Under no external perturbation or field, p-n junction can be represented as the schematic shown in figure 1.2a. When p-type and n-type materials come in contact, holes and electron recombine, generating a region depleted of free charge carriers, known as depletion region or space charge region. This region extends in both p and n sides of the junction and the built in field created by this

region dynamically prevents any further crossover of the charge carriers across the junction. Fermi levels of the materials also align due to the electron hole flow during junction formation. Typically, charge current flows if any Fermi level gradient exists in the system. In the absence of any external perturbing field, under equilibrium a single Fermi level can be used to describe the entire system as can be seen in figure 1.2b.

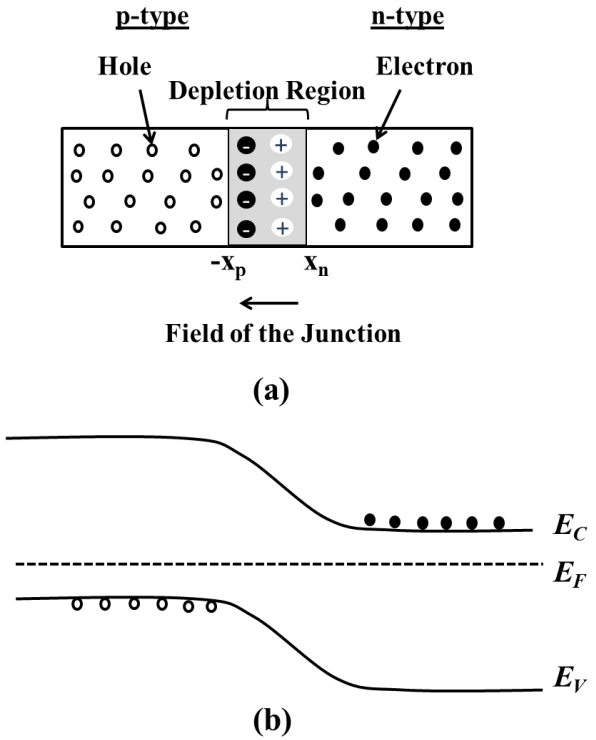

Figure 1.2: (a) Schematic of a p-n junction with depletion region formed due to the recombination of electrons and holes. Field of this region prevents any further crossover of the charge carriers across the junction. (b) Equilibrium band diagram of the p-n junction under no external bias (at a finite temperature). System can be described by a single Fermi level $E_{F.}$

While developing the analytical understanding of the p-n junction it is assumed that in the depletion region, densities of free charge carriers *n* (electrons) and *p* (holes) are negligible as compared to the density of acceptor atoms N_A and donor atoms N_D. This approximation is known as *Depletion Approximation*[3, 4]. Under this condition, the depleted region is sensitive to even the minutest change in charge carrier density (due to defects for example) hence it remains at the heart of the junction related analyses and

characterization techniques. Under the depletion approximation the built-in potential (ϕ) across the junction can be calculated by using electrostatic Poisson's equation as follows:

$$\frac{d^2\phi}{dx^2} = -e\frac{N_A}{\varepsilon} \qquad \text{for } -x_p < x < 0 \qquad (1.7a)$$

and

$$\frac{d^2\phi}{dx^2} = e\frac{N_D}{\varepsilon} \qquad \text{for } 0 < x < x_n \qquad (1.7b)$$

These equations can be used to calculate the electric field, width of the junction and capacitance. Investigation of junction capacitance can further reveal many properties of the p-n junction and other related physical parameters as will be discussed in coming section.

When reverse bias is applied to the junction diode, depletion region widens within the material since the free charge carriers are attracted away from the junction. However, in case of forward bias, charges can be injected across the junction and depletion region narrows down. An ideal p-n junction tries to oppose any conduction of charge in reverse bias (except for the contribution from holes in the n-type side and electrons in the p-type side or minority charge carriers). However, in the forward bias, conduction happens after built in potential of the junction is overcome. Unless a very high forward bias is applied, conduction current in the diode flows due to the diffusion of charge carriers. Current-voltage (*I-V*) characteristics of an ideal p-n junction diode are given by Shockley equation[4]

$$I = I_0\left[\exp\left(\frac{eV}{k_BT}\right) - 1\right] \qquad (1.8)$$

where I_0 is the reverse saturation current.

In a real p-n junction, defect states can be present within the depletion region which can capture/ release charge carriers. The exchange of charge carriers by these defects with band edges can contribute to the free charge carrier density and hence

current. However, the defect energy band should lie below the Fermi level for it to be occupied with charge carriers. Variations in temperature and applied bias affect the position of Fermi level and hence the defect contribution (will be discussed in chapter 2, figure 2.8). Thermal rate ($1/\tau$) of charge carrier exchange from defects is given by[35]:

$$\frac{1}{\tau} = \upsilon \exp\left(-\frac{E_{Th}}{k_B T}\right) \tag{1.9}$$

Where E_{Th} is the defect activation energy and υ is thermal prefactor. In section 1.5 we will discuss in brief how capacitance based measurements are used to characterize defect response in junction structures.

1.3.1 Depletion capacitance

Depletion capacitance can be defined as the increment in total charge of the junction (ΔQ) upon an incremental change in applied voltage (ΔV) i. e. $C=\Delta Q/\Delta V$. Under zero bias, reverse bias and small positive bias, the junction behaves like a dielectric between two conducting plates as shown in figure 1.2a. In this case its capacitance is mainly dominated by depletion capacitance. One can then write:

$$C = \frac{\varepsilon A}{x} \tag{1.10}$$

where A is the area and x is the width of the junction. As mentioned above, with increase in reverse bias, width x of the junction increases which decreases the depletion capacitance.

To calculate the exact change in the width x with applied voltage V, it is easy to assume a junction configuration, where depletion region spreads in one particular side of the junction (Schottky junction, for details see chapter 3 of reference 4), say n-type. This can be achieved either by heavily doping the other side of the junction (p^+-n or n^+-p) or by making metal-semiconductor junction. Then it can be shown by using equation (1.7) under depletion approximation that [4, 36]:

$$N_D(x) = \frac{2}{e\varepsilon A^2 \frac{d(1/C^2)}{dV}} \tag{1.11}$$

Experimentally, by measuring C with varying reverse bias V one can calculate N_D using the above equation (1.11). This technique is called C-V profiling (similar expression can be written for N_A in case of p-type materials).

It is important to note that C-V profiling actually gives free charge carrier density which might be different from the actual value of N_D whenever charge density is non-uniform[37]. This non-uniformity affects the capacitance measurements. One can show that this differential capacitance actually measures the mean position $\langle x \rangle$ of the differential charge ΔQ and can be written as[37]:

$$C = \frac{\Delta Q}{\Delta V} = [(\varepsilon \int_0^\infty \Delta n(x)dx) / (\int_0^\infty x\Delta n(x)dx)] = \frac{\varepsilon}{\langle x \rangle} \tag{1.12}$$

Where Δn is the displaced electron distribution due to ΔV.

It is worth mentioning here that as a quantity to measure stored charge, junction capacitance can be used to track any changes in the total available charge density of the junction e.g. due to the dynamics of defects. Hence capacitance based techniques are widely used to probe electronic transitions involving charge carriers and helpful in calculating defect related parameters. This will be discussed in further detail in section 1.5.

1.3.2 p-n junction under high charge carrier injection: diffusion capacitance and negative capacitance

When a p-n junction is forward biased, energy can be supplied to charge carriers for crossing the barrier. This way electron or holes can be '*injected*' into p-type and n-type regions respectively where they can be treated as minority carriers.

In general, under the injection of charge, minority charge carrier densities start to become comparable to majority charge carrier densities and hence drift as well as

diffusion of charge carriers becomes important. In this case, it is not possible to describe the system with the help of one Fermi level and hence electron and hole populations are described with two separate quasi-Fermi levels as shown in figure 1.3.

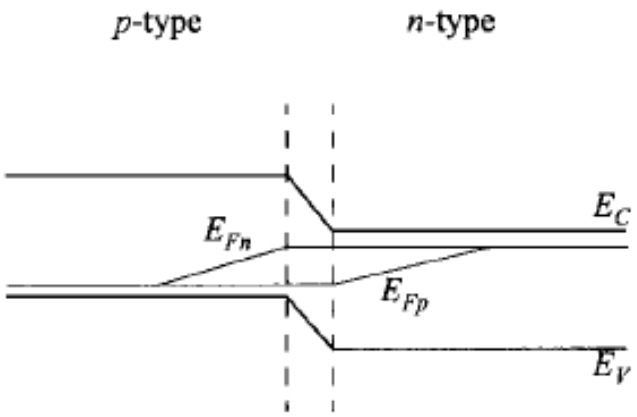

Figure 1.3: Schematic of the p-n junction under external applied field (taken from reference 4). Due to the change in barrier potential and injection of charge carriers, a single Fermi level cannot be used to describe both electrons and holes population and Fermi level splits in quasi Fermi levels for electrons and holes in the junction region.

According to the conventional diode theories, due to the narrowing of depletion region with increasing forward bias, depletion capacitance does not remain significant. Contribution to junction capacitance mainly comes from the diffusion of minority carriers across the junction. This is called the diffusion capacitance and given by[38]:

$$C_{Diff} = \int 2e \frac{\partial N(x,V)}{\partial V} dx \tag{1.13}$$

Where $N(x,V)$ is the charge density as a function of position (x) and bias (V).

Diffusion capacitance decreases with increasing frequencies[4]. However, we will see in following chapters that even diffusion capacitance is not enough to explain the capacitance characteristics of the junction under high charge injection. We will demonstrate that the reactive component of the junction impedance acquires an inductive like behavior with increasing forward bias, which is manifested as negative capacitance (NC)[39]. NC will be discussed in detail in chapter 2 and 3. However, it can be immediately observed that, such response is beyond the diffusion capacitance model of the forward

bias junction. This creates a scope for further experimental and theoretical investigation of diodes in the regime of high charge carrier injection. It becomes important to ask if the electrostatic description of diodes based on depletion approximation remains valid in this situation.

1.3.3 Semiconductor heterostructures and nanostructures

Heterostructures are junctions between two different materials, proposed by Shockley[40] and developed in 1950-60s by Kroemer, Alferov and many others[41, 42]. Using heterostructures, one can achieve quantization of electron motion restricting it to less than three dimensions as compared to a free electron in bulk. Invention of heterostructures gave a new direction to semiconductor physics with increasing scope of using various materials and their combinations. Development and use of these heterostructures was largely supported by the availability of growth techniques which can grow epitaxial layers of materials with abrupt changes. These structures are used in a lot of different devices[43, 12] for example light emitting diodes, lasers, solar cells etc. but their physics is not as established and understood as for a simple p-n junction.

The immediate breakthrough following the development of heterostructures was the development of double heterostructure based devices which used a sandwich layer in between two different materials. In these structures, the dynamics of charge carriers happens primarily in the sandwiched layer. The idea of double heterostructures became very useful for optoelectronic devices like light emitting diodes and lasers and led to the Nobel prize in physics for year 2000[44]. Figure 1.4 shows a schematic of the double heterojunction structure.

If the width of the sandwiched layer is less than the de Broglie wavelength of electron inside the material i.e. $w < \lambda_{de-Broglie}^{electron}$ we observe quantization of electron energy levels. This wavelength range is on the order of few nanometers and these structures are generally referred to as nanostructures. Electron is said to be quantum confined and its dynamics are governed by quantum mechanics. With three translational degrees of freedom available for electron, three types of nanostructures can be constructed:

(i) Quantum wells: when one of the three dimensions is less than $\lambda_{de-Broglie}^{electron}$.

(ii) Quantum wires: when two of the three dimensions are less than $\lambda_{de-Broglie}^{electron}$.

(iii) Quantum dots: when all three dimensions are less than $\lambda_{de-Broglie}^{electron}$.

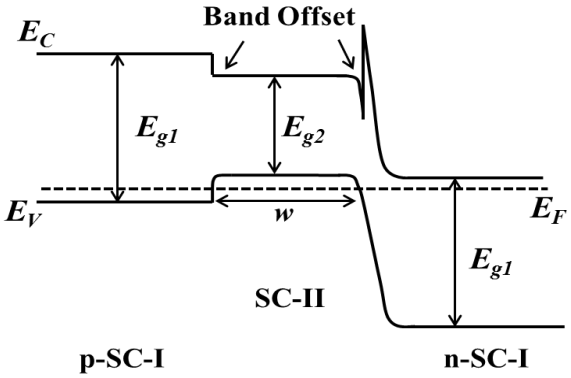

Figure 1.4: Schematic of a double heterojunction. A lower band gap (E_{g2}) semiconductor (SC) material (p-type in this case) is sandwiched between higher band gap (E_{g1}) materials to make a potential well. Dynamics of charge carriers change drastically due to this confinement. When width of the sandwich layer w is less than $\lambda_{de-Broglie}^{electron}$ we start to observe quantum behavior[45].

Density of states[2] (DOS), also changes due to confinement effect as compared to bulk as shown in figure 1.5.

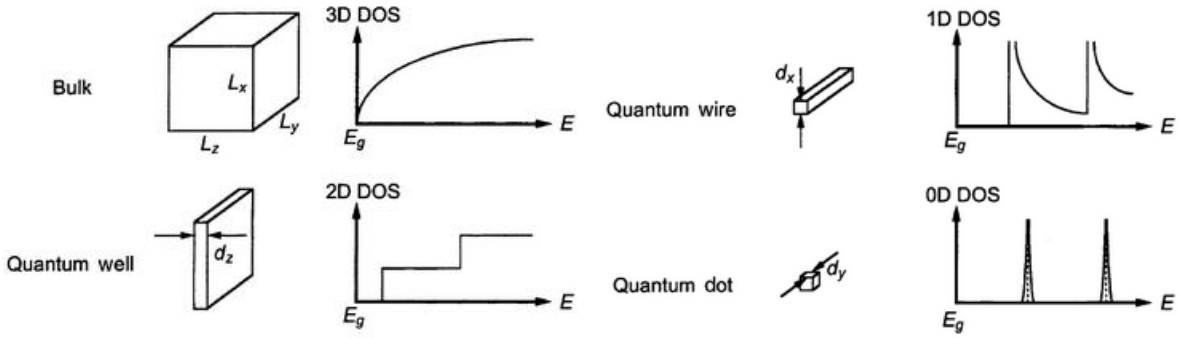

Figure 1.5: Effect of quantum confinement on joint density of states (DOS). As we go from 3D to 0D, DOS becomes non-monotonic function of energy. (Taken from reference 19.)

Development of such quantum structures using semiconductor materials presented a direct system to test and study quantum physics. A rich new physics of quantum structures opened up a whole new direction for devices based on them. These structures

played a significance role for semiconductor based electroluminescent diodes as we will discuss in the following section.

1.4 Electroluminescent diodes (ELD)

When electrically injected charge carriers recombine radiatively, we observe luminescence which is called electroluminescence due to the electric source of its existence. This is the process used in our current diode based electroluminescent structures i.e. lasers and LEDs. Essentially ELDs consist of a material where radiative recombination is more probable or efficient as compared to any other recombination process which is non-radiative. This condition can easily be fulfilled in case of direct band gap materials. But even in case of some indirect band gap materials, radiative recombination can be achieved with the help of a non-radiative channel[46]. These diodes are a part of our day to day technology and can be found in laser pointers, DVD writers, display, optical communication etc.

1.4.1 Physics of light emission in semiconductors

Light emission in semiconductors happens through radiative transitions. These transitions can be of different types, depending on where the electrons and holes are coming from and recombining. Broadly they can be divided into

(i) Transitions involving excitons which happen in relatively pure lattice structures and are much more pronounced at low temperatures and quantum confined structures when the probability of the existence of excitons is sufficient (they are not broken off due to local field due to impurities or thermal energy). Exciton transitions can involve free excitons, bound excitons or their interaction complexes with different quasi particles inside the lattice e.g. exciton-polaritons[14, 18].

(ii) Band to band transitions which occur between conduction and valence band. These transitions can either directly be band to band in case of direct band gap

materials or can be phonon assisted to conserve momentum in case of indirect band gap materials[14].

(iii) Trap assisted transitions where shallow or deep impurity levels take part in the transition[46].

Generally, spectral features of the radiative transition at low or varying temperatures are studied to probe the mechanism of light emission. For example excitonic luminescence peaks are sharp as compared to band to band luminescence[47]. Excitonic peak does not suffer any red spectral shift with increasing excitation[24]. However, in case of band to band transitions which happen due to the presence of free electron-hole density, band gap renormalization[48] effects generate a red shift at higher excitation densities. This broadening can also be present due to different homogeneous or nonhomogeneous effects[12], excitonic peaks can also show broadening in linewidth due to increase in temperature[49] and even at low temperatures due to increased carrier interaction[50], [51]. In such cases, it becomes difficult to identify or understand the transition mechanisms using optical means only.

In case of bulk material, radiative recombination probability is governed by equation (1.4). In case of quantum well, probability of radiative transition increases due to the overlap of electronic wavefunctions under the presence of confinement of charge carriers in a small region. Also, the density of states gets altered and becomes discrete as we discussed in section 1.3.3 and figure 1.5. Now the modified transition probability between any two sub bands of conduction (n) and valence band (m) is given by the corresponding element of the transition matrix (M)[12, 45]:

$$M_{Cn,Vm} \propto \left\langle \varphi^{C}{}_{n}(z) \middle| \varphi^{V}{}_{m}(z) \right\rangle \times \left\langle u^{C}{}_{k}(r) \middle| \vec{e}.\vec{p} \middle| u^{V}{}_{k}(r) \right\rangle \qquad (1.14)$$

where $\left\langle \varphi^{C}{}_{n}(z) \middle| \varphi^{V}{}_{m}(z) \right\rangle$ is the overlap between the components of the envelope wavefunctions of the quantum well in the conduction (C) band and valence (V) band, and $\left\langle u^{C}{}_{k}(r) \middle| \vec{e}.\vec{p} \middle| u^{V}{}_{k}(r) \right\rangle$ is the momentum matrix element, $u^{C}{}_{k}(r)$ and $u^{V}{}_{k}(r)$ are the cell periodic parts of the Bloch functions.

It is worth mentioning that due to the overlapping wavefunctions in case of quantum wells, existence of excitons becomes probable even at room temperatures[52]. Presence of excitons has been reported in many experimental studies on quantum well structures showing excitonic luminescence (photoluminescence as well as electroluminescence) at room temperature[24-26]. For bulk semiconductors, excitonic effects are observed at low temperatures as discussed in section 1.2.2.

1.4.2 Condensed matter physics of electroluminescent diodes

Figure 1.6 shows the structure of a typical quantum well based laser diode[53] available commercially. In our work, we have used laser diodes with similar structures. They essentially have a quantum well which is a special case of double heterojunction diode. We have discussed above that quantum well structures provide much more efficient radiative recombination as compared to simple double heterojunction diodes.

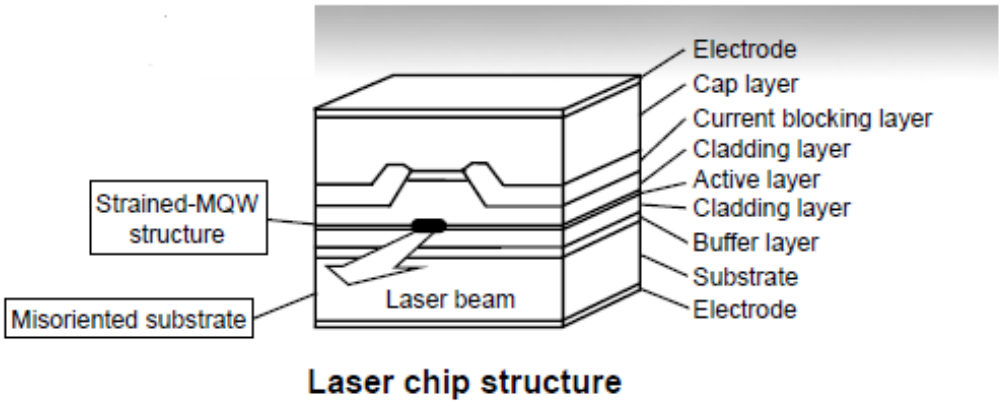

Figure 1.6: A typical structure (taken from reference 53) of strained-multi quantum well (MQW) laser diode available commercially. Presence of different constituent semiconductor layers as well as different time scale processes in the active regime of light emission makes them difficult to be analyzed using simplified depletion approximation based diode model.

To understand and quantify the properties of any material, a very basic device form is constructed. Only then can the depletion approximation based electrostatic description be used to interpret the results. Then each constituent layer can be characterized using conventional techniques, for its physical or more importantly electronic properties. However, for a full device structure, which is operated under high

charge injection, it is not logical to simply extrapolate the behavior of constituent layers based on their conventional characterization (using depletion approximation based techniques). Due to the presence of many different layers and their junctions, the understanding of such complicated structures is far beyond our conventional understanding of a diode. Moreover, in an active ELD, different time scale processes involving charge carriers happen simultaneously e.g. light emission, defect response, non-radiative transitions etc. Coupling of these processes or their mutual competition can give rise to interesting many body physics beyond the electrostatic description.

In addition, to mention briefly, a special case of ELDs are Lasers. Unlike gas lasers or more conventional lasers[54], in diode based lasers we have fermionic charge carriers. Hence the condition of population inversion[55], which is a basic step toward lasing action, can be achieved by exciting (using electrical injection or optical excitation) more and more electrons from valence band to conduction band (as shown in the figure 1.7).

Necessary condition for lasing i.e. going from spontaneous emission[56] to stimulated emission regime is given by[4, 57]:

$$E_g < h\nu < E_{Fn} - E_{Fp} \tag{1.15}$$

Where E_{Fn} and E_{Fp} are electron and hole quasi Fermi levels respectively. This condition is shown in figure 1.7c.

It is interesting to understand what kind of dielectric changes occur in a laser structure, when light emission starts or when lasing starts? Also what is the effect of inherent structure itself on light emission under electrical modulation?

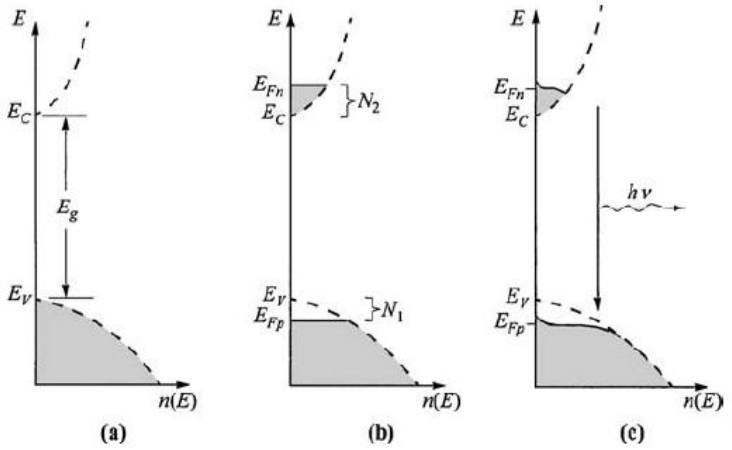

Figure 1.7: Schematic of an ideal semiconductor band structure (taken from reference 4) (a) at 0K with no free charge carrier (b) at 0K with population inversion and (c) at higher temperature with population inversion.

1.4.3 Semiconductor material systems used in ELDs

Popular elemental semiconductors Si and Ge do not exhibit light emission in bulk state due to indirect band gap. GaAs, GaSb, SiC, Si-Ge alloys etc. are some of the earlier materials used for light emission[58]. With the development of epitaxial growth techniques and double heterostructures, various ternary (e.g. AlGaAs) and quaternary alloys (e.g. AlGaInP) of III-V materials became popular for light emission[59]. Variation of material composition allows a large range of visible spectrum to be covered in these alloys and their lattice matching with GaAs provides a good growth condition. With recent technologies, nitrides of III-V materials have gained popularity for high energy emission[60, 61]. Most commonly used device structures are quantum well based[62]. Many different materials like ZnO[63], ZnSe[64] have also been used. For next generation devices, lower dimension structures like quantum wires[65-68] and quantum dots[69-72] are also being studied extensively where theoretical predictions suggest better efficiencies. However, they are yet to achieve commercial success. As a cheap alternative and for flexible electronics, organic (polymer) materials based devices[73, 74] are also being studied. However, they generally suffer from stability issues.

In our work, we have mainly used commercially available ELDs based on III-V based multi quantum well structures. For the purpose of generalizing our technique and

analyses, we have also used III-V based quantum dot ELDs as well as Si-based devices (also available commercially) which do not emit light.

1.5 Admittance (impedance) spectroscopy

Admittance spectroscopy is a technique where capacitance (C) and conductance (G) are measured as a function of temperature and frequency[35, 75-77]. Since, G ($G/2\pi f$ to be precise) and C are the real and imaginary part of the impedance response, they are connected by Kramers-Kronig[78, 79] relations. Any of these can be used to fetch out similar information. When all the free charge carriers can follow the modulation frequency *f*, *C* relates to the width of the space charge layer or depletion region as described in section 1.3.1. This happens when a *p*-*n* junction contains only shallow donors and acceptors. This response is limited by the dielectric relaxation $\tau_d=\varepsilon/\sigma$. Where ε is dielectric constant and σ is conductivity. When modulation frequency exceeds the inverse of the time scale of this relaxation, whole structures behaves like a dielectric. In this case, capacitance reduces to the minimum value governed only by geometry and called geometric capacitance.

We have already discussed before how semiconductors are very sensitive to any impurities and intentional introduction of impurities (doping) can be used to get desired physical properties and device functionalities. However, there can be incorporation of some undesired impurities or lattice irregularities which we consider as defects. Defects modify the band structure in uncontrolled way and can affect dynamics of charge carriers inside the material or device to depending upon their concentration and activation energy.

Charge carrier trapping and de-trapping from these defects can also affect device capacitance. This can happen when modulation establishes an equilibrium between defect carrier capture and their thermal relaxation. In other words, modulation can be felt by the defect states. Hence this poses a restriction on the frequency range where defect response can be seen in capacitance, which should be on the order of the rate of this trapping and de-trapping process. This rate is given by equation (1.9) hence we can write

$$f = \upsilon \exp\left(-\frac{E_{Th}}{k_B T}\right) \tag{1.16}$$

where υ is the thermal prefactor and E_{Th} is the defect activation energy. When this energy matches with electron (or hole) quasi Fermi level E_{Fn} (or E_{Fp}) inside the band gap, frequency dependent conductance shows a peak and capacitance goes through an inflection point[35]. Now we write equation (1.16) as:

$$E_{Th} = k_B T \ln\left(\frac{\upsilon}{f}\right) \tag{1.17}$$

Clearly, when temperature is changed, frequency of defect response also changes and vice versa. Hence by a frequency and temperature scan of capacitance (or conductance or both) one can calculate the defect activation energy and thermal prefactor which is given by:

$$\upsilon = 2N_{C,V}\ \mathrm{v_{Th}}\sigma_{n,p} \tag{1.18}$$

where, $N_{C,V}$ represents effective density of the band (conduction band or valence band), $\mathrm{v_{Th}}$ and $\sigma_{n,p}$ are the thermal velocity and capture cross section for involved charge carriers respectively. Temperature dependence of prefactor is governed by all of these quantities.

To present an example, in figure 1.8 we show admittance (impedance) spectroscopy results for hot wire chemical vapor deposition (HWCVD) grown a-Si,Ge;H on p^+ crystalline-Si sample with 30% Ge and greater than $10^{20}/cm^3$ density of O_2 as defects[80].

Re-writing equation (1.14) gives:

$$\ln f_{Max} = \ln \upsilon + \left(-\frac{E_{Th}}{k_B}\right)\frac{1}{T} \tag{1.19}$$

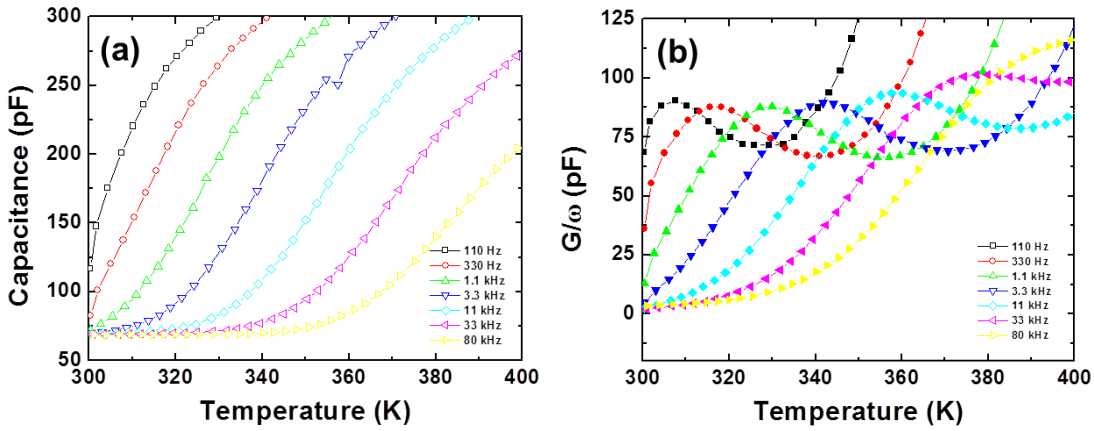

Figure 1.8: Impedance spectroscopy for a-Si,Ge;H on p^+ crystalline-Si sample (Schottky diode configuration) with 30% Ge and >10^{20}/cm^3 density of O_2 as defects (Taken from reference 80) . Change in capacitance (a) and peak in G/ω (ω=2πf) (b) is visible due to the defect activation. Position of the peak shifts to lower temperature for lower applied modulation frequency in accordance with the response rate equations (1.9) and (1.16) of these defects.

Therefore, Arrhenius plot[81, 82] between lnf_{Max} and T gives a straight line, slope of which is related to activation energy E_{Th} and intercept provides information about carrier capture cross section for defect states as per equation (1.18).

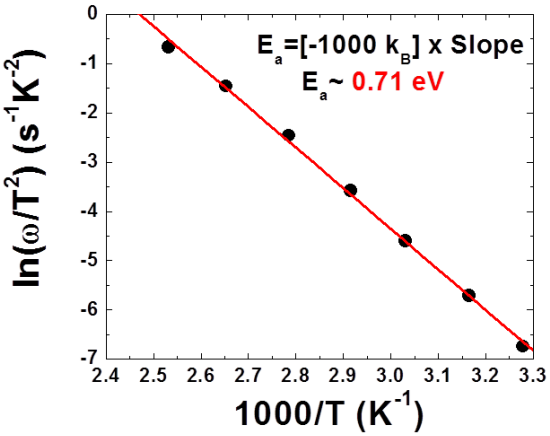

Figure 1.9: Shows resulting Arrhenius plot from figure 1.8 to calculate E_{Th} which is represented as E_a here. ω=2πf.

Admittance/ impedance spectroscopy is an important and widely used tool to probe defect dynamics in semiconductor junctions. It is clear from above analysis that it is best

to carry out when we have a single type of free carriers (majority carriers) present in the device, which keeps the analysis simple. Hence one has to be careful while using above analysis and its interpretations.

1.6 An outline of the thesis

We have discussed how condition of charge injection is important for the operation of diode based light emitting devices. However, due to the presence of large number of free charge carriers, this regime cannot be explained by the conventional theory of p-n diodes presented here. Modifications in the theory are required to extend it to understand the behavior of a junction diode under high charge injection. One needs to understand how process of light emission couples with different processes inside the junction to affect its dielectric behavior. Therefore, in this thesis we present our work on ELDs (mainly AlGaInP based multi quantum well) under their operating condition of light emission (under charge carrier injection). Surprisingly, such studies, trying to understand the electrical transport in these *active* devices are not many in the literature. We will show how the interdependence of electrical and optical properties in these devices throws light on the basic physical processes they undergo. We will also show that these studies aimed at probing basic condensed matter physics can, in fact, help in improving device efficiencies for various applications.

We will discuss the techniques and analyses we have developed to study these devices beyond the conventional understanding including the electrical signatures of excitonic state and its subsequent Mott transition to free electron-hole plasma state. These states are generally probed by optical means only.

In **chapter 2**, we will describe the low frequency electrical (< 2 MHz) and optical (< 100 kHz) response from ELDs and their observed interdependence under charge carrier injection. We studied impedance of these active devices and developed the technique of voltage modulated electroluminescence to measure its connection with light emission. We will describe the crossover of capacitive reactance to inductive like

reactance which happens simultaneously with the onset of modulated light emission. Observed inductive reactance seen as negative capacitance and modulated light emission also follow similar frequency dependence. We will explain observed connection and similarity in frequency dependent optical and electrical response by considering the role of sub-band gap defects in radiative recombination dynamics. We will argue how our techniques using low frequency characterization can be used to qualitatively predict and improve the response of ELDs under high frequency modulation (~ GHz) used in optical communication. We will also discuss the features observed in both capacitance and conductance when the process of lasing starts.

In **chapter 3**, we will present the theoretical basis of observed negative capacitance (NC) phenomenon by analyzing the variation in frequency dependent impedance after the application of small forward bias voltage pulse. We will describe how time variation of current transient following the voltage step dictates the effective behavior of frequency dependent capacitance. We will experimentally demonstrate the signatures of negative capacitance as the monotonically increasing positive valued current transient. We will also show how our understanding of NC based on the competition of slow defects and fast radiative recombination processes fits into the theoretical analyses and provides a most general explanation for NC.

To establish and test the model of defect mediated radiative recombination process, we will discuss temperature domain studies of observed low frequency modulated electrical and optical response in **chapter 4**. We will discuss that the observed counterintuitive increase in modulated light emission with increasing temperature (unlike usual CW light emission which decreases with increasing temperature) supports our model for lower temperature ranges. However, after a certain temperature range, carrier escape from inbuilt quantum well structure of the ELD starts to affect the observed low frequency response. This results in a temperature range where modulated light emission maximizes. We suggest that it should be brought to the device's working temperature for better efficiency of the device under modulation. We will show that the negative capacitance also behaves like modulated light emission during temperature scan, indicating the correlation between electrical and optical response.

In continuation with our understanding of correlated electrical and optical properties, we studied small signal impedance response in frequency domain to probe the light emission process. At a constant temperature, this response shows bias activation, as will be discussed in **chapter 5**, following a phenomenological rate equation we have developed. Frequency dependence of this bias activated response inverts after the onset of light emission indicating the presence of negative activation energy. We will describe that the occurrence of negative activation energy could be attributed to the presence of an excitonic state in these devices. We will show that at higher injection biases, this possible signature of excitonic state vanishes, indicating Mott transition of excitonic state to free electron-hole plasma state. Thus, for the first time we identify the electrical signatures, which can possibly be associated with excitonic presence and its Mott transition. We will also show optical results in agreement with our interpretation.

Since charge carrier injection is an essential condition for ELDs, we have used these systems mainly to probe the physics of semiconductor diodes under charge carrier injection using modulated electrical and optical response. However, our results are generalized and applicable to a wider range of diodes which we will present in **chapter 6**. We applied our techniques to study quantum dot based ELDs, which show qualitatively similar behavior like quantum well based ELDs. Importantly, will show that the qualitatively dissimilar behavior of Si based diodes (which do not emit light) under small signal modulation can also be explained by the techniques and analyses we have developed.

Finally we will summarize the work and present important conclusions in **chapter 7**. We will also discuss the directions in which this work is being extended, or can be pursued further.

1.7 References

[1] P. Y. Yu and M. Cardona, *Fundamentals of Semiconductors: Physics and Materials Properties* (Springer, 4th Edition, 2010), Chapter 1.

[2] C. Kittel, *Introduction to Solid State Physics* (Wiley-India, 7th Edition, 2007).

[3] M. Shur, *Physics of Semiconductor Devices* (Prentice Hall-India, 1st Edition, 1995).

[4] S. M. Sze and K. K. Ng, *Physics of Semiconductor Devices* (Wiley-Interscience, 3rd Edition, 2006).

[5] J. C. Philips, *Phys. Rev*. **125**, 1931 (1962).

[6] L. T. Canham, *Appl. Phys. Lett*. **57**, 1046 (1990).

[7] O. Bisi, S. Ossicini and L. Pavesi, *Surf. Sci. Rep*. **38**, 1 (2000).

[8] M. L. Cohen and J. R. Chelikowsky, Electronic Structure and Optical Properties of Semiconductors (Springer, 2nd Edition, 1989).

[9] M. Grundmann, *The Physics of Semiconductors: An Introduction Including Devices and Nanophysics* (Springer, 2nd Edition, 2010).

[10] J. R. Chelikowsky and M. L. Cohen, *Phys. Rev. B* **14,** 556 (1976).

[11] J. Millman and C. C. Halkias, Integrated Electronics (Tata McGraw-Hill, 1st Edition, 1991).

[12] J. Singh, *Physics of Semiconductors and Their Heterostructures* (McGraw-Hill, International Edition, 1993).

[13] D. V. Shroeder, *An Introduction To Thermal Physics* (Addison-Wesley, 1st Edition, 1999).

[14] J. I. Pankove, *Optical Processes in Semiconductors* (Dover Publications, 1st Edition, 1975).

[15] C. T. Sah, R. N. Noyce, and W. Shockley, *Proc. IRE* **45**, 1228 (1957).

[16] R. N. Hall, Phys. *Rev.* **87**,387 (1952).

[17] W. Shockley and W. T. Read, Phys. *Rev.* **87**, 835 (1952).

[18] C. F. Klingshirn, *Semiconductor Optics* (Springer, 2nd Edition, 2004).

[19] E. Kapon, *Semiconductor Lasers I: Fundamentals* (Academic Press, 1st Edition, 1999).

[20] J. Nelson, *The Physics of Solar Cells* (Imperial College Press, 1st Edition, 2003).

[21] J. Frenkel, *Phys. Rev.* **37**, 17 (1931).

[22] G. H. Wannier, *Phys. Rev*. **52,** 191 (1937).

[23] M. A. Lampert, *Phys. Rev. Lett*. **1**, 450 (1958).

[24] M. Noriyasu and K. Fujiwara, *Appl. Phys. Lett*. **97**, 031103 (2010).

[25] R. P. Stanley, B. J. Hawdon, J. Hegarty, R. D. Feldman and R. F. Austin, *Appl. Phys. Lett.* **58**, 2972 (1991).

[26] K. Fujiwara, N. Tsukada and T. Nakayama, *Appl. Phys. Lett*. **53**, 675 (1988).

[27] L. V. Keldysh and Y. V. Kopaev, *Sov. Phys. Solid State* **6,** 2219 (1965).

[28] L. V. Butov, A. C. Gossard, and D. S. Chemla, *Nature* **418,** 751 (2002).

[29] Fabrice P. Laussy, Alexey V. Kavokin, and Ivan A. Shelykh, *Phys. Rev. Lett.* **104,** 106402 (2010).

[30] L. V. Butov, C. W. Lai, A. L. Ivanov, A. C. Gossard and D. S. Chemla, *Nature* **417**, 47 (2002).

[31] Kosuke Yoshioka, Eunmi Chae, and Makoto Kuwata-Gonokami, *Nat. Commun*. **2,** 328 (2011).

[32] A. A. High, J. R. Leonard, A. T. Hammack, M. M. Fogler, L. V. Butov, A. V. Kavokin, K. L. Campman, and A. C. Gossard, *Nature* **483,** 584 (2012).

[33] F. Manni, Y. Léger, Y.G. Rubo,R. André and B. Deveaud, *Nat. Commun***. 4,** 2590 (2013).

[34] Hui Deng, Hartmut Haug, and Yoshihisa Yamamoto, *Rev. Mod. Phys.* **82,** 1489 (2010).

[35] T. Walter, R. Herberholz, C. Muller and H. W. Schock, *J. Appl. Phys.* **80**, 4411 (1996).

[36] W. Shockley, *Electrons and Holes in Semiconductors With Application To Transistor Electronics* (D. Van Nostrand Company, 1950).

[37] H. Kroemer and W. Y. Chien, *Sol. State. Electron*. **24**, 655 (1981).

[38] J. Strologas and K. Hess, *IEEE Trans. Electron. Devices*, **51**, 506 (2004).

[39] See reference 3-23 of chapter 2.

[40] W. Shockley, U. S. Patent, 2,569,347 (1951).

[41] Z. I. Alferov, *Semiconductors* **32,** 1 (1998).

[42] Z. I. Alferov, *Rev. Mod. Phys.* **73**, 767 (2001).

[43] J. J. Coleman, *Semiconduc. Sci. Technol.* **27**, 090207 (2012).

[44] http://www.nobelprize.org/nobel_prizes/physics/laureates/2000/

[45] J.H. Davies, *The Physics of Low-dimensional Semiconductors* (Cambridge University Press, 1st Edition, 1998).

[46] C. H. Henry, P. J. Dean and J. D. Cuthbert, *Phys. Rev*. **166**, 754 (1968).

[47] R. Dingle, W. Wiegmann and C. H. Henry, *Phys. Rev. Lett*. **33**, 827 (1974).

[48] S. D. Sarma, R. Jalabert and S. R. Eric Yang, *Phys. Rev. B* **41**, 8288 (1990).

[49] H. Qiang, F. H. Pollak, C. M. S. Torres, W. Leitch, A. H. Kean, M. A. Stroscio, G. J. Iafrate and K. W. Kim, *Appl. Phys. Lett.* **61**, 1411 (1992).

[50] W. Liu, D. Jiang, K. Luo, Y. Zhang and X. Yang, *Appl. Phys. Lett*. **67**, 679 (1995).

[51] T. S. Koh, Y. P. Feng and H. N. Spector, *J. Appl. Phys*. **81**, 2236 (1997).

[52] J. Feldmann, G. Peter, E. O. Gobel, P. Dawson, K. Moore, C. Foxon and R. J. Elliott, *Phys. Rev. Lett*. **59**, 2337 (1987)

[53] Taken from 'SanyoLDCatalogue2008' and 'Sanyo_databook'

[54] K. Thyagarajan and A. Ghatak, *Lasers: Fundamentals and Applications* (Springer, 2nd Edition, 2010).

[55] O. Svelto, *Principles Of Lasers* (Springer, 5th Edition, 2010).

[56] R. Loudon, *Quantum Theory Of Light* (Oxford University Press, 3rd Edition, 2000).

[57] M. G. A. Bernard and G. Duraffourg, *Phys. Status Solidi* **1**, 699 (1961).

[58] E. F. Schubert, *Light-Emitting Diodes* (Cambridge University Press, 2nd Edition, 2006).

[59] E. Kapon, *Semiconductor Lasers II: Materials and Structures* (Academic Press, 1st Edition, 1999).

[60] S. Nakamura, S. Pearton and G. Fasol, *The Blue Laser Diode: The Complete Story* (Springer, 2nd Edition, 2000).

[61] S. Nakamura and S. F. Chichibu, *Introduction to Nitride Semiconductor Blue Lasers and Light Emitting Diodes* (Taylor and Francis, 1st Edition. 2000).

[62] H. Zhao, G. Liu, J. Zhang, J. D. Poplawsky, V. Dierolf and N. Tansu, *Optics Express*, **19**, A991 (2011).

[63] A. Tsukazaki, M Kubota, A. Ohtomo, T. Onuma, K. Ohtani, H. Ohno, S. F. Chichibu and M. Kawasaki, Jap. *J. Appl. Phys*. **44**, 643 (2005).

[64] J. Ren, K. A. Bowers, B. Sneed, D. L. Dreifus, J. W. Cook Jr., J. F. Schetzina, and R. M. Kolbas, *Appl. Phys. Lett.* **57**, 1901 (1990).

[65] Z. Tang, N. A. Kotov and M. Giersig, *Science* **297**, 237 (2002).

[66] S. D. Sarma and D. W. Wang, *Phys. Rev. Lett*. **84**, 2010 (2000).

[67] K. Tomioka, J. Motohisa, S. Hara, K. Hiruma and T. Fukui, *Nano Lett*. **10**, 1639 (2010).

[68] T. Frost, S. Jahangir, E. Stark, S. Deshpande, A. Hazari, C. Zhao, B. S. Ooi and P. Bhattacharya, Nano Lett. 14, 4535 (2014).

[69] C. W. Snyder, B. G. Orr, D. Kessler, and L. M. Sander, *Phys. Rev. Lett*. **66**, 3032 (1991).

[70] A. Polimeni, M. Henini, A. Patane` , L. Eaves, P. C. Main and G. Hill, *Appl. Phys. Lett*. **73**, 1415 (1998).

[71] L. Qian, Y. Zheng, J. Xue and P. H. Holloway, *Nat. Photon.* **5**, 543 (2011).

[72] N. N. Ledentsov, *Semiconduct. Sci. Technol.* **26**, 014001 (2011).

[73] C. W. Tang and S. A. VanSlyke, *Appl. Phys. Lett*. **51**, 913 (1987).

[74] S. Reineke, M. Thomschke, B. Lüssem, and K. Leo, *Rev. Mod. Phys.* **85**, 1245 (2013).

[75] D. K. Schroeder, *Semiconductor Material Device Characterization* (Wiley Interscience, 2nd Edition, 1998).

[76] R. Herberholz, M. Igalson and H. W. Schock, *J. Appl. Phys.* **83**, 318 (1998).

[77] J. V. Li and D. H. Levi, *J. Appl. Phys*. **109**, 083701 (2011).

[78] J. D. Jackson, *Classical Electrodynamics* (Wiley, 3rd Edition, 1998).

[79] D. A. B. Miller, D. V. Lang and L. C. Kimerling, *Ann. Rev. Mater. Sci*. **7**, 377 (1977).

[80] Unpublished data from Dr. Shouvik Datta, reproduced with permission.

[81] A. Frost, R. Pearson, *J. Phys. Chem.* ***65,*** 384 (1961).

[82] K. J. Laidler, *J. Chem. Educ.* **61**, 494 (1984).

Chapter 2

Low Frequency Electrical and Optical Properties

2.1 Introduction

In our effort to understand the physics of electroluminescent devices (ELDs), we studied how the impedance characteristics are affected by light emission or charge carrier injection. We are interested in probing the response of charge carriers inside the device and the importance of studying impedance in this context has already been discussed in chapter 1, section 1.5. We observed characteristic change in the frequency dependence of conductance (G) after the onset of light emission. However, more interestingly, we observed that under high carrier injection, reactive component of impedance acquires inductive like behavior. This phenomenon is manifested in negative values of capacitance and does not follow frequency dependence of a pure inductance. Also, due to the geometry of the device, which supports the presence of capacitance over inductance, it is preferred to call it as negative capacitance (NC) effect. This behavior cannot be explained by the conventional, text-book based understanding of junction diode based on depletion approximation[1, 2]. In general, under charge carrier injection, as a signature of inductive reactance[3, 4], negative capacitance has been reported in many semiconductor devices/structures like Schottky barriers[5, 6], solar cells[7, 8], Silicon based diodes[9-12], p-i-n junctions[13], TiO_2 films[14], III-V nitrides based diodes[15, 16], light emitting diodes (LED)[17-19] and laser diodes (LD)[20]. In application of diode based detectors for high energy particle detection, NC has been observed in Si based p^+-n junctions irradiated with fast electrons[21]. In case of LEDs, onset of NC has been associated with the threshold of light emission[22] and for LDs, it has even been correlated with the onset of lasing[20]. Variation of voltage[22] and current[23] modulated electroluminescence has also been studied in this

context. Observed increase in modulated electroluminescence with high injection levels and low frequencies had been somewhat correlated[22] with the observed NC, which also follows the same trend. However, presence of NC has also been reported in case of Silicon based devices and solar cells, which are intrinsically inefficient for light emission. Hence its connection with light emission, as presented previously, cannot be used alone to provide a generalized mechanism for NC.

To sum up, occurrences of NC have always been associated with junctions under charge injection and a variety of explanations have been proposed to justify its presence. Theoretical calculations showing the occurrence of NC have also been presented for metal insulator junction[24] and junction diodes in general[25]. These calculations are based on a much more careful consideration of junction current components improving the conventional text-book understanding of a simple diode structure and will be discussed in a bit more detail in following chapters. Nevertheless, basic overall understanding of physical mechanisms of NC which should be extendable to various kinds of devices is required. Here we present the detailed investigation of NC and related phenomena in AlGaInP based red LDs and red LEDs. We will discuss the generalized prescription of NC we came up with, by considering the role of sub-band gap states in the light emission process. We will also discuss how the dynamic competition between these processes actually affects both NC and modulated light emission in a significant way by studying and analyzing their dependence on modulation frequency. Experimental investigations of such influence of sub-band gap defects on the physics of NC as well as on modulated light emission in light emitting devices is the main focus of the work presented in this chapter. By and large, we will extend and generalize our explanations of NC to non-electroluminescent devices. We also suggest that better understanding of these interconnected phenomena can be used to characterize as well as to improve the performance of these semiconductor devices.

Presence of electronic sub-band gap defects is often a limiting factor for the performance of any electronic device[26, 27]. Specifically, in electroluminescent devices, defects can degrade long term radiative efficiency and stability by introducing non-radiative recombination pathways. Here we will also discuss the importance of using the

above characterization techniques like modulated light emission spectroscopy to optimize the material parameters and device designs of laser diodes. Specifically, we argue that such optimizations are necessary to minimize the contribution of slowly responding defect states in light emission processes. We will emphasize that this can, in principle, significantly improve the performance of high speed (~GHz) operation of electroluminescent devices used in optical communication.

In this study, we employed low frequency ($f \leq 2$ MHz) impedance spectroscopy and voltage modulated electro-luminescence spectroscopy (VMEL) ($f \leq 100$ kHz) at room temperature under small signal condition to investigate commercially available AlGaInP based red LDs and red LEDs. Here we report – (i) the onset of relatively dispersion-less region in the measured steady state conductance soon after the growth of significant continuous wave (CW) light output, (ii) a generic physical mechanism for NC, (iii) connection between the onset of negative capacitance with the onset of VMEL signal at a particular modulation frequency and forward bias (I_{dc}) and (iv) contribution of sub-band gap defects to the spectral line shapes of VMEL with the variation of injection level as well as the modulation frequency. Although here we will be discussing results only for red light emitting edge-emitter diodes but we will argue that the scope of this work and subsequent analysis can be extended to include general behavior of negative capacitance seen in many different types of junction diodes.

2.2 Experimental methods

2.2.1 Sample details

We used commercially available diode laser DL 3148-025 from Sanyo at current injection levels below the lasing threshold for most of our studies. These are AlGaInP based edge emitting, strained multi-quantum well structures with lasing wavelength 635 nm (data is taken from ‘SanyoLDCatalogue2008’ and ‘Sanyo_databook’). Results which we will be discussing are also reproduced for many DL-3148-025 LDs and similar red

LDs like RLD-65-NE from Rohm (657 nm) as well as for a number of red LEDs. Internal circuit diagram of laser diodes used is shown in figure 2.1. They consist of three terminals. However, the photodiode (PD) terminal was kept disconnected during our measurements. For different applications this connection is used to monitor the light output from laser diode and to maintain the current injection without damaging the diode. In case of LEDs, having only two terminals, connections were made according to the required forward bias condition.

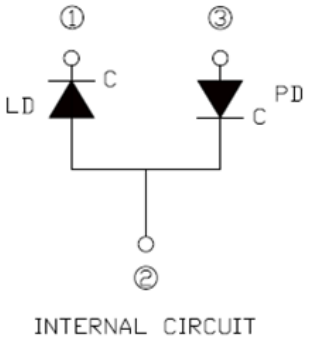

Figure 2.1: Internal circuit of the commercially available diode lasers used in our work (figure taken from Sanyo_databook). LD represents laser diode and PD represents photo diode. For all the measurements terminal 1 and 2 were connected in forward bias configuration leaving terminal 3 disconnected.

2.2.2 Instrumentation

A significant part of this work was devoted to integrating different instruments and components for experimental setup. We established various techniques to study the physics of semiconductors and their devices in the lab including: electrical techniques such as impedance spectroscopy, drive level capacitance profiling (DLCP), deep level transient spectroscopy (DLTS) etc. and optical techniques like photoluminescence (PL), electro-reflectance modulated spectroscopy (ER), surface photo voltage spectroscopy (SPV), transient photo capacitance spectroscopy (TPC) etc. An introduction of these techniques and their applications can be found in reference 28. Fully automated experimental modules were developed with real time data acquisition and plotting. LabVIEW 8 by National Instruments was used as an interface to integrate different components of the experimental setup.

In the work presented in this thesis, some of the above mentioned techniques were used along with the modification required for the conventionally different regimes where we target to study the devices. Wherever necessary, we will describe these modifications in techniques or analysis methodology as we will go through the results and discussion part presented in the thesis.

We have extensively used impedance (reactance and conductance) measurement as a tool for probing various processes in the ELDs for relatively low frequency range. For impedance measurements, we used E4980A precision LCR meter from Agilent (frequency $\leq$ 2 MHz). Forward bias injection current level and voltage was monitored by the same instrument which we refer to as I_{dc} and V_{dc} respectively. A simple equivalent circuit model as shown in figure 2.2a consisting of a capacitance (C) and a conductance (G) in parallel has been used for impedance analysis by neglecting any contribution of series resistance at the low current injection levels. C represents the stored charge and G in parallel represents any parallel path for the flow of current in the device other than the junction itself.

We have developed modulated light output or voltage modulated electroluminescence spectroscopy (VMEL) to probe the connection between observed electrical and optical properties. Experimental setup for this is shown in figure 2.2b. E4980A was used for dc-biasing and the sinusoidal output of SR850 lock-in amplifier (f $\leq$ 100 kHz) from Stanford Research System for voltage modulation. Modulated electroluminescence signal was dispersed using an Acton Monocromator-2555i from Princeton Instruments and was finally detected by a Si photodiode (FDS010) in phase with the applied voltage modulation. The current signal from the photodiode was amplified with a SR570 current preamplifier from Stanford Research System before being fed to SR850 lock-in amplifier for final measurement.

Under small signal condition (V_0^{rms}= 30 mV), measured I_{ac}^{rms} was kept at least an order of magnitude smaller than I_{dc}. To couple the dc bias and ac modulation signal, we used a home built adder-amplifier circuit (with IC CA3240E) which currently limits I_{dc} to less than 10 mA. For CW light detection, emitted light was externally chopped at 35 Hz using a SR540 chopper controller from Stanford Research Systems. We monitored the

temperature of all samples using a Lakeshore 340 temperature controller along with DT-670B-SD Silicon diode sensor at all stages of bias currents (with an experimental accuracy of ±0.1 K). For this purpose device was mounted on a closed cycle Helium cryostat (through a sample holder) from Advance Research Systems. We placed a diode sensor on the cryostat cold head, output of which was used by Lakeshore 340 to control the Joule heating and maintain the desired temperature. For monitoring device temperature more accurately, we placed another sensor on the sample holder.

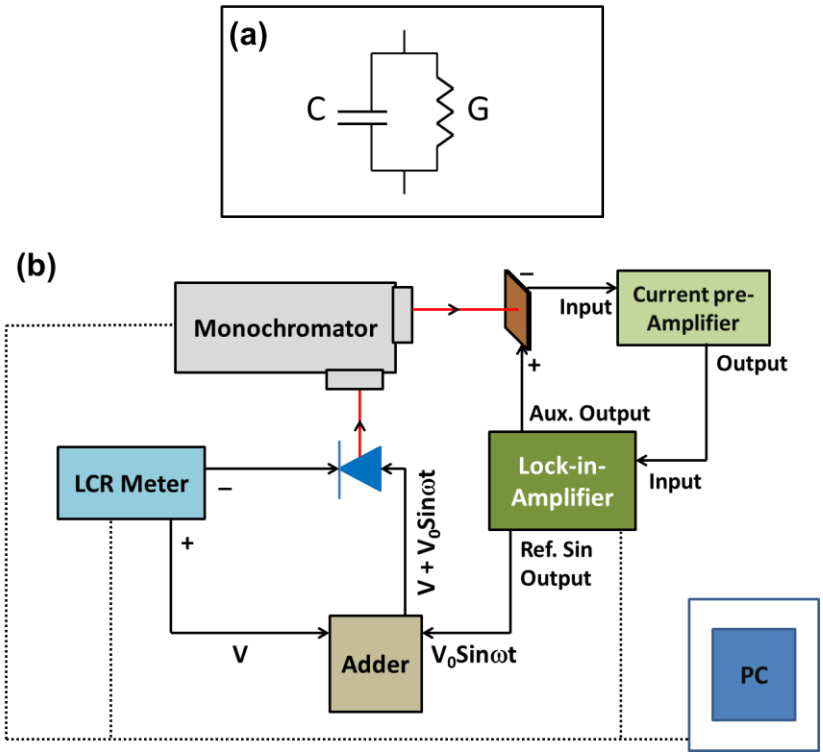

Figure 2.2: (a) Simple circuit model used for the measurement of capacitance (C) and conductance (G). (b) Schematic of the experimental setup for modulated light output measurements. Different components were integrated using LabVIEW with automated data acquisition facility.

2.2.3 **Sample holder**

Schematic of the sample holder used is shown in the figure 2.3. It was made by using a copper strip of sufficient thickness. This ensured good thermal conductivity and efficient heat transfer between the cold head of the cryostat and the sample holder. To insulate the sample electrically from holder (and cold head), an insulating strip was

screwed on the sample holder. Electroluminescent diode (ELD) was soldered on this insulating strip as shown in the figure 2.3.

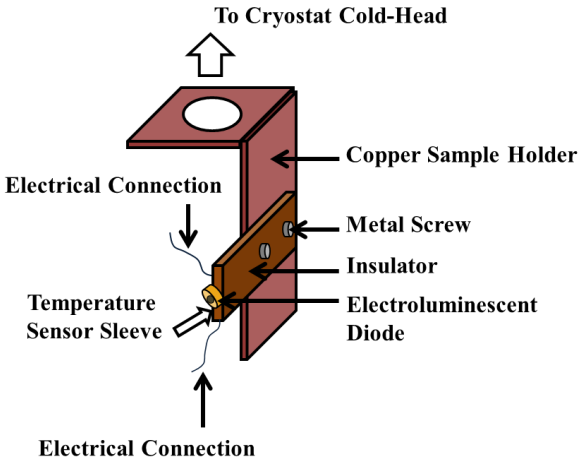

Figure 2.3: Schematic of the sample holder used.

2.3 Results and discussion

Figure 2.4 shows characteristics of the laser diodes (DL-3148-025) to identify the light emitting threshold, lasing threshold and spectral features of the laser. Figure 2.4a is the typical light emission vs injection current (L-I) curve for the laser showing the onset of lasing around 27 mA. The onset of spontaneous light emission occurs much earlier, around only a few μA. Figure 2.4b shows spectra at different current injection levels. As the applied current injection level increases, the peak intensity increases. After lasing threshold, emission spectrum becomes sharp with very narrow line width centered at 635 nm, as shown in the inset.

We observe a slight asymmetry in the spectral shape around the peak position. An emission tail is observed on the low wavelength (high energy) regime. The high energy feature is due to the band-to-band recombination of electrons and holes occupying higher energy states away from the conduction and valence band edges or so called hot carriers[29, 30].

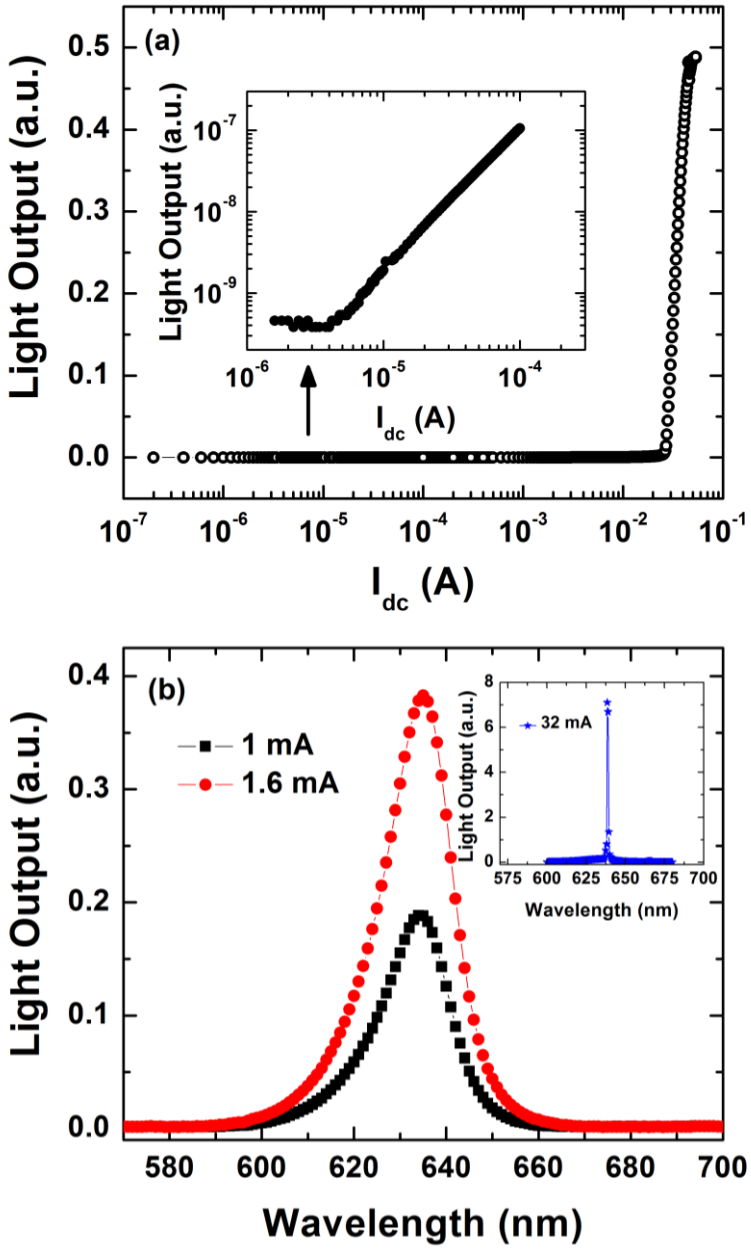

Figure 2.4: Characteristics of laser diode DL-3140-025 (a) L-I curve depicting lasing threshold around 27 mA and light emission threshold (inset) around few μA and (b)Light emission spectra before and after (inset) lasing onset. In the regime of spontaneous light emission spectra are broad as compared to sharp emission line centered at 635 nm after lasing threshold.

2.3.1 Impedance characteristics of electroluminescent diodes (ELD) and the signatures of light emission

To observe any change or effect of light emission on the dielectric behavior, we measured impedance of the devices under charge injection condition up to 100 mA. Figure 2.5 shows the variation of conductance (G) and capacitance (C) with applied current injection level for different modulation frequencies.

Two distinct frequency dependent regions for injection currents – (i) < 20 μA and (ii) > 3 mA can be seen in G which have qualitatively opposite behavior. For I_{dc} < 20 μA, the junction is dominated by diffusion of injected minority charge carriers from bulk, hence G increases monotonically with both the injection level and modulation frequency. Whereas, in this range of bias current (< 20 μA), C increases with increasing injection level but decreases with increasing modulation frequency. This is again the characteristic diffusion capacitance like behavior where minority carrier storage near the junction plays a major role[26]. However, we notice a relatively non-dispersive region in G, triggered after significant light output, for 20 μA < I_{dc} < 3 mA. Interestingly C remains highly dispersive in this range of bias current, which starts to decrease as the injection current starts to drift the charge carriers[31] and eventually turns negative with increasing I_{dc}. For lower frequencies, this NC is more prominent and observed at lower injection levels.

Being real and imaginary parts of the same dielectric response function, qualitatively different frequency dependence of G and C may look confusing. To clarify, we plot G/ω (ω=2π*f* being angular frequency of modulation) in the inset of figure 2.5a. They are connected through Kramers-Kronig relations for linear dielectric responses[32]. As in case of C, we do not observe any dispersion-less region in G/ω, as expected.

Clearly frequency dependent NC can neither be caused by CW light emission which starts at quite low current (~4 μA; inset of figure 2.4a) nor by the lasing action which starts at a comparatively higher current (> 27 mA; figure 2.4a).

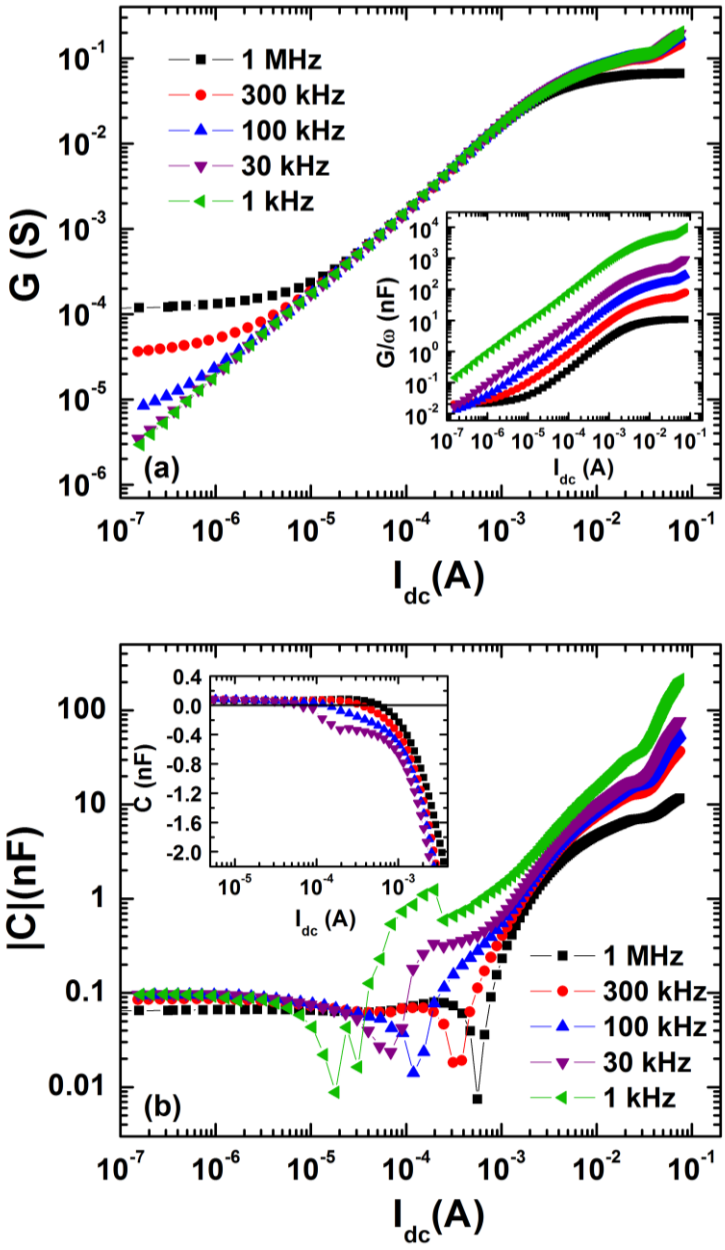

Figure 2.5: (a) Conductance (G) of the light emitting device vs I_{dc} at different frequencies, showing two distinct dispersive regions separated by a relatively non-dispersive region. Frequency dependences of dispersive regions are characteristically opposite. Span of non-dispersive region varies for different samples. Inset shows the plots for G/ω to compare directly with capacitance. (b) Capacitance (C) vs I_{dc}, plotted as absolute value, turning of the curve after sudden kink is the starting of negative capacitance (NC). Inset shows that the onset of NC happens at lower I_{dc} for lower modulation frequencies (f).

At this point, we postpone any further discussion on the cause of NC to the later part of this chapter. It is evident from the variation of C with such low modulation

frequencies (≤ 2 MHz) that sub-band gap states with transition rates much slower than the radiative transitions are playing a significant role. However, a dispersion free region for G in the same range of currents points to the fact that the modulation at different frequencies couples the energy used in the injection process with the surrounding heat bath[32] in a similar fashion. Usually, Shockley-Read-Hall type of recombination, mediated by sub-band gap trap states, dissipates heat[28] through lattice vibrations or phonons (joule heating ~ i^2R). So it is expected that sub-band gap states can notably affect the reactive response under different modulation rates. Nevertheless, we observe that the conductance and associated steady state dissipation of energy is practically independent of modulation frequency in the intermediate current injection levels (figure 2.5a). Comparing figures 2.4a and 2.5a, it is also evident that this non-dispersive region in G starts only after a significant growth of CW light emission. In order to understand this event, we presume that the energy spent in increasing the forward bias and subsequent increase in minority carrier injection is wholly being utilized by the radiative light emission of those injected minority carriers without significant coupling of the excess energy to the heat bath in the frequency range of operation. At higher current injection levels, increased joule heating is possibly significant enough to change this dispersion-less situation and G starts showing variations with modulation frequency for I_{dc} > 3 mA. This is supported by the fact that the sample temperature remains flat around 298 ± 0.1 K for I_{dc} ≤ few mA and sharply increases thereafter.

It is interesting to note the qualitative difference in frequency variation of G below (diffusion capacitance like behavior) and above (significant joule heating) the relatively dispersion free region. We must also mention that the overall span of this dispersion-less regime with respect to the forward current levels in fact varies for different types of laser diodes and LEDs.

With increase in the current a hump in both G and C has been observed near the lasing threshold for different modulation frequencies. In figure 2.6a we plot conductance (G) and capacitance (C) in the region of the lasing onset. Figure 2.6b shows the first and second derivatives of output light power (P) with respect to applied injection current I_{dc}. Since the onset of lasing increases the light output power drastically, this change can be easily visualized in the derivatives. Second derivative (d^2P/dI_{dc}^2) is exclusively used in

the calculation of lasing threshold while first derivative provides a measure of external quantum efficiency also. In figure 2.6a, lasing threshold can be clearly identified. It can be observed that both G and C deviate from their regular behavior around this threshold. This behavior can be understood in the following way:

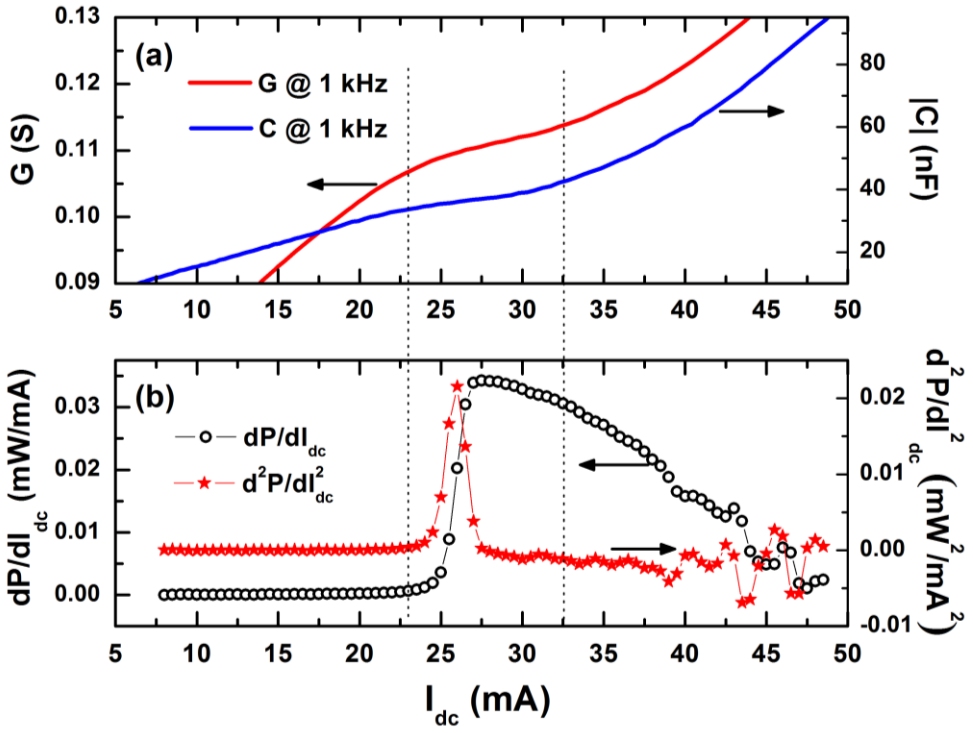

Figure 2.6: (a) Change in the conductance (G) and the capacitance (C) with the onset of lasing around 27 mA. (b)Current derivatives of light output power (P) marking the onset of lasing.

As the stimulated emission starts, the rate of radiative recombination increases[33]. However due to the pinning of quasi Fermi levels near lasing threshold[34], sufficient supply of charge carriers is obstructed. This results in a temporary saturation in G and C. With increase in injection level, a steady state supply of charge carriers is maintained. As a result, G and C also keep increasing in magnitude.

2.3.2 Correlated optical and electrical properties: role of sub-band gap defects in radiative recombination dynamics

To understand the physical mechanism of NC, we have also measured VMEL to see any effect of applied modulation frequency on light emission. Figure 2.7 shows

variation of VMEL magnitude vs I_{dc} curves (< 10 mA, as limited by the adder amplifier circuit) with different modulation frequencies.

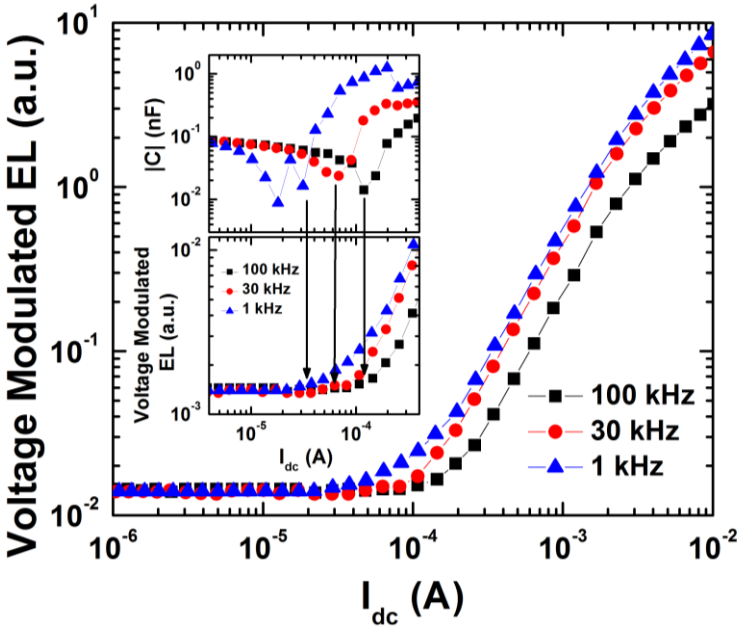

Figure 2.7: Voltage modulated electroluminescence (VMEL) as a function of applied injection level/bias for different applied modulation frequencies. As the frequency decreases, onset of the VMEL shifts to lower applied bias and its magnitude also increases. VMEL and negative capacitance (NC) follow similar frequency dependence as shown in the inset. Arrows indicate the simultaneous onsets of NC and VMEL.

This indicates: (i) signal increases with increasing bias, (ii) for lower frequency, onset of signal is at lower values of I_{dc} and (iii) signal is larger for lower values of modulation frequency. To compare NC and VMEL, we look at the zoomed in plots in the inset of figure 2.7. This indicates that *VMEL* signal also starts to increase significantly around the current bias values where C turns fully negative for a specific modulation frequency. Such low frequency response of VMEL again suggests participation of slowly responding defect states in the modulated light emission processes. Good correlation of the onset of NC with the significant rise in modulated light emission rules out the possibility of it being an artifact due to bad contacts and emphasizes on the presence of basic underlying mechanics. Moreover, the magnitude of NC does not scale with the modulation frequency like a normal inductor even for $f \sim 1$ MHz, which also rules out[5] any contribution from external parasitic inductances. Generally, any inductive like response originates when a sample builds resistance to changing current levels and the

modulated current lags behind the applied voltage. Quasi Fermi levels which track the injected minority carrier densities are influenced by both radiative recombination and contributions from sub-band gap defect states. Onset of radiative recombination irreversibly depletes minority carrier reservoirs stored on either side of the junction with increasing forward bias. This radiative consumption of minority carriers happens at a rate faster than the rate of replenishment of such carriers by injection and by carrier trapping-de-trapping processes. In this way, active participation of slowly responding sub-band gap defects can delay the dynamic response of quasi Fermi levels. If the contribution of sub-band gap states to overall density of *available* minority carriers is significant, then quasi Fermi levels cannot follow the applied modulation. Thus, steady state separation between these levels goes through a transient change over a full cycle of sinusoidal variation. These points will be elaborated in figure 2.8 (and in chapter 3) and subsequently discussed in more detail in the next few paragraphs. Such transient changes further induce a transient variation of the steady state current level, which is proportional to the spatial gradient of these quasi Fermi levels. *As a consequence, small signal reactive response of the device acquires the so called 'inductive' like component which resists any such deviations from the steady state current level.* Resultant induced voltage ultimately tries to compensate any such momentary changes in the separation of quasi Fermi levels over a cycle of applied modulation and steady state condition is regained. An increase in I_{dc} increases the number of injected minority carriers and enhances the amount of radiative recombination, it also increases the contribution from shallower defects near the band edges by shifting the quasi Fermi levels apart. This in turn requires larger 'inductive' like response to restore and maintain the steady state separation of quasi Fermi levels over a full cycle of voltage modulation. As a consequence, reactance part measured as capacitance becomes more and more negative with increasing I_{dc} as is evident in figure 2.5b.

Here, it is important to note that the conventional techniques (like deep level transient spectroscopy[28, 35], transient photo-capacitance spectroscopy[36-38] etc.) used to characterize defect states have been *developed primarily for junctions held under reverse bias* and cannot be used directly with their usual interpretations in the present case. Currently, we are working in a forward bias regime where the all-important *depletion*

approximation is not valid because of the presence of a large number of injected charge carriers near the junction. Positions of quasi Fermi levels also move towards the band edges under increasing forward bias. Thereby significantly *more participation of relatively shallow states* is possible in the capacitance/current of a forward biased junction.

To sum up, *dynamic competition between 'fast' (radiative recombination) and 'slow' (defect response) processes* can generate a compensatory negative capacitance response where modulated current will lag behind the modulating voltage like that of an inductor to negate any transient change of steady state current level. At this stage, we would like to add that any past observations[9-12] of such frequency dependence of NC in predominantly non-luminescent Silicon based structures/devices may also require the presence of mutually competing 'fast' and 'slow' non-radiative channels near the active junction. However, this has to be verified by experiments on a case by case basis and will be discussed in chapter 6.

In order to explain the variation of VMEL with current bias and modulation frequency as observed in figure 2.7, we will now try to understand the mechanism by which sub-band gap defect states contribute towards the net minority carrier density *available* for radiative recombination. For better understanding, we present figure 2.8 which depicts a schematic energy (E) level diagram illustrating the contribution of defect states to the total minority carrier (here electrons) density $n_{injected}^{Total}(E)$ available at the conduction band edge (E_C) in the active region of the device. Here we assume that the electron quasi Fermi level (E_{Fn}) may be extended in the active region to describe the population of injected minority electrons. Similar diagrams can be made for minority holes too.

As per the diagram, the total density of injected minority electrons $n_{injected}^{Total}(E)$ in the active region is the sum of free minority electron density $n_{injected}^{Free}(E)$ and the density of trapped minority electrons as

$$n_{injected}^{Total}(E) = n_{injected}^{Free}(E) + n_{injected}^{Trapped}(E) \qquad (2.1)$$

Where, $n_{injected}^{Trapped}(E) = \int_{E_C - E_{Th}}^{E_{Fn}} g(E)dE$ and g(E) is the sub-band gap defect density at an energy E below the conduction band.

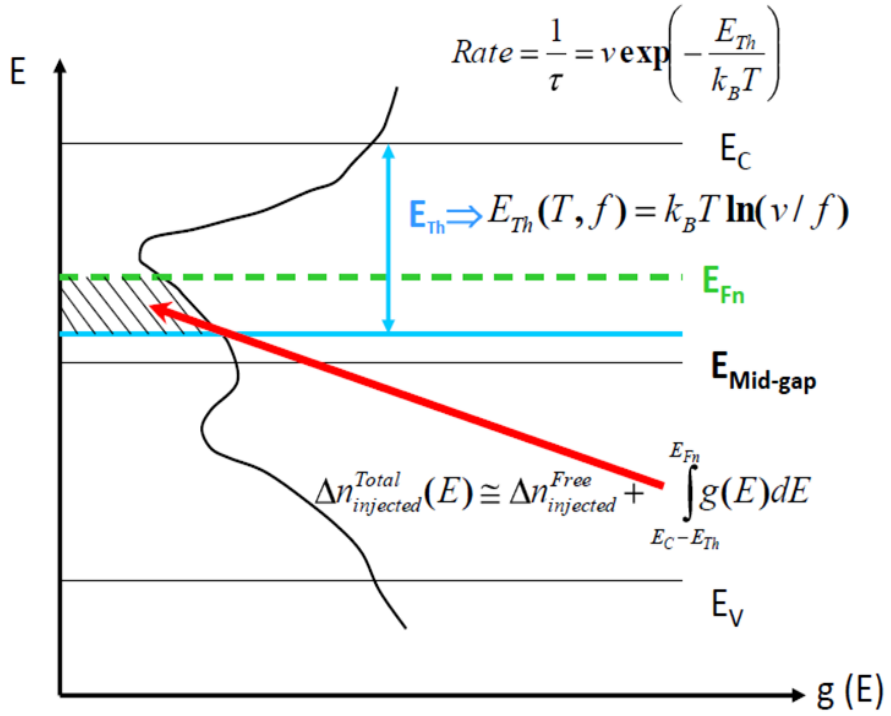

Figure 2.8: Effective band diagram to understand the contribution of sub-band gap defects to the injected minority carriers (electrons in the p-type side of the junction) available for recombination at a particular temperature and frequency. Here we have assumed that the quasi Fermi level of minority electrons (E_{Fn}) can be extended to describe the population of injected minority electrons near the active region. The shaded area represents the energy range of the sub-band gap states which are actively contributing minority carriers for band-to-band recombination. Sub-band gap states above E_{Fn} are effectively empty and states below E_{Th} cannot follow the modulation and cannot contribute to steady state minority carrier density available at the band edges. More participation of shallower states is expected at increasing forward bias.

At a particular T (in Kelvin) and f (in Hz), $n_{injected}^{Trapped}(E)$ have contributions only from sub-band gap defects which lie within E_{Fn} and E_{Th} (shaded area in figure 2.8). E_{Th} is the characteristic thermal activation energy of sub-band gap states, given by:

$$E_{Th} = k_B T \ln(\nu / f) \tag{2.2}$$

If the rate at which these states can exchange carriers with the band edge is $\sim\frac{1}{\tau}$, then equation (2.2) can be rewritten as $\frac{1}{\tau}=\nu\exp\left(-\frac{E_{Th}}{k_BT}\right)$, where τ is the characteristic time, ν is the thermal prefactor of such transitions and k_B is the Boltzmann constant. With increasing forward bias, E_{Fn} moves closer to the conduction band and the difference $\left(E_C-E_{Fn}\right)$ decreases. Depending on *T* and *f*, defects will contribute to the steady state value of band edge carrier density only if $\left(E_C-E_{Th}\right)>\left(E_C-E_{Fn}\right)$.

It is clear from equation (2.2) that sub-band gap states responding at low frequencies stay away from the band edges and satisfy the above criterion at a smaller forward bias. As a result, in figure 2.7, we see that the onsets of VMEL and negative capacitance occur at smaller forward biases for lower frequencies. With increasing E_{Th} and decreasing *f*, contribution of defect states towards $n_{injected}^{Trapped}(E)$ increases. As a result, net minority carrier density [$n_{injected}^{Total}(E)$] available for radiative recombination process also increases. Therefore, we notice in figure 2.7 that room temperature VMEL signal at a fixed forward bias is higher for lower modulation frequencies. Defect states responding at low frequency are also considerably slower in terms of their response time. That way the re-equilibration of minority carriers takes longer time and quasi Fermi level separation as well as current response lags the voltage modulation by a bigger margin. This in turn requires stronger inductive like response to maintain the steady state. As a result, observed negative capacitance is more negative for lower frequencies (figure 2.7) at a particular I_{dc}. When I_{dc} is increased at a fixed modulation frequency, radiative recombination increases which ultimately causes the negative capacitance effect to increase as well.

Strong dependence of radiative recombination on steady state contribution of minority carriers from sub-band gap states may also signify that radiative and non-radiative recombinations of these minority carriers are no longer mutually exclusive events. Subsequently this may also imply that $\frac{1}{\tau_{Effective}}\neq\frac{1}{\tau_{radiative}}+\frac{1}{\tau_{Non-radiative}}$, where

$\tau_{effective}$ represents the effective time scale of modulated electroluminescence. Here the equality sign applies only in case of non-interconnected probabilistic processes assuming a particular minority carrier cannot take part in both radiative and non-radiative processes which is not strictly true under the current circumstances. Moreover, any major contribution of $n_{injected}^{Trapped}(E)$ towards the total density of minority carriers (equation (2.1)) available for radiative recombination can have significant impact on the efficiency of any electroluminescent device. Minority carriers trapped by existing deep defects will not respond at high frequency (~GHz) and will be *missing in action* from the final radiative recombination processes as per equation (2.1) and figure 2.8. This can effectively suppress the amount of minority carriers accessible for radiative recombination, thereby reducing the overall light intensity. Therefore, these slower processes can, in principle, compromise the efficiency of these light emitting devices during high frequency applications like optical communications.

2.3.3 Spectral properties of modulated light emission

In figure 2.9a, we plot the in-phase VMEL spectra at different current injection levels for a fixed f = 10 kHz. For comparison, continuous wave (CW) light emission spectra of LD at different I_{dc} are shown in figure 2.9b. Expected increase in the light emission intensity with increasing I_{dc} can easily be noticed. We also notice that VMEL signal level increases at higher forward biases as expected.

It has been reported[39, 40] earlier that it is necessary to consider the modulation frequency dependence of only the in-phase component of the modulated photoreflectance signal to appreciate the detailed role of sub-band gap defects in the context of modulation spectroscopy. However, it is not necessary that the theoretical analyses widely used for modulated reflectance spectra of a reverse biased junction depleted of free carriers will also be valid for modulated electroluminescence spectra of a device experiencing strong radiative recombinations of injected minority carriers under large forward bias. In this case, shape of the measured VMEL spectra resembles the first derivative line shapes of modulated reflectance spectroscopy where the external modulation does not significantly perturb the translational invariance[41] of the solid. It seems that the voltage modulation

also does not change the electric field of the forward biased junction enough, either to cause any field induced acceleration of the charge carriers or to modulate the energy level structure in the active region.

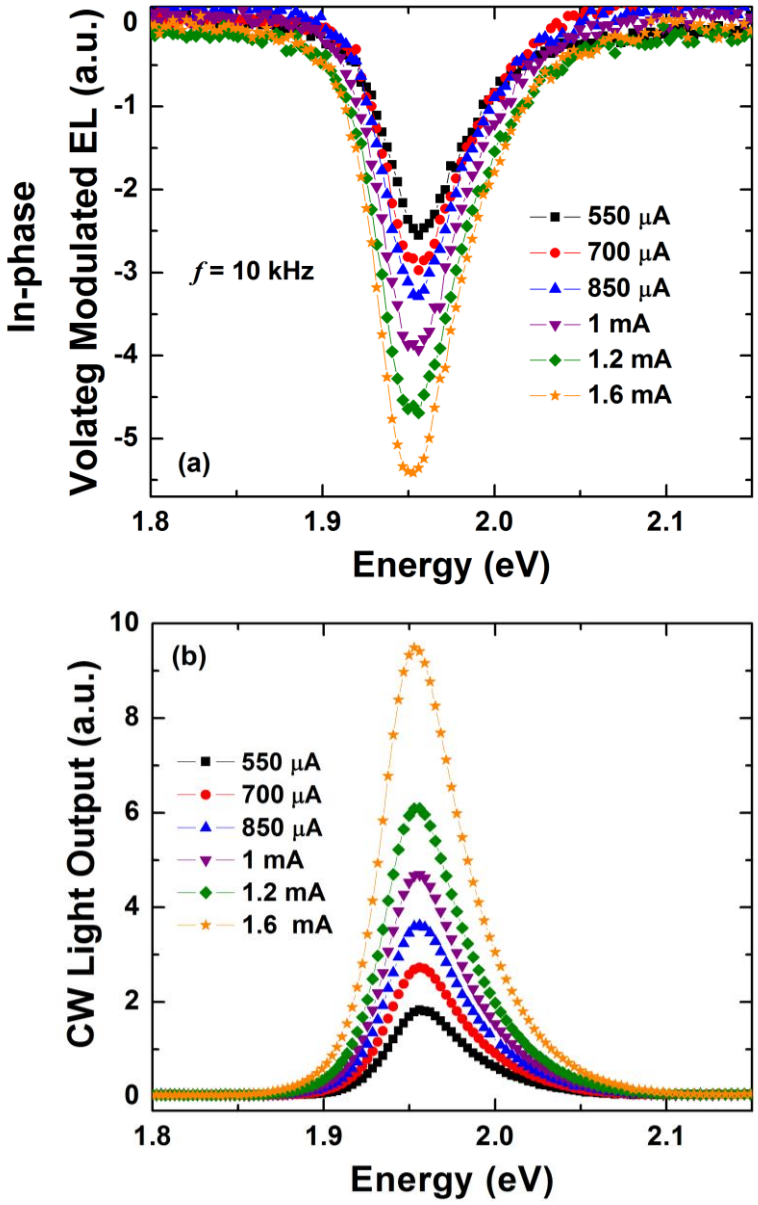

Figure 2.9: (a) In-phase VMEL spectra at different forward bias currents below the lasing threshold. The in-phase VMEL signal progressively gains a distinct negative component near its peak for all bias levels shown in the figure. This is a manifestation of bi-molecular recombination rate as discussed in the text. Current VMEL measurements are limited by the adder amplifier circuit to < 10mA. (b) The usual CW electroluminescence spectra from DL 3148-025 red laser diode below the lasing threshold for comparison.

From these spectral line shapes, it can be concluded that there is no effect of modulation on lattice periodicity which could have resulted in much more complicated spectral line shapes[41]. Instead, most of the voltage modulation related effects come from changes in the minority carrier density. We can write the net rate of recombination when the system is driven away from the steady state as:

$$R_{Net} = \frac{(n+\Delta n)(p+\Delta p)}{np} R_{Steady} \approx R_{Steady} + \Delta R \tag{2.3}$$

where n, p are steady state densities of injected minority electrons and minority holes respectively, R_{Steady} is the generic van Roosbroeck-Schokley type recombination rate for electroluminescence in the steady state and ΔR is the deviation of radiative recombination rate from the steady state. After neglecting small second order terms, it can be shown (following chapter 6 of reference 27) that:

$$\frac{\Delta R}{R_{Steady}} \approx \frac{\Delta n}{n} + \frac{\Delta p}{p} \tag{2.4}$$

Assuming $\Delta n = \Delta p = \Delta c$, one can arrive at:

$$\Delta R \sim \Delta c \tag{2.5}$$

where Δc is the excess minority carrier density along with a proportionality constant consisting of only steady state parameters. Therefore, any increase/decrease in minority carrier density (Δc) following the voltage modulation (ΔV) can proportionately modulate the radiative recombination as well as the resultant electroluminescence intensity. In figure 2.8 this can be viewed as a modulation in the shaded area between E_{Fn} and E_{Th}, through quasi Fermi levels modulation, affecting the amount of minority carriers available for recombination. Hence, these types of modulated changes in VMEL are due only to modulation of the pumping levels as illustrated in figure 2.10a. Here we are assuming that there is no significant pinning of quasi Fermi levels for both types of minority carriers in this smaller range of applied injection current.

Moreover, it is evident from figure 2.5b that reactive response at a particular modulation frequency is affected strongly by the change in the net injection level.

Therefore, it will not be wrong to assume that voltage modulation induced perturbation of minority carrier density not only modulates the radiative recombination but also concurrently varies the dielectric response of the diode. We also note that the measured in-phase VMEL signal (figure 2.9a) becomes increasingly negative as the spectral scan goes through its peak. We have earlier pointed out the connection between the onset of VMEL signal with the onset of NC at a particular modulation frequency (figure 2.7), whereas, any such connection between the measured conductance data (figure 2.5a) and onset of VMEL signal is not very apparent.

Since the steady state reactive response of minority electrons (n) and minority holes (p) depends on respective densities, therefore, VMEL signal is directly proportional to the steady state reactive response of both, minority electrons and minority holes, as VMEL ~ R ~ np. We know that the time varying current through a reactive component is always out-of-phase with the small signal voltage modulation. Therefore, prevailing reactive contributions at high forward biases for both minority electrons $\left(n \sim e^{\frac{i\pi}{2}} \right)$ and minority holes $\left(p \sim e^{\frac{i\pi}{2}} \right)$ combined together can produce the overall negative factor $\left[VMEL \sim R \sim np \sim e^{\frac{i\pi}{2}} \times \sim e^{\frac{i\pi}{2}} \cong e^{i\pi} = -1 \right]$ of the in-phase VMEL signal. This characteristic negative sign of the in-phase VMEL is, therefore, a testimony to the bi-molecular recombination process involving both electrons and holes.

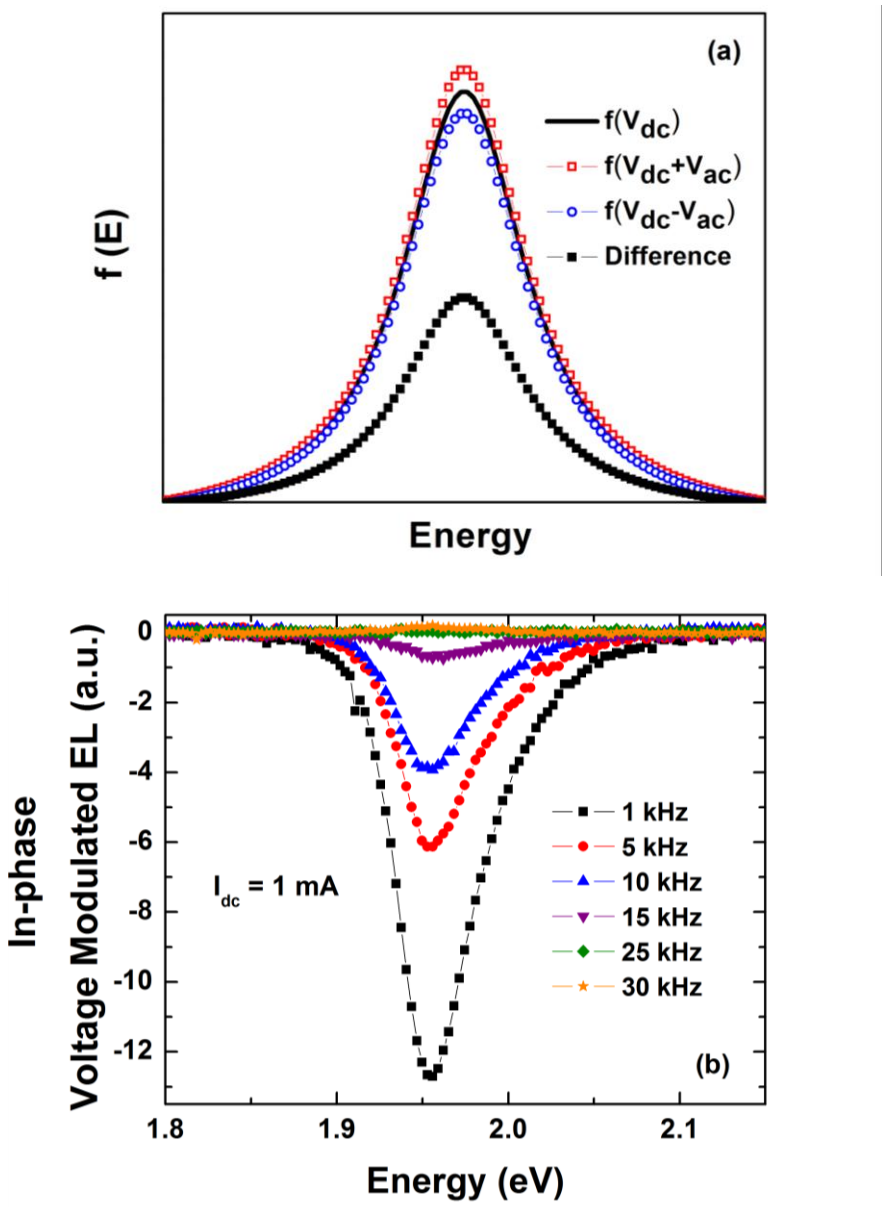

Figure 2.10: (a) Schematic of CW spectrum presenting optical transitions (solid line) as a function of energy (f(E)) *and effect of modulation on pumping levels (Δn and Δp) by small signal voltage modulation (empty symbols). Absolute difference between modulated and un-modulated functions (solid symbol) which resembles measured spectral lines verifying that the applied voltage modulation only affects the charge carrier density. (b) Variation of in-phase VMEL spectra with modulation frequency. Lower frequencies produce cumulatively larger VMEL signal as explained by figure 2.8.*

In figure 2.10b, we plot the VMEL (in-phase) spectra for different modulation frequencies at a fixed forward current bias (I_{dc}) of 1 mA. Here we see the increase in VMEL signal level with decreasing modulation frequency as also explained in connection

with figure 2.7. Strong dependence of VMEL on modulation frequency is a clear sign of the active presence of defect states in modulating the total injected minority carrier density at the band edges inside the active region and consequently affecting their radiative recombination.

2.4 Conclusions

We have studied the low frequency impedance response from quantum well based electroluminescent diodes under charge carrier injection. We observed a prominent negative capacitance (NC) for high applied biases and low modulation frequencies. We perceive it as a result of significant contribution of sub-band gap defect states in the active region towards the overall radiative recombination process. Simultaneous onset and similar dependence of negative capacitance and voltage modulated electroluminescence on low modulation frequencies also confirms the participation of sub-band gap states in the minority carrier dynamics even at low injection levels. We can relate the onset of negative capacitance with the presence of 'inductive' like response necessary to compensate any transient effect arising out of a *dynamic competition between the fast radiative recombination pathways and the slowly responding electronic defects*. Device designs should minimize any considerable contribution from such slower carrier trapping-de-trapping processes towards the overall density of minority carriers *available* for radiative recombination. Only then can we expect a noteworthy enhancement in the intensity of emitted light when device is directly modulated at very high frequencies (~GHz) useful for applications like optical communication. A qualitatively similar consideration may also apply for high frequency applications of Silicon based devices. Behavior of in-phase VMEL signal connects the dielectric properties of the junction with the bimolecular nature of light emission in electroluminescent devices.

Studies on time evolution of current transients and temperature dependence of VMEL are required to develop more understanding of the role of sub-band gap states in modulated electroluminescence spectra and will be presented in the following chapters.

However, to obtain the quantitative estimates and to comment on the nature of electronic defects a detailed knowledge of device structure is required.

A major part of the work presented in this chapter has been published in Journal of Applied Physics, Vol. 110, p. 114509, 2011 and Physica Status Solidi C, Vol. 10, p. 593, 2013.

2.5 References

[1] S. M. Sze and K. K. Ng, *Physics of Semiconductor Devices* (Wiley-Interscience, 3rd Edition, 2006).

[2] M. Shur, *Physics of Semiconductor Devices* (Prentice Hall-India, 1st Edition, 1995).

[3] A. K. Jonscher, J. Chem. Soc., *Faraday Trans. 2*, **82**, 75 (1986).

[4] M. Ershov, H. C. Liu, L. Li, M. Buchanan, Z. R. Wasilewski, and A. K. Jonscher, *IEEE Trans. Electron. Devices*, **45**, 2196 (1998).

[5] X. Wu, E. S. Yang and H. L. Evans, *J. Appl. Phys*. **68**, 2845 (1990).

[6] J. Werner, A. F. J. Levi, R. T. Tung, M. Anzlowar and M. Pinto, *Phys. Rev. Lett*. **60**, 53 (1988).

[7] I. Mora-Sero´, J. Bisquert, F. Fabregat-Santiago, G. Garcia-Belmonte, G. Zoppi, K. Durose, Y. Proskuryakov et al. *Nano Lett*. **6**, 640 (2006).

[8] J. Bisquert, *Phys. Chem. Chem. Phys.* **13**, 4679 (2011).

[9] R. Tadros-Morgane, G. Vizdrik, B. Martin, and H. Kliem, *J. Appl. Phys.* **109**, 014501 (2011).

[10] C. D. Wang, C. Y. Zhu, G. Y. Zhang, J. Shen, and L. Li, *IEEE Trans. Electron Devices* **50**, 1145 (2003).

[11] Ş. Altındal and H. Uslu, *J. Appl. Phys.* **109**, 074503 (2011).

[12] I.S. Yahia , G.B. Sakr , S.S. Shenouda , M. Fadel, S.S. Fouad and F. Yakuphanoglu, *Appl. Phys. A* **112**, 275 (2013).

[13] F. Lemmi and N. M. Johnson, *Appl. Phys. Lett*. **74**, 251 (1999).

[14] V. Kytin, Th. Dittrich, F. Koch and E. Lebedev, *Appl. Phys. Lett.* **79**, 108 (2001).

[15] Y. Li, C. D. Wang, L. F. Feng, C. Y. Zhu, H. X. Cong, D. Li, and G. Y. Zhang, *Appl. Phys. Lett.* **101**, 233506 (2012).

[16] L. E. Byrum, G. Ariyawansa, R. C. Jayasinghe, N. Dietz, A. G. U. Perera,S. G. Matsik, I. T. Ferguson, A. Bezinger, and H. C. Liu, *J. Appl. Phys.* **106**, 053701 (2009).

[17] L. F. Feng, Y. Li, C. Y. Zhu, H. X. Cong, and C. D. Wang, *IEEE J. Quantum Electron.*. **46**, 1072 (2010).

[18] Y. Li, C. D. Wang, L. F. Feng, C. T. Zhu, H. X. Cong, D. Li, G. Y. Zhang, *J. Appl. Phys.* **109**, 124506 (2011).

[19] J. Bisquert, G. Garcia-Belmonte, A´. Pitarch, H. J. Bolink, *Chem. Phys. Lett.* **422**, 184 (2006).

[20] L. F. Feng, D. Li, C. Y. Zhu, C. D. Wang, H. X. Cong, X. S. Xie and C. Z. Lu, *J. Appl. Phys.* **102**, 063102 (2007).

[21] N. A. Poklonski, S. V. Shpakovski, N. I. Gorbachuk and S. B. Lastovskii, *Semiconductors,* **40**, 803 (2006).

[22] C.Y. Zhu, L. F. Feng, C. D. Wang, H. X. Cong, G. Y. Zhang, Z. J. Yang and Z. Z. Chen, *Solid-State Electron*. **53**, 324 (2009).

[23] T. Azuhata, T. Homma, Y. Ishikawa, S. F. Chichibu, T. Sota, and T. Mukai, *Appl. Phys. Lett.* **79**, 1100 (2001).

[24] H. H. P. Gommans, M. Kemerink, and R. A. J. Janssen, *Phys. Rev. B* **72**, 235204 (2005).

[25] S. E. Laux and K. Hess, *IEEE Trans. Electron. Device* **46**, 396 (1999).

[26] P. Bhattacharya, *Semiconductor Optoelectronic Devices* (Prentice-Hall, Inc., Englewood Cliffs, New Jersey., U.S.A, 1994).

[27] J. I. Pankove, *Optical Processes in Semiconductors* (Prentice-Hall, Inc., Englewood Cliffs, New Jersey, U.S.A, 1971).

[28] D. K. Schroder, *Semiconductor Material and Device Characterization* (John Wiley & Sons, Inc. 3rd Edition, 2006).

[29] J. Shah, R. F. Leheny, R. E. Nahory, and H. Temkin, *Appl. Phys. Lett.* **39**, 618 (1981).

[30] M. Yamanishi, I Suemune, K. Nonomura and N. Mikoshiba, *Jpn. J. Appl. Phys.* **21**, L240 (1982)

[31] D. C. Tripathi and Y. N. Mohapatra, *Appl. Phys. Lett.* **102**, 253303 (2013).

[32] G. L. Miller, D. V. Lang, and L. C. Kimerling, *Ann. Rev. Mater. Sci*. **7**, 377 (1977).

[33] D. Li, W. Yang, L. Feng, P. W. Roth, J. He, W. Du, Z. Yang, C. Wang, G. Zhang and X. Hu, *Appl. Phys. Lett.* **102**, 123501 (2013).

[34] T. Paoli and P. Barnes, *Appl. Phys. Lett.* **28**, 714 (1976).

[35] D. V. Lang, *J. Appl. Phys*. **45**, 3023 (1974).

[36] S. Datta, J. D. Cohen, Y. Xu, A. H. Mahan and H. M. Branz, *J. Non-Cryst. Solids* **354**, 2126 (2008).

[37] A. V. Gelatos, K.K. Mahavadi, J. D. Cohen and J. P. Harbison, *Appl. Phys. Lett.* **53**, 403 (1988).

[38] J. D. Cohen and A. V. Gelatos, in: Hellmut Fritzsche (Ed.), *Amorphous Silicon and Related Materials, vol. A* (Worlds Scientific, Singapore, 1989) p. 475.

[39] H. Shen, F. H. Pollak, J. M. Woodall and R. N. Sacks, *J. electron. Mater.* **19**, 283 (1990).

[40] F. H. Pollak and H. Shen, *Mat. Sci. Engg.* R **10**, 275 (1993).

[41] D. E. Aspnes, *Surf. Sci*. **37**, 418 (1973). Figure 1a.

Chapter 3

Negative Capacitance Effect and the Evolution of Transient Current under Charge Carrier Injection

3.1 Introduction

We have observed a non-trivial negative capacitance (NC) response under high carrier injection in case of light emitting structures along with a correlated frequency dependent modulated light emission. We explained NC and its correlation with optical properties as an outcome of the defect participation (slow process) in radiative recombination (fast process) and their mutual competition for the consumption of available charge carriers. Negative capacitance behavior has generally been reported in many different types of diodes with different functionalities[1] under the condition of high charge carrier injection. It is true that the NC effect carries special importance in the context of diodes which are meant to be operated under carrier injection, like electroluminescent diodes (ELDs), but to better understand NC in general, its occurrences in all different type of structures should be considered.

Generally, NC is observed for high injection levels and is more prominent for lower modulation frequencies. It arises due to the presence of a non-equilibrium like situation as compared to the steady state reverse biased behavior of a diode[2, 3]. A non-equilibrium like situation is also desirable to accept NC intuitively as a 'decrease in stored charge (q) with increasing voltage' (C=dq/dV).

3.1.1 A general consideration of negative capacitance (NC)

In chapter 2 we briefly discussed the description of NC given in the literature especially for electroluminescent diodes (ELD). However, generally in the context of junction diodes, explanations for NC are as many as the number of devices based on them. Occurrence of negative capacitance was observed a long time ago (1955) in Silicon and Germanium diodes under forward bias[4]. It was realized that the diode characteristics deviate from Shockley theory[5] under significant charge injection. However, this phenomenon was overlooked initially considering it to be an outcome of the bad contact or parasitic effects[6]. NC was also observed in semiconductor chalcogenides thin films with temperature increase accompanying the dielectric phase change from resistive to conducting state[7-11]. In these disordered materials, NC was explained to be caused due to the charge redistribution of low mobility carriers lagging behind the applied ac signal. Successively, NC in Shottky diodes or metal insulator junction of different materials[12-16] was studied to gain a physical insight of the phenomenon. Due to the presence of NC under charge carrier injection or a more conducting state, NC was believed to be an outcome of conductivity modulation due to minority charge injection in the bulk[17-20]. NC was also understood under plasma like treatment[21, 22] of quantum confined charge carriers due to the presence of some process like tunneling other than recombination. A systematic dependence of NC on frequency led to the belief that it is due to the effect of trap states on charge carrier dynamics[1, 12, 23-28]. NC has also been correlated with the presence of trap states in polymer-nanocrystal composites[29] and diodes made of organic semiconductors[30-32] (having lower carrier mobility). NC has also been studied in case of quantum confined structures like quantum wells[33, 34] and quantum dots[35-37]. With these studies, negative capacitance phenomenon, in the context of junction diodes, has come out of its perception of being an artifact or experimental errors, however, its various explanations do not seem to converge on a common description at first. On the other hand, reported traits (high injection and low frequency) of NC remain similar in different devices. There have been some theoretical as well as experimental studies coming up with a relatively generalized description or signatures of NC[38-44]. Jonscher et al.[38, 39] have developed a generalized model for describing NC through the description of current transients. Jones et al.[40] suggested that in case of Shottky structures or highly resistive

samples, NC is due to the relaxation like behavior where dielectric relaxation time is more than the recombination life time. Laux and Hess[41] have used a modified approach to calculate the junction capacitance by considering all the components of junction currents along with the revised boundary conditions. Their analysis includes the presence of a recombination center and can qualitatively describe the presence of NC. Different current components included by them can be ascribed to different physical phenomena in different material or device systems based on semiconductor junction. Gommans et al.[42] have suggested that NC observed in low mobility solids can be described by solving time dependent drift-diffusion equations for bipolar transport in metal-insulator-metal configuration. They found junction capacitance to be highly sensitive for recombination rates. Shulman et al.[43] suggested that NC in fluids can appear when dc-ac signals are superimposed (like injection situation created by dc bias), I-V characteristics are super-linear and relaxation process has nonlinearities.

All of these studies directly or indirectly emphasize on the presence of different competing processes to be at the root of the causing negative capacitance phenomenon and agree with the generalized description of NC we have proposed[1, 45] and discussed in chapter 2.

Recently (between 2011 and 2013)[27, 46-48], some more efforts have been made to understand the physical mechanism of NC and correlate it with different device parameters related to the dynamics of charge carriers. For example, Feng et al.[47] have used frequency and bias dependence of NC to calculate recombination life time of charge carriers for InGaN based didoes; Anutgan and Atilgan[27] have used forward bias capacitance to estimate the energy distribution of the density of states for the sub-band gap states in hydrogenated amorphous Silicon based p-i-n diodes. Presence of NC has been used to qualitatively comment on the device performance in case of solar cells[49, 50]. It has been understood as an effect of addition recombination pathway reducing charge accumulation capacity of the cell. Studies with wider material and device ranges are required along with rigorous verification of results using other techniques; only then can these proposed techniques be established which are claimed to be easy and

straightforward. Definitely, this would require some more attention in the field of probing a junction diode under charge carrier injection.

Moreover, as we suggested and has been pointed out by others as well, one can use negative capacitance effect in different applications. For example, as we argued[1, 45] low frequency negative capacitance reflects the participation of sub-band gap defects in charge carrier recombination in case of ELDs. This qualitatively suggests that some of the charge carriers are being captured by these slowly responding states which would totally be missing in action if diode is modulated directly at very high frequency (~ GHz), used in applications like optical communication. Keeping in mind that the application of ELDs in optical communication covers a large part of their total application chart, negative capacitance based characterization techniques can provide a quick and economical way of characterizing and improving the efficiency of ELDs for such applications. To mention a few more, it had been proposed by Salahuddin and Datta[51] that use of ferroelectric insulator in field effect transistors can produce effective negative capacitance effect under specific parameter conditions (due to decreasing polarization with increasing electric field). This can be utilized to lower the switching voltage and hence power consumption, effectively reducing the heat production in an integrated system[51, 52]. Recently, this concept has been demonstrated experimentally[53]. Also, NC has been predicted to be used to increase the tunneling range of a varactor diode[54] in monolithic-microwave integrated circuits.

Clearly a comprehensive and generalized understanding of NC and related phenomena is required not only to gain better knowledge of device physics but also can be exploited in various applications. In this chapter we will discuss how the occurrence of NC can be visualized theoretically in a very general manner along with the physical mechanism. We will consider the admittance change of a diode, in general, in response to a small voltage step[39]. We will calculate the admittance under this perturbation by using the Fourier transformation of time varying current under the application of a voltage step. We will identify the connection of frequency dependent capacitance with the nature of relaxation transient current after the small voltage perturbation. We will explain that the different behavior or shapes of the current transient can be used to

explain both, negative and positive capacitance behavior. A monotonically increasing or non-monotonic transient describes NC, while for positive capacitance regime, transient remains monotonically decreasing[39]. The analysis presented here remains valid for different junction based devices with different functionalities involving different physical phenomena. We will also support the theoretical analysis by measuring the current transients of ELD during the application of a small voltage pulse, in different ranges of applied bias. We will point out the drastic change in the shape of current transient marking the crossover between positive capacitance and negative capacitance behavior. We will also discuss how the qualitative understanding of NC developed by us[1] based on mutual competition of fast and slow processes (chapter 2) fits into the theoretical picture of NC based on the behavior of current transients.

3.2 Diode admittance under small forward bias voltage step

To develop the analytical understanding of NC, we consider the junction diode as a two terminal device, consisting of a Capacitance (C) and conductance (G) in parallel (as described in chapter 2 section 2.2.2). Capacitance and conductance of the device can be defined as:

$$C(\omega) = \frac{1}{\omega}\,\mathrm{Im}[Y(\omega)] \tag{3.1a}$$

and

$$G(\omega) = \mathrm{Re}[Y(\omega)] \tag{3.1b}$$

where $\omega=2\pi f$ and $Y(\omega)$ is the device admittance given by:

$$Y(\omega) = \frac{\delta I(\omega)}{\delta V(\omega)} \tag{3.2}$$

δI is the small signal current in the device after the application of small voltage δV.

We will use the Fourier analysis method to calculate C and G by looking at the transient behavior of the device after the application of small, time dependent voltage excitation at *t=0*.

Under the application of a step voltage, such that:

$$\delta V(t) = \Delta V \theta(t) \tag{3.3}$$

where $\theta(t)$ is the unitary step function, current in response can be written as:

$$\delta I(t) = I(t) - \lim_{\tau \to 0} I(\tau) \tag{3.4}$$

This current involves both transient component and a step like component. If $I[\infty]$ represents current at a much later time (as $t \to \infty$) then the current $\delta I(t)$ can be written as:

$$\delta I(t) = [I(t) - I(\infty)]\theta(t) + [I(\infty) - \lim_{\tau \to 0} I(\tau)]\theta(t) \tag{3.5}$$

First term in equation (3.5) represents transient current (say $\delta J(t)$) which vanishes as $t \to \infty$.

To calculate Y using equation (3.2), we take Fourier transformed components of equation (3.3) and (3.5):

$$Y(\omega) = \frac{\int_{-\infty}^{\infty} \delta I(t) e^{-i\omega t} dt}{\Delta V \int_{-\infty}^{\infty} \theta(t) e^{-i\omega t} dt} \tag{3.6}$$

We assume here that ΔV is small enough to cause any nonlinearity in transient behavior and can be taken out of the integral. For practical purposes, it should be just enough to clearly visualize the effect of perturbation.

Now, considering $X = \int_{-\infty}^{\infty} \theta(t) e^{-i\omega t} dt$ and performing integration by parts:

$$X = -\theta(t) \frac{e^{-i\omega t}}{i\omega}\Bigg|_{-\infty}^{\infty} - \int_{-\infty}^{\infty} \frac{d\theta(t)}{dt} \left(-\frac{e^{-i\omega t}}{i\omega} \right) dt \tag{3.7}$$

Since $\theta(t)$ is a unitary step function, first term in the above integral will vanish and second term will survive only for $t=0$ with $d\theta(t)/dt=1$. Hence,

$$X = \frac{1}{i\omega} \tag{3.8}$$

now we will use this value of X in equation (3.6) and will also take into account that perturbation exists only after $t=0$

$$Y(\omega) = i\omega \int_0^\infty \delta I(t) e^{-i\omega t} dt \tag{3.9}$$

using $e^{-i\omega t} = \cos \omega t - i \sin \omega t$ and then separating real and imaginary parts:

$$C(\omega) = \frac{1}{\Delta V} \int_0^\infty \delta J(t) \cos \omega t dt \tag{3.10}$$

$$G(\omega) = \frac{I(\infty) - \lim_{\tau \to 0} I(\tau)}{\Delta V} + \frac{\omega}{\Delta V} \int_0^\infty \delta J(t) \sin \omega t dt \tag{3.11}$$

where $\delta J(t)$ is the transient current as given by the first term in equation (3.5). This transient current is composed of an impulse like component and a relaxation component ($\delta j(t)$):

$$\delta J(t) = \delta j(t) + \delta j'(t) \tag{3.12}$$

where intuitively $\delta j'(t) = C_0 \Delta V \delta(t)$, $\delta(t)$ being delta function to describe the step like behavior and C_0 is the geometric capacitance. Using this in equation (2.10),

$$C(\omega) = C_0 + \frac{1}{\Delta V} \int_0^\infty \delta j(t) \cos \omega t dt \tag{3.13}$$

integrating by parts:

$$C(\omega) = C_0 + \frac{1}{\Delta V} \left[\delta j(t) \frac{\sin \omega t}{\omega} \Big|_0^\infty - \int_0^\infty \frac{d\delta j(t)}{dt} \left(\frac{\sin \omega t}{\omega} \right) dt \right] \tag{3.14}$$

since $\delta j(t) \to 0$ as $t \to \infty$,

$$C(\omega) = C_0 + \frac{1}{\omega \Delta V} \int_0^{\infty} \left(- \frac{d\delta j(t)}{dt} \right) \sin \omega t dt \tag{3.15}$$

It is clear from equation (3.15) that the ultimate value of C(ω) will depend on the second term in equation (3.15) which is governed by the transient current itself. Depending upon the time variation of the transient current, integral value can be positive or negative leading to an effective positive or negative value of capacitance respectively. If transient is positive valued and monotonically decreasing to zero, the integral will give positive values and resultant capacitance will be positive. If transient is positive valued and increasing or non-monotonic such that its negative time derivative is negative valued approaching zero then the integral will give negative values. In that case, total capacitance will be negative in frequency ranges which generate a higher magnitude of negative second term than C_0. Qualitatively, a positive and increasing current transient or effectively increasing transient (with non-linear behavior) will lead to an effective negative capacitance value, while a decreasing transient will signify positive capacitance. In coming sections we will focus on experimental observation of how the different shapes of current transients can represent different regimes of capacitance and their physical origin.

3.3 Experimental methods

In addition to the sample details and instrumentation discussed in the chapter 2 (section 2.2) for transient current measurements, SR850 lock-in amplifier from Stanford Research Systems and AFG 3022B function generator from Tektronix were used for dc biasing and voltage pulsing respectively. Resultant transient currents were recorded using SR570 current pre-amplifier from Stanford Research Systems and DPO 4034 digital oscilloscope from Tektronix. Figure 3.1 shows a schematic of the measurement setup used. To measure transient current response, a 50 mV forward bias voltage pulse was applied while maintaining a particular level of injection or dc bias.

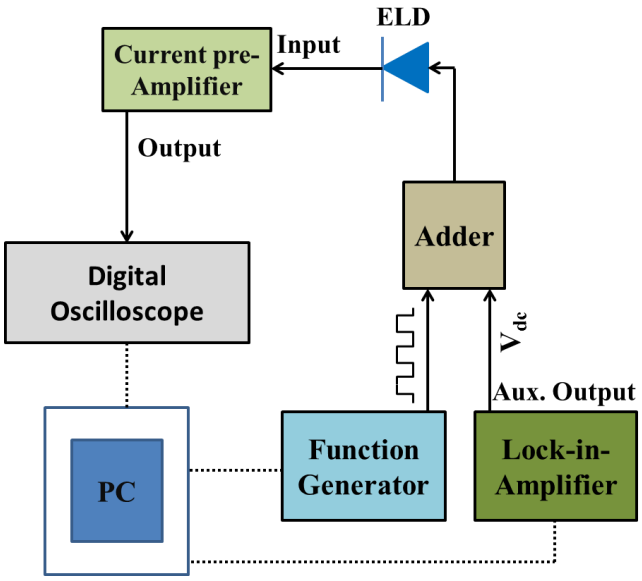

Figure 3.1: Schematic of the current transient measurement setup.

3.4 Results and discussion

Figure 3.2 shows the variation of negative capacitance and voltage modulated electroluminescence with applied modulated frequency. We can observe a continuous increase in both as the frequency decreases. This remarkable connection between optical and electrical techniques can be exploited to understand the physics of an active light emitting device. In the context of negative capacitance, which was at one point considered to be a parasitic effect or problem of improper contacts, this physical connection rules out any such possibility. Besides this connection, dominance of negative capacitance effect on lower frequencies also suggests that it is not like a pure inductor which should have dominance at higher ranges of the frequencies. As discussed in section 3.2, we would like to elaborate on the time domain behavior of this frequency dependent response and attempt to understand it better.

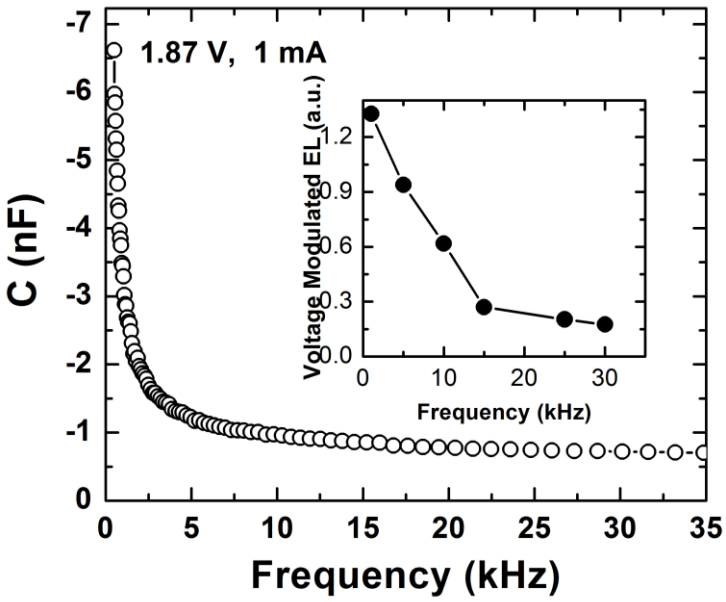

Figure3.2: Variation of negative capacitance and voltage modulated electroluminescence (inset) with applied modulation frequencies. We observe continuous increase in both the quantities as the applied frequencies decrease.

3.4.1 Transient current under small forward bias voltage step

Figure 3.3a shows the capacitance response of the diode DL 3148-025 for varying bias level (V_{dc}) for modulation frequency of 10 kHz. We observe that as the bias increases, capacitance acquires inductive like behavior and shows negative values. After approximately 1.7 V, we observe a prominent negative capacitance behavior.

In figure 3.3b, we are showing current transients after a small voltage step while maintaining particular injection levels. We applied a voltage pulse as also shown in the plot (black line). We used 10 kHz square wave pulse with 20% duty cycle. Amplitude of the pulse was kept at 50 mV to ensure that it provides only required perturbation to the system without producing any undesirable non-linear effect as assumed in the calculation (section 3.2). We observed the behavior of current transients during the application of this pulse. As we increase the bias we observe a change in the current transient behavior. In the regime where NC is observed (~ 1.7 V) transient becomes monotonically increasing (marked as inductive in the figure). For a positive capacitance regime transient remains monotonically decreasing after a sudden jump due to the change in applied electric field.

We also observe nonlinearity in current transient, before acquiring monotonically increasing nature, as the system approaches negative capacitance regime.

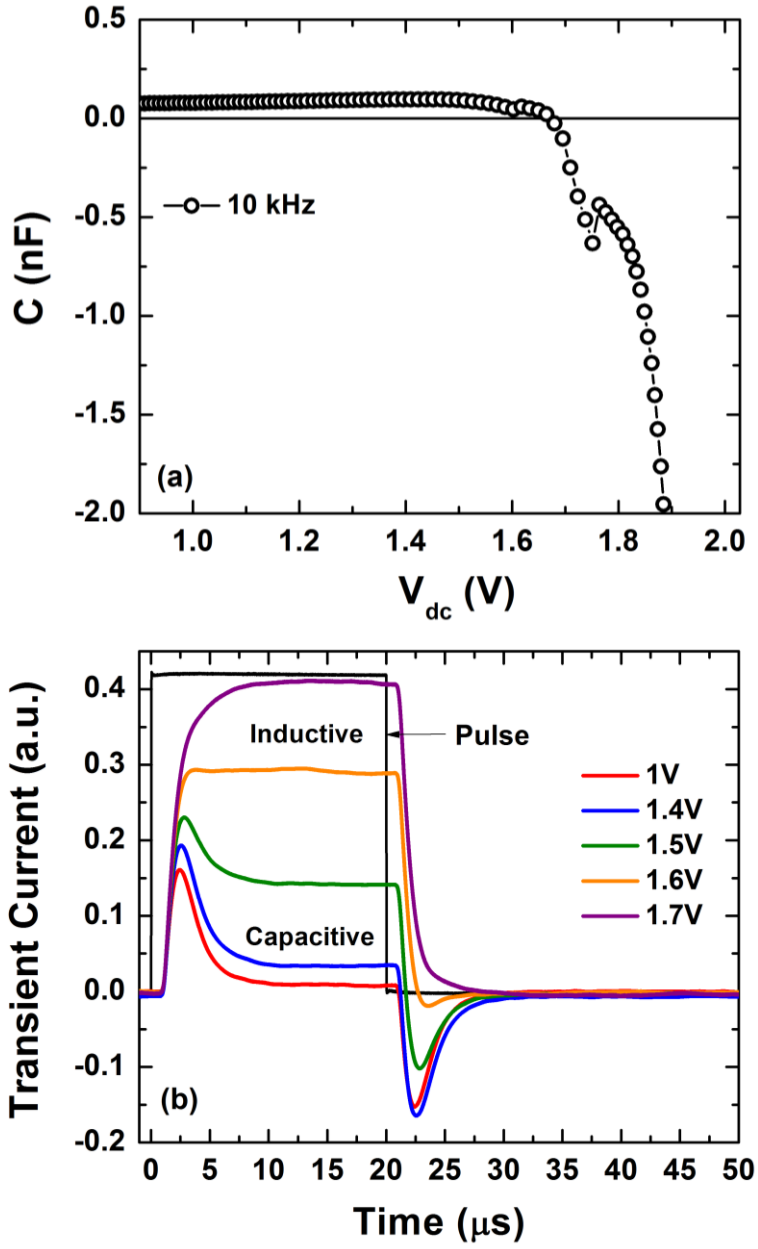

Figure 3.3: (a) Capacitance of DL 3148-025 measured at 10 kHz, shows prominent NC effect above 1.7 V. (b) Current transient after the application of voltage pulse (50 mV, 10kHz with 20% duty cycle, also shown in the plot) for different injection levels. As the NC effect starts to dominate transient approaches monotonically increasing behavior (shown as inductive). However, for positive capacitance regime it remains monotonically decreasing.

To have a better correlation of measured current transients with the theoretical expression, we further present figure 3.4. We present the current transient for 1.8 V where NC effect is prominent. We observe a smooth, monotonically increasing transient. In the inset of figure 3.4 we show (a) ($-d\delta j(t)/dt$) calculated for the measured current transient which is negative and monotonically increasing to zero, (b) simulated sinusoidal signal and (c) the final product $[(-d\delta j(t)/dt)\times \sin \omega t]$. It is very easy to observe in the inset (c) now that the negative half of the resultant periodic variation is significantly larger in this case. This leads to the negative contribution from the second term in the equation (3.15) and implies the presence of NC for wide range of frequencies.

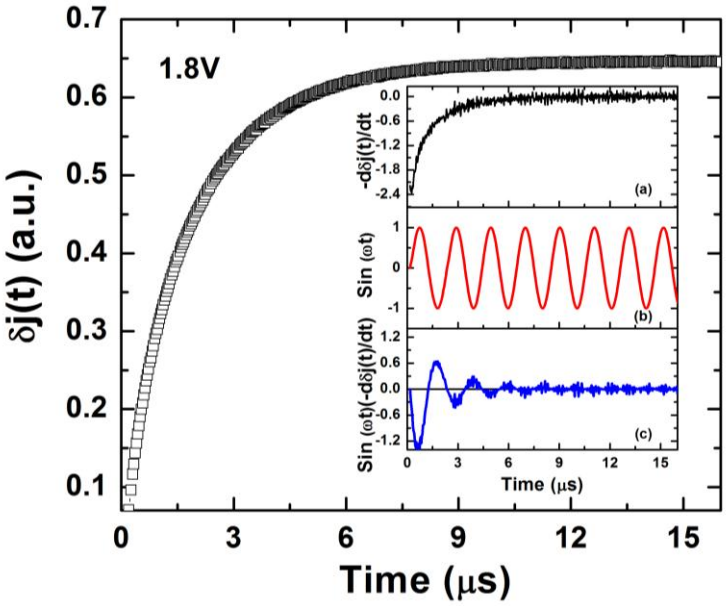

Figure 3.4: Evolution of current transient under a 50 mV forward voltage pulse when device is held at forward bias of 1.8 V. The voltage pulse stays at 50 mV for the whole duration of the transient shown above. Current monotonically increases to saturation value. Insets show (a) negative time derivative $(-d\delta j(t)/dt)$ of the transient (b) simulated sinusoidal signal and (c) product $[(-d\delta j(t)/dt)(\sin \omega t)]$ is dominated by the negative part of the oscillating output which makes the reactive response to simulate negative capacitance like behavior. Monotonically increasing transient indicates the occurrence of negative capacitance for all measurement frequencies.

In figure 3.5 we consider current transients for two different bias levels i.e. 1.6 V and 1.8 V. For lower bias (1.6 V), negative capacitance behavior is not very prominent and current transient shows increasing shape with non-monotonic nature (solid blue line

in figure 3.5). Its time derivative (line with circles) acquires a very sharp decreasing behavior with small non-monotonic behavior with the time. [$(-d\delta j\ (t)/dt)\times sin\ \omega t$] product for this transient would not generate a dominant negative half. In fact, the difference in magnitudes of the positive and negative halves will die down like the transient derivative itself. This will lead to an effective positive capacitance behavior for a wide range of frequencies. However, a negative capacitance effect can be predicted for lower frequency range. As the bias is increased (1.8 V) negative capacitance effect is prominent. As a result the current transient (solid black line) becomes smooth and monotonically increasing. Its derivative (line with squares) also acquires decreasing and more monotonic behavior. Lag in the current transient also becomes more prominent with increasing bias. This description clarifies the significance of monotonically increasing and non-monotonic transients in the context of NC.

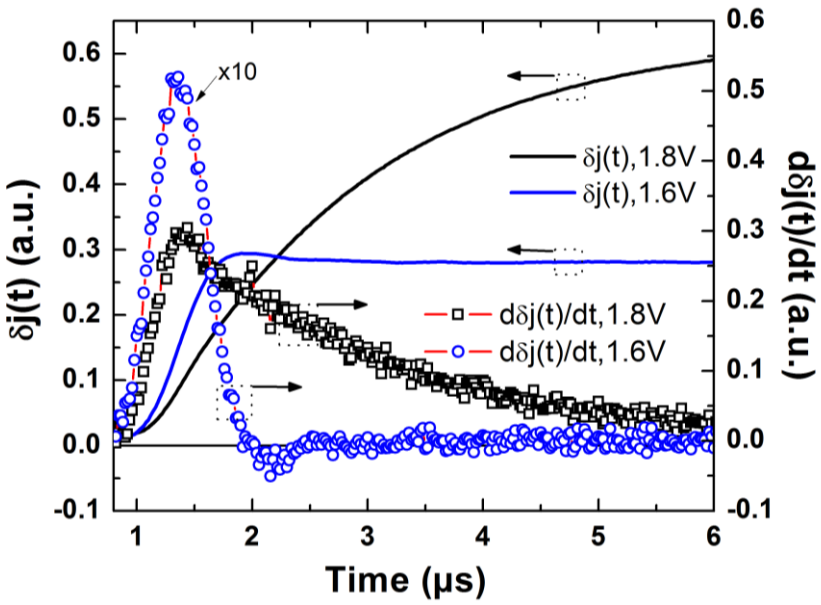

Figure 3.5: Current transients and their derivatives for DL-3148- 025 laser diode under the application of 50 mV step voltage. As the applied bias increases, current transient (derivative) becomes monotonically increasing (decreasing) which is the characteristic of negative capacitance behavior.

Presence of monotonically increasing current transient or non-monotonic transient can be understood by the effect of impurity and interface states on the dynamics of charge carriers[26, 39, 55]. We understand that NC is due to the significant contribution of sub-band gap defect states to overall charge carrier density[1, 45]. This disables quasi Fermi levels

from following applied modulation. As a result, we observe a transient change in the steady state separation values of the quasi Fermi levels after a complete cycle of sinusoidal modulation. Subsequently a transient current is generated which lags behind the applied voltage generating inductive like effect. Resultant induced voltage ultimately tries to compensate any such momentary changes in the separation of quasi Fermi levels over a cycle of applied modulation and steady state condition is regained. When step voltage is applied to an initially forward biased diode, it increases the charge carrier density even more. Due to the perturbation in quasi Fermi level positions, contribution from trap states also changes. Simultaneously radiative recombination will consume charge carriers faster than the response from the traps. Trapping rate of holes and electrons and hence their effective availability will also be different at respective interfaces generating a time varying potential across the device[56]. This will result in increased interface barriers but ultimately increasing the drift for charge carriers. We observe this as a slow increase in transient current during the voltage pulse when contribution from defect states is significant. We also observe the effect that the transient current derivative slowly dies (figure 3.5) when the net current level approaches its steady state value as governed by I_{dc}.

3.5 Conclusions

We have presented a theoretical description of negative capacitance which can be generalized to different junction devices. We described frequency dependent capacitance in terms of the transient current produced after a small voltage perturbation. A monotonically increasing transient or non-monotonically increasing positive valued transient describes NC behavior. However for positive capacitance regime transient has decreasing behavior. This description not only produces negative and positive capacitance mathematically but has also been verified experimentally in this work. We presented a physical mechanism for observing increasing transients in case of NC behavior by considering the role of defect states in charge carrier recombination dynamics. This is consistent with the explanation we proposed for NC and its optical correlation in chapter 2 and can be generalized for a variety of devices other than

electroluminescent devices. As we have pointed out earlier, probing mechanism of NC has provided a better understanding of the different processes taking place in the device.

A part of the work presented in this chapter has been published in Physica Status Solidi C, Vol. 10, p. 593, 2013 and MRS Proceedings, 1635, t07-05 (2014).

3.6 References

[1] K. Bansal and S. Datta, *J. Appl. Phys.* **110**, 114509 (2011). (See references 4-17 cited therein).

[2] S. M. Sze and K. K. Ng, *Physics of Semiconductor Devices* (Wiley-Interscience, 3rd Edition, 2006).

[3] M. Shur, *Physics of Semiconductor Devices* (Prentice Hall-India, 1st Edition, 1995).

[4] Y. Kanai, *J. Phys. Soc. Jpn.* **10**, 718 (1955).

[5] W. Shockley, *B. S. T. J.* **28**, 435 (1949).

[6] K. S. A. Butcher, T. L. Tansley, and D. Alexiev, *Solid-State Electron.* **39**, 333 (1996).

[7] R. Vogel and P. J. Walsh, Appl. Phys. Lett. 14, 216 (1969).

[8] J. Allison and V. R. Dawe, *Electron. Lett*. **7**, 706 (1971)

[9] H. K. Rockstad, *J. Appl. Phys*. **42**, 1159 (1971).

[10] G. S. Nadkarni, N. Sankarraman and S. Radhakrishnan, *J. Phys. D: Appl. Phys*. **16**, 897 (1983).

[11] B. S. Doyle, *J. Phys. D: Appl. Phys.* **19**, 1129 (1986).

[12] X. Wu and E. S. Yang, *J. Appl. Phys.* **65**, 3560 (1989).

[13] C. H. Champness and W. R. Clark, *Appl. Phys. Lett*. **56**, 1104 (1990).

[14] X. Wu, E. S. Yang and H. L. Evans, *J. Appl. Phys.* **68**, 2845 (1990).

[15] M. Beale and P. Mackay, *Phil. Mag. B* **65**, 47 (1992).

[16] E. E. Kamel, P. Gonon, F. Jomni and B. Yangui, Appl. Phys. Lett. 93, 042904 (2008).

[17] T. Misawa, *J. Phys. Soc. Jpn.* **12**, 882 (1957).

[18] J. Werner, A. F. J. Levi, R. T. Tung, M. Anzlowar and M. Pinto, *Phys. Rev. Lett*. **60**, 53 (1988).

[19] M. Matsumura and Y. Hirose, *Jpn. J. Appl. Phys*. **39**, L123 (2000).

[20] M. Matsumura and Y. Hirose, Jpn. J. Appl. Phys. 39, L123 (2000).

[21] R. Merlin and D. A. Kessler, *Phys. Rev. B* **41**, 9953 (1990).

[22] J. Shulman, S. Tsui, F. Chen, Y. Y. Xue and C. W. Chu, *Appl. Phys. Lett*. **90**, 032902 (2007).

[23] T. Noguchi, M. Kitagawa and I. Taniguchi, *Jpn. J. Appl. Phys*. **19**, 1423 (1980).

[24] G. Blatter and F. Greuter, *Phys. Rev. B* **34**, 8555 (1986).

[25] C. C. Wang, G. Z. Liu, M. He and H. B. Lu, *Appl. Phys. Lett*. **92**, 052905 (2008).

[26] L. E. Byrum, G. Ariyawansa, R. C. Jayasinghe, N. Dietz, A. G. Perera, S. G. Matsik, I. T. Ferguson, A. Bezinger and H. C. Liu, *J. Appl. Phys*. **106**, 053701 (2009).

[27] M. Anutgan and I. Atilgan, *Appl. Phys. Lett.* **102**, 153504 (2013).

[28] W. Z. Shen and A. G. U. Perera, *Appl. Phys. A* **72**, 107 (2001).

[29] L. Bakueva, G. Konstantatos, S. Musikhin, H. E. Ruda and A. Shik, *Appl. Phys. Lett*. **85**, 3567 (2004).

[30] F. A. Castro, P. R. Bueno, C. F. O. Graeff, F. Nuesch, L. Zuppiroli, L. F. Santos and R. M. Faria, *Appl. Phys. Lett.* **87**, 013505 (2005).

[31] L. S. C. Pingree, B. J. Scott, M. T. Russell, T. J. Marks and M. C. Hersam, *Appl. Phys. Lett.* **86**, 073509 (2005).

[32] J. Bisquert, G. Garcia-Belmonte, A. Pitarch and H. J. Bolink, *Chem. Phys. Lett*. **422**, 184 (2006).

[33] A. G. U. Perera, S. G. Mastik, H. C. Liu, M. Gao, M. Buchanan, W. J. Schaff and W. Yeo, *Appl. Phys. Lett*. **77**, 741 (2000).

[34] M. Ershov, H. C. Liu, L. Li, M. Buchanan, Z. R. Wasilewski and V. Ryzhii, *Appl. Phys. Lett*. **70**, 1828 (1997).

[35] S. D. Wang, Z. Z. Sun, N. Cue, H. Q. Xu and X. R. Wang, *Phys. Rev. B* **65**, 125307 (2002).

[36] A. J. Chiquito, Y. A. Pusep, S. Mergulhao, J. C. Galzerani and N. T. Moshegov, *Phys. Rev. B* **61**, 5499 (2000).

[37] S. D. Lin, V. V. Ilchenko, V. V. Marin, N. V. Shkil, A. A. Buyanin, K. Y. Panarin and O. V. Tretyak, *Appl. Phys. Lett.* **90**, 263114 (2007)

[38] A. K. Jonscher, *J. Chem. Soc., Faraday Trans. II* 82, 75 (1986).

[39] M. Ershov, H. C. Liu, L. Li, M. Buchanan, Z. R. Wasilewske and A. K. Jonscher, *IEEE Trans. Electron. Devices* **45**, 2196 (1998).

[40] B. K. Jones, J. Santana and M. McPherson, *Solid State Commun*. **107**, 47 (1998).

[41] S. E. Laux and K. Hess, *IEEE Trans. Electron. Devices* **46**, 396 (1999).

[42] H. H. P. Gommans, M. Kemerink and R. A. J. Janssen, *Phys. Rev. B* **72**, 235204 (2005).

[43] J. Shulman, Y. Y. Xue, S. Tsui, F. Chen and C. W. Chu, *Phys. Rev. B* **80**, 134202 (2009).

[44] M. B. Partenskii and P. C. Jordan, *Phys. Rev. B* **80**, 011112 (2009).

[45] K. Bansal, *Phys. Status Solidi C* **10**, 593 (2013).

[46] R. Tadros-Morgane, G. Vizdrik, B. Martin and H. Kliem, *J. Appl. Phys.* **109**, 014501 (2011).

[47] L. F. Feng, Y. Li, D. Li, X. D. Hu, W. Yang, C. D. Wang and Q. Y. Xing, *Appl. Phys. Lett*. **101**, 233506 (2012).

[48] D. C. Tripathi and Y. N. Mohapatra, *Appl. Phys. Lett.* **102**, 253303 (2013).

[49] I. Mora-Sero´, J. Bisquert, F. Fabregat-Santiago, G. Garcia-Belmonte, G. Zoppi, K. Durose, Y. Proskuryakov, I. Oja, A. Belaidi, T. Dittrich, R. Tena-Zaera, A. Katty, C. Le´vy-Cle´ment, V. Barrioz and S. J. C. Irvine, *Nano Lett*. **6**, 640 (2006).

[50] J. Bisquert, *Phys. Chem. Chem. Phys*. **13**, 4679 (2011).

[51] S. Salahuddin and S. Datta, *Nano Lett.* **8**, 405 (2008).

[52] V. V. Zhirnov and R. K. Cavin, *Nat. Nanotech*. **3**, 77 (2008).

[53] A. I. Khan, D. Bhowmik, P. Yu, S. J. Kim, X. Pan, R. Ramesh, and S. Salahuddin, *Appl. Phys. Lett*. **99**, 113501 (2011).

[54] S. Kolev, B. Delacressonniere and J. Gautier, *IEEE Trans. Microw. Theory Tech*. 49, 2425 (2001).

[55] R. Tadros-Morgane, G. Vizdrik, B. Martin and H. Kliem, *J. Appl. Phys.* **109**, 014501 (2011).

[56] F. Lemmi and N. M. Johnson, *Appl. Phys. Lett.* **74**, 251 (1999).

Chapter 4

Temperature Variation of Negative Capacitance and Modulated Electroluminescence: Role of Quantum Well Structure

4.1 Introduction

So far, we have discussed the presence of an inductive like response from ELDs under low frequency modulation and high charge injection[1, 2]. This response, seen as negative capacitance (NC) is exciting, technologically important[3-5], yet a less understood phenomenon. A remarkable connection of this electrical property with voltage modulated electroluminescence (VMEL) has been established. Frequency dependent NC and VMEL are understood as an outcome of the dynamic competition between radiative recombination process in the quantum well (QW) and the steady state response from defects states[1]. We have also discussed a general description of NC, given in the context of different functionality devices and its theoretical explanation based on the behavior of current transients after a small forward bias voltage step[6]. We have already shown in previous chapters how our explanation of NC, considering the competition of fast and slow processes in general, involving available charge carriers, provides a generalized explanation for its occurrence. However, this description is incomplete without probing the temperature dependence of these properties for the following reasons: (a) as per equation (2.2) contribution from sub-band gap states is temperature dependent and must affect NC as well as VMEL and (b) strictly room temperature studies, as discussed so far, overlook (under thermal equilibrium) any effect of temperature dependent processes

inside the quantum well, on measured modulation properties. Notably, in this context, there are very few (and very recent) reports in the literature concerning temperature dependent behavior of a diode under charge carrier injection[7, 8]. These studies report the sensitivity of negative capacitance for temperature variation. However, a clear cut connection with light emission is not probed.

Therefore in this chapter we will show how the ELDs we are probing under high carrier injection behave with temperature variation. In the work presented in previous chapters, *while working on a particular constant temperature*, we assumed thermal equilibrium condition. This ensures that the *steady state* population of charge carriers inside the QW is unaffected by any thermally activated escape of carriers from the QW barrier. Hence, any change in the measured response was solely due to applied modulation.

In this chapter, we will discuss the temperature variation of both NC and VMEL and their interdependence. In addition to probing basic physical processes, it is necessary to study the interdependence of electronic and optical properties of ELDs under their operating condition of light emission for their efficiency improvement. In fact, improvement in the performance efficiency of ELDs is the primary goal of physicists as well as engineers working in the field of optoelectronics. Continuous research is going on to achieve better efficiency devices and materials for a vast variety of technological applications[9].

During a temperature scan, unlike usual[10] continuous wave (CW) light emission, which expectedly decreases continuously with increasing temperature, both NC and VMEL show an increase when temperature increases from a very low value (~60 K). They achieve a maximum around a certain temperature range and then start to fall down with further increase in temperature. Position of this maximum systematically shifts towards higher temperature with increasing forward bias. Contribution from defect states at applied modulation frequency explains the increase of NC as well as VMEL with temperature for lower temperature regime. However, as the temperature becomes sufficiently high, charge carrier escape from the inbuilt quantum wells becomes dominant, effectively reducing both NC and VMEL. Resultant peak or maxima in

modulated light emission indicates that the device can have maximum efficiency at different temperatures for different biases. Thus, we suggest that for efficient working of ELDs under direct modulation, the temperature of maximum light emission must be tailored to their operational temperature. This can be achieved either by careful choice of materials and/or by clever device engineering.

4.2 Experimental methods

4.2.1 Temperature variation

For variation of temperature we mounted the sample (on the sample holder shown in figure 2.3 in chapter 2) inside the closed cycle Helium cryostat (from Advance Research Systems). For better transfer of thermal energy, we used a Silver-Indium ring between the cold head and sample holder. For primary temperature sensing Si diode temperature sensor (DT-670B-SD from Lakeshore) was mounted on the cold head directly. This sensor was used along with the Lakeshore 340 temperature controller to monitor and control the temperature by controlling the current through the electric heater strip around the cold head. To monitor the sample temperature accurately we used another sensor in the vicinity of the sample itself. To improve the thermal contact between the sample holder and the sensor, we used Cryogenic High Vacuum Grease form Apiezon (N Grease). We measured the temperature with an experimental accuracy of ±0.1 K.

We know that the dependence of injection current and hence the number of free charge carriers available in the diode, on applied voltage during temperature variation[11], is non-linear (chapter 1, equation (1.8)). Therefore we performed the experiments at a constant forward bias current (I_{dc}). This allows us to ignore any effect of changing charge carrier density due to temperature variation only on the mechanisms we are probing.

4.3 Results and discussion

Figure 4.1 shows the variation of CW light output/ electroluminescence with temperature. We can observe a continuous decrease in the light emission intensity as the temperature increases.

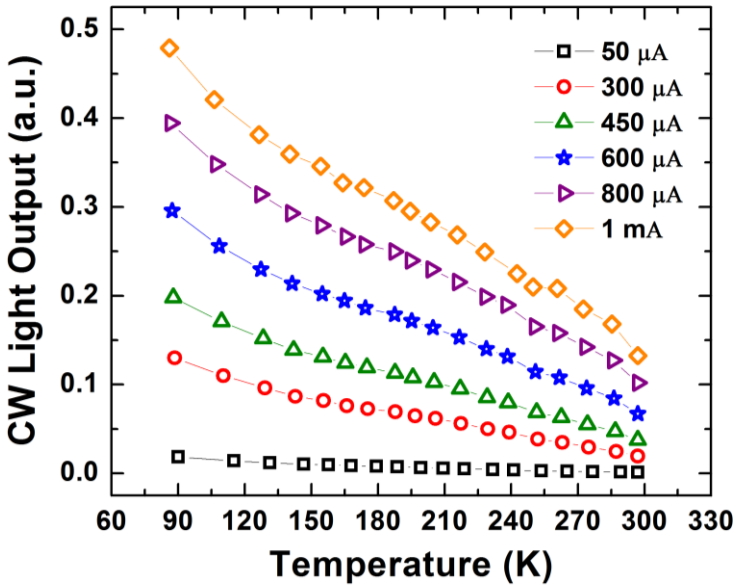

Figure 4.1: Continuous wave (CW) light emission from laser diode DL-3140-025 decreases monotonically with increasing temperature for all the values of current (I_{dc}). This follows general reduction in radiative recombination efficiency with temperature increase as discussed in the text.

Generally, efficiency of light emission decreases with increasing temperature and can be attributed to various processes affected by temperature variation[12-17]. In case of quantum well based structures, fall of luminescence intensity with temperature can be attributed to two major reasons[18]: (i) activation of non-radiative recombination processes mediated by trap states[19-23] and (ii) thermal escape of charge carriers from quantum wells and their effective non-radiative recombination in the barrier layer[24-30]. These processes effectively increase the radiative recombination life time with increasing temperature making the process inefficient[31].

4.3.1 Temperature dependence of modulated light emission and negative capacitance response

Results in figure 4.1 can be treated as the control experiment for the functionality of the diode, giving standard reported results. Now, in figure 4.2, we show similar plots for VMEL. It is clear from the figure that the behavior of modulated electroluminescence or modulated light emission is not a monotonic function of temperature.

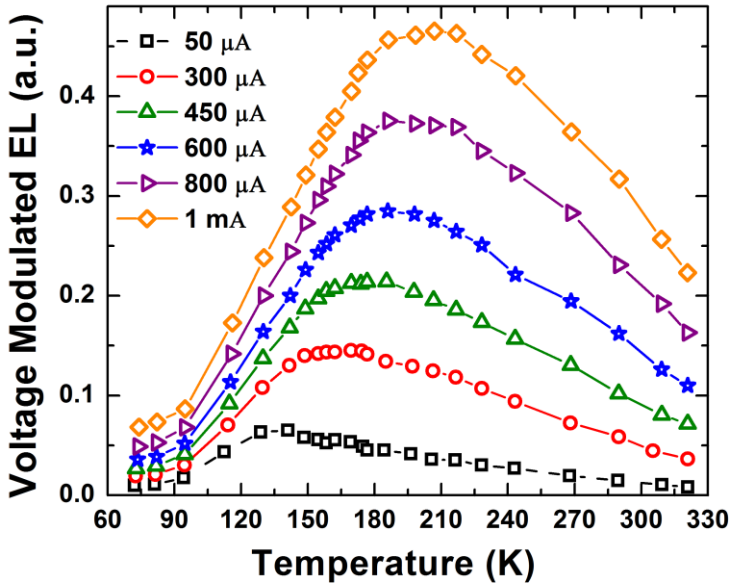

Figure 4.2: Temperature scan of modulated light emission from laser diode (DL-3148-025) at different I_{dc}, measured at 1 kHz. Scan goes through a maximum at certain temperatures (T_{Max}). With increasing bias, T_{Max} shifts to higher temperature. For cost effective performance, this maximum should be around operational temperature of the ELD.

For a given I_{dc}, when the sample temperature is increased form a very low value (~ 60 K) we observe that VMEL signal increases. This is contrary to what has been discussed above in the context of figure 4.1 where CW light emission expectedly decreases with increasing temperature. After acquiring a range of temperature (~140K – 210K), further heating causes VMEL to reverse its trend and it starts to decrease. Interestingly, this results in a temperature point where VMEL signal maximizes. We named this temperature of maximum emission as $T_{Max.}$ It is apparent from figure 4.2 that T_{Max} shifts systematically to higher temperature side as the bias (I_{dc}) increases. Absence

of any maximum in the case of CW light emission indicates that the observed features in VMEL are only due to the steady state response of charge carriers to applied voltage modulation.

Our previous results indicated a correlation between VMEL and NC[1, 2], hence to verify this correlation of light emission with the capacitance behavior we measured impedance of the devices under charge injection condition with temperature variation. Figure 4.3a and 4.3b show the variation of capacitance (C) and conductance (G) respectively with temperature for frequency 1 kHz and varied I_{dc} levels.

These measurements are done under the circuit model containing capacitance and conductance in parallel as described in chapter 2 (section 2.2.2). We have discussed in chapter 2 that the onset of VMEL accompanies the onset of negative capacitance (NC). As shown in figure 4.3a, we observe NC effect in the same bias regime where we were observing significant modulated emission (figure 4.2). NC also increases in magnitude as the temperature increases from a very low value, acquires maximum value and then reverses its course to decrease with increasing temperature. Temperature where NC effect is maximum (T_{Max}) also shifts to higher values with increasing forward bias or I_{dc} values. In conductance, as shown in figure 4.3b, we observe an increase with increasing temperature, however above the range of T_{Max}, it saturates with a slow decrease thereafter. Figures 4.2 and 4.3a strongly support the correlation between NC and VMEL throughout the range of temperature variation. This correlation can be explained by considering the active participation of defects in radiative recombination dynamics.

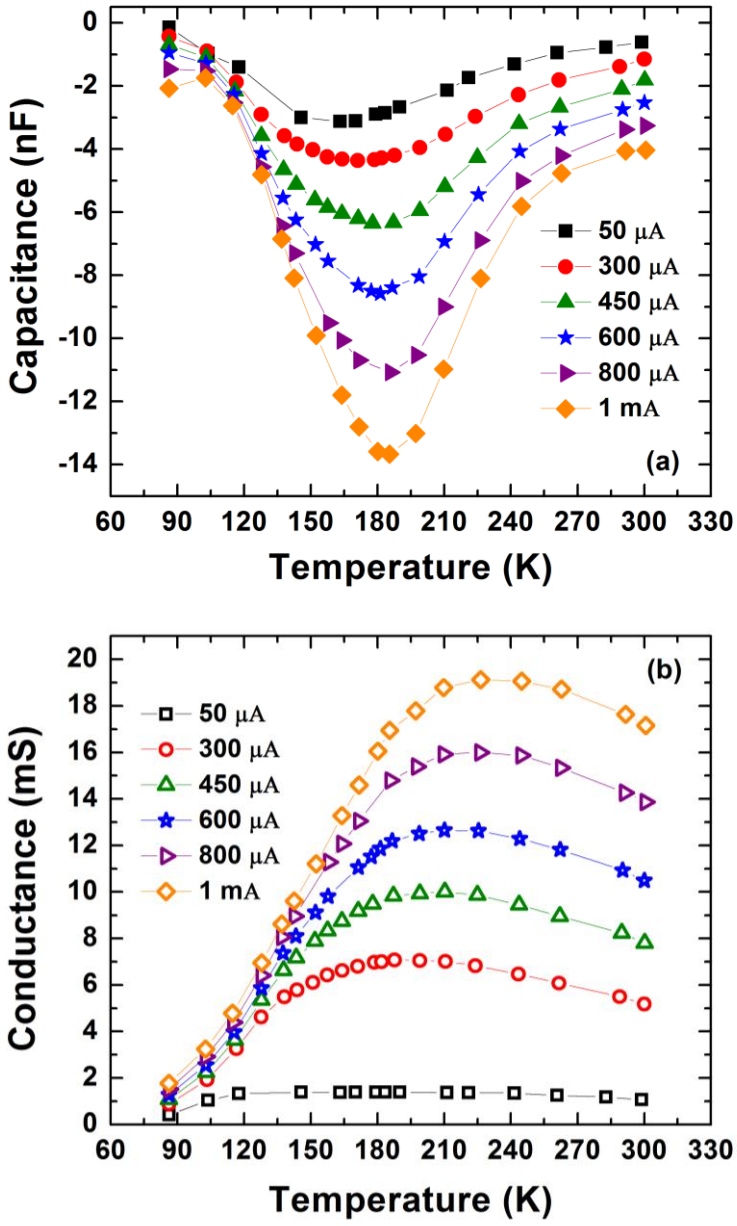

Figure 4.3: Temperature scan of (a) negative capacitance and (b) conductance for laser diode at 1 kHz for different I_{dc}. A maximum is observed in capacitance at certain temperature (T_{Max}), which shifts to higher side for higher bias. Behavior of negative capacitance is similar to that of VMEL as shown in figure 4.2.

Defect states can only contribute to the VMEL and NC signal if their thermal rate of carrier exchange with the band edges ($1/\tau$) is comparable to applied frequency (f). Here ($1/\tau$) is related to the thermal activation energy (E_{Th}) of the defect level by $1/\tau = \nu \exp(-E_{Th}/k_B T)$ where k_B is the Boltzmann constant, ν is the thermal prefactor, hence we can write:

$$E_{Th} = k_B T \ln(\nu / f) \tag{4.1}$$

steady state charge carrier (e.g. electrons) contribution from defects is given as, $n^{Trapped} = \int_{E_C - E_{Th}}^{E_{Fn}} g(E)dE$, g(E) is the sub-band gap defect density. Limits of integration represent the total defect states which can respond to the applied signal (shaded area in figure 2.8) as given by equation (4.1) and also by the position of quasi Fermi level (E_{Fn}) and band edges (conduction band E_C in case of electrons). At any given temperature, lower frequency allows defect levels with higher E_{Th} also to respond to the applied modulation, thereby, increasing the defect contribution towards total charge carrier density available for radiative recombination. This is why we observe higher VMEL and NC signals at lower frequencies as discussed in chapter 2 (figure 2.7). Similarly, at a given bias and frequency, defect contribution to charge carrier density available for radiative recombination increases with the increasing temperature. As a result we see counterintuitive increase in the magnitude of VMEL and NC signal as shown by figures 4.2 and 4.3a, when temperature is increased from a significantly low value (~ 60 K). This signature is missing in case of CW light emission as is evident from figure 4.1. However this increase is rather slow for relatively low temperatures (≤ 100 K) due to the inability or inertia of charge carriers to respond to the applied voltage modulation. In such case, one would expect that for even lower temperatures both VMEL and NC will saturate to a small value.

As we increase the temperature further above T_{Max}, VMEL and NC reverse the behavior and start to decrease. In this regime, behavior of VMEL matches with that of CW light emission and hence the likely causes of this can be[18] (i) the loss of charge carriers to thermally activated defects with very large response time as compared to the applied modulation. Charge carriers can get trapped in these slow defects becoming unable to follow the applied modulation or (ii) the increasing loss of charge carriers available for radiative recombination due to their field assisted thermal escape from the active quantum well (QW) region. Both of the processes can contribute simultaneously as well.

To probe this process further and to figure out the dominant reason, we studied frequency dependence of temperature scan of VMEL and NC maintaining a particular I_{dc}. We present the results in figures 4.4a and 4.4b respectively.

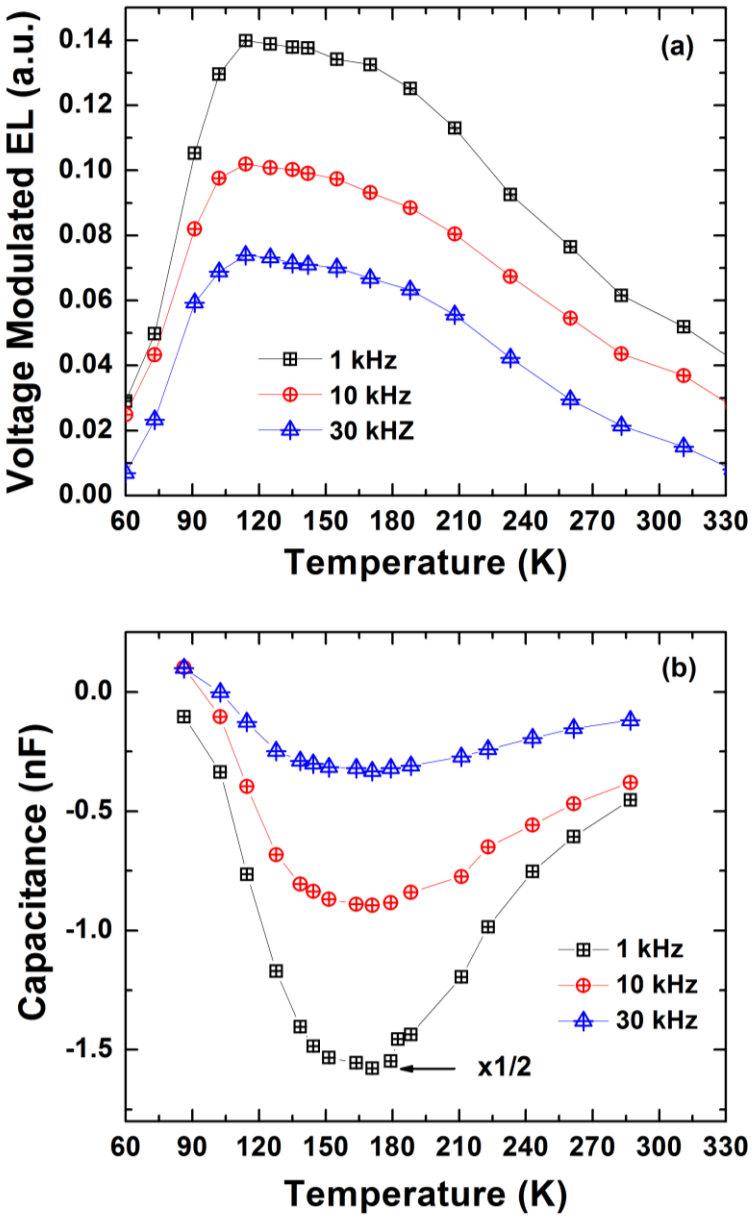

Figure 4.4: Frequency dependence of temperature scan of (a) modulated light emission and (b) negative capacitance at I_{dc}=250 μA. Note that the T_{Max} is relatively independent of applied modulation frequencies in both the cases.

For the frequency variation results presented here, I_{dc} was kept at 250 µA. Similar behavior was obtained for other values of I_{dc} also. For any given temperature, lower frequency produces higher VMEL signal and negative capacitance. This is again in support of our previously discussed results in chapter 2. Noticeably, T_{Max} is relatively independent of the frequency (for frequencies ≤ 100 kHz) for both VMEL and NC. This indicates that the process causing VMEL and NC to decrease after T_{Max} is not affected by the applied modulation. This can happen when the process occurs at a very fast rate as compared to the time scale of the modulation. This favors the presence of QW escape processes to be the cause of the reversal observed in VMEL and NC. Also, in the dominance of slow defects we would have observe a peak in conductance response rather than capacitance response as discussed in chapter 1 section 1.5. Thermally activated escape of charge carriers from quantum well, being a very fast process[32] (~ 100 ps) remains independent of the applied modulations frequency in the used frequency range. Hence it starts affecting the properties of the device we are measuring under modulation, around the same temperature irrespective of the applied modulation frequency. The escape process is supported by the remnant field of the junction. Higher thermal activation is required, as the bias becomes more positive which nullifies the field of the junction. As a result, we observe that the T_{Max} shifts to higher temperature side with increasing I_{dc}.

4.3.2 Field assisted thermally activated escape of charge carriers from quantum wells

It would be interesting to probe the thermally activated escape process but in the present case we have injected charge carriers, defect responding to applied modulation, emission of light and escape process happening simultaneously. Hence it becomes difficult to directly probe the escape process itself. However, in this case, continuous charge carrier escape from QW is a complimentary process to light emission in a sense that it depletes the number of charge carriers available for radiative recombination. To probe the escape process we measured the variation of CW light emission with temperature for different I_{dc} values, as shown in figure 4.5a. We also measured the variation in I_{dc} with temperature while maintaining certain light emission intensity, as

shown in figure 4.5b. In our case, a major contribution to this I_{dc} comes from charge injection to active region, QW escape, radiative recombination and trapping by defects etc.

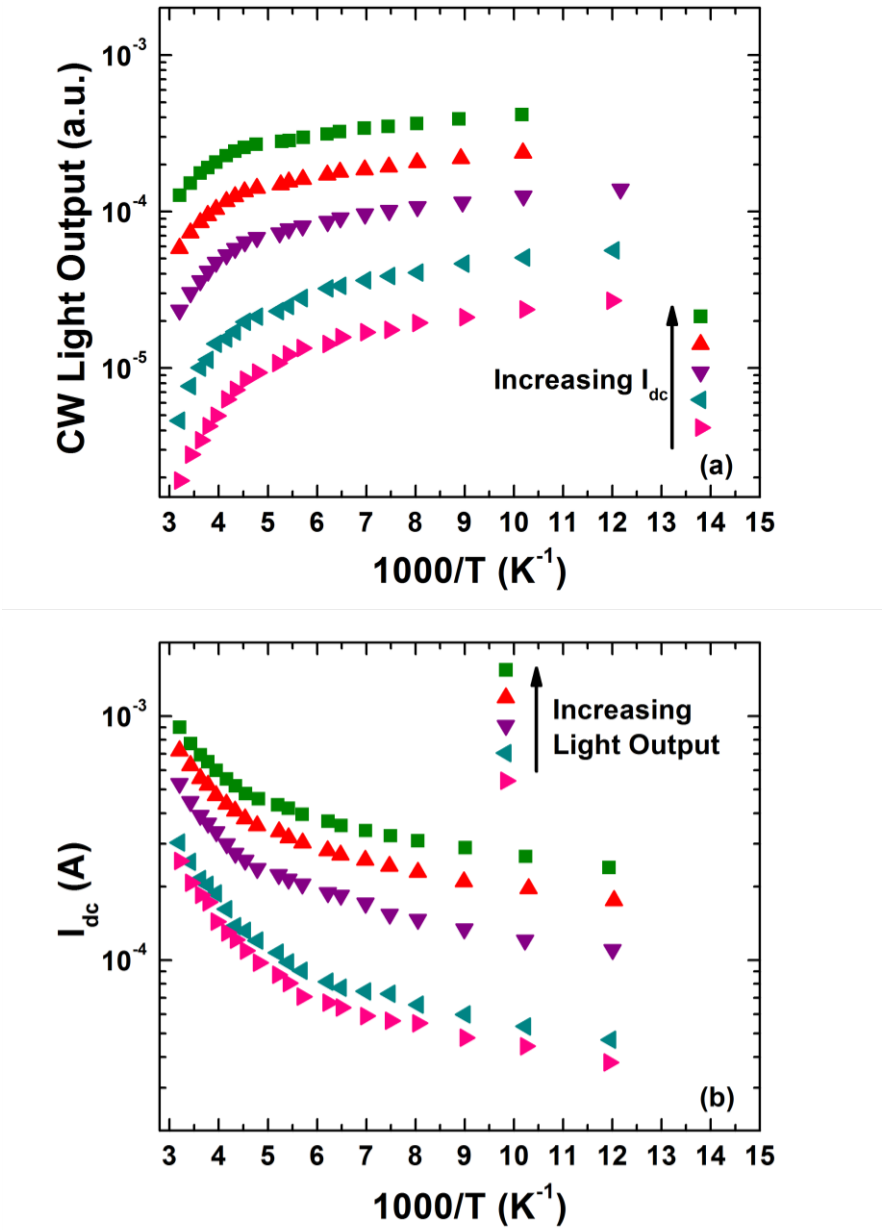

Figure 4.5: (a) showing increase in the rate of light emission with decreasing temperature and increasing I_{dc} (0.1, 0.2, 0.45, 0.7 and 1.3 mA). As the thermal escape starts, change in the slope of light output decrease can be noticed. (b) Variation in the rate of charge injection in the form of I_{dc} with temperature to maintain certain CW light output intensity. As the temperature increases, higher I_{dc} (rate of charge injection) is required to maintain the light output intensity. Again we observe a sharp change in the I_{dc} values after the escape process starts. (notice the logarithmic y axes in the figures)

Current density of escape J_E for electrons is directly proportional to the density of charge carriers available in the QW and inversely proportional to the escape life time. It can be written in the form[33]:

$$J_E = \frac{n_{QW} eL}{\tau_E} \tag{4.2}$$

where L is the width of the QW, n_{QW} is the carrier density inside the well, e is the electronic charge and $1/\tau_E$ is the rate of thermal escape. As the temperature increases, $1/\tau_E$ for charge carriers in the QW increases, and escape process starts to dominate around 1000/T ~ 4 - 6.5 K^{-1}. This is also evident in figure 4.5a: for low temperatures, radiative recombination falls slowly, probably due to the activation of non-radiative defect channels. After the range of 1000/T ~ 4 - 6.5 K^{-1}, which matches with the range of T_{Max} or the temperature range where reversal is observed in VMEL and NC, light emission output falls sharply with 1000/T. This happens due to the higher consumption rate of the charge carriers by thermally activated QW escape process at a particular I_{dc}. This region of the figure 4.5a fits well with the equation of the form $N=N_0\text{-}exp(\text{-}E_I/k_BT)$ indicating an Arrhenius like process [$N'=(N_0\text{-}N) \approx exp(\text{-}E_I/k_BT)$]. Arrhenius equation describes the variation of a temperature dependent rate process[34, 35]. In this context it signifies the relative fall of radiative recombination rate with increasing temperature after the charge carrier escape starts. At a particular temperature, more light emission is observed for higher I_{dc} as expected.

Similarly in figure 4.5b, as the temperature increases (beyond 1/T ~ 6.5 K^{-1}), higher rate of charge injection in terms of I_{dc} is required to maintain constant light emission intensity. This is again due to the increase in thermally activated QW escape process with increasing temperature. Linear behavior of I_{dc} (plotted in log scale) with 1000/T after the onset of escape process indicates an Arrhenius like process. This signifies the increasing charge injection rate required to maintain certain light output intensity with increasing temperature. At a particular temperature, required I_{dc} to maintain light emission, increases with increasing light emission intensity, as is also discussed in the context of figure 4.5a.

We can obtain Arrhenius like plots from the region 1000/T ~ 4 - 6.5 K^{-1} of figures 4.5a and 4.5b after the onset of thermal escape of charge carriers from the QW. Calculated values of respective activation energies E_I and E_{II} are shown in figure 4.6a and 4.6b respectively.

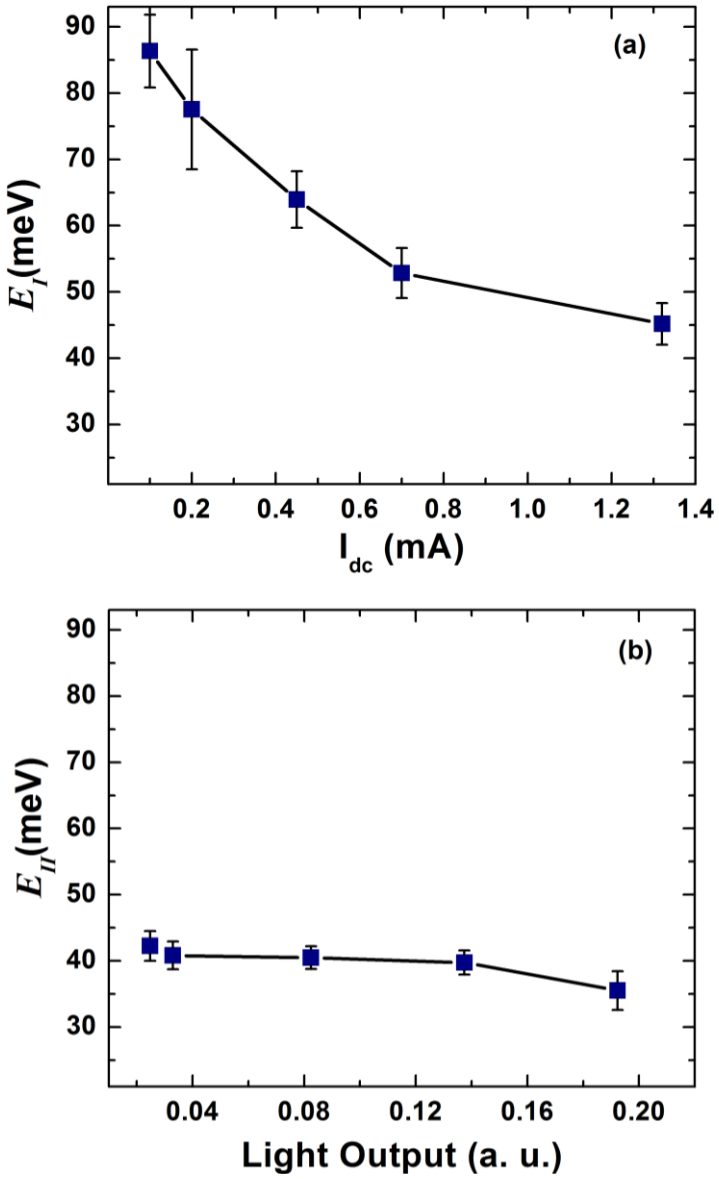

Figure 4.6: (a) Absolute value of the activation energy for light emission E_I as calculated from the straight line portion of the Arrhenius like plot of figure 4.5a. For this calculation we considered the process as $[N=N_0\text{-}exp(-E_{II}/k_BT)]$ in figure 4.5a and then obtained Arrhenius like plot by first obtaining the value of N_0. This signifies the recovery of charge carriers to maintain the light output by further charge injection or (increasing I_{dc}) after their consumption by escape process. (b) Activation energy for charge injection E_{II} as calculated from the straight line portion of the Arrhenius like plot of figure 4.5b.

The rate for any thermally activated QW escape process can be given as[31]

$$\frac{1}{\tau_E} = \left(\frac{k_B T}{2\pi Q}\right)^{1/2} \exp\left(-\frac{E_B}{k_B T}\right) \tag{4.3}$$

where $Q = L^2 m^*$, m^* is the effective mass of the charge carrier inside the well and E_B is the effective thermal barrier height for the escape. In the present case of active light emitting device under voltage modulation, thermal rate of one process is intricately connected with the other competing processes like charge injection, recombination, escape and defect trapping etc. Many of these processes are also intrinsically thermally activated with different barrier heights. Hence it is difficult to directly associate the calculated activation energies solely to any particular barrier height of field assisted thermal escape from QW. However we understand E_I as the activation energy of light emission which goes down with increasing bias ($\sim I_{dc}$) suggesting that the QW escape process which is complimentary to light emission decreases with increasing I_{dc}. This happens due to the field assisted behavior of QW escape process which is also evident in figures 4.2 and 4.3a. In absence of any forward bias, built-in field of the p-n junction efficiently separates thermally escaped charge carriers[36]. However, with increasing forward bias (I_{dc}) this net field contribution to field assisted thermally activated escape of carriers from QW decreases. Hence for higher value of I_{dc} further increase in temperature (as compared to lower current) is required for the activation of escape process. As a result T_{Max} shifts towards higher temperature for higher $I_{dc.}$ E_{II} is understood as the activation energy of charge injection which remains relatively unchanged with light emission intensity within our range of measurements and mainly depends on p-n junction parameters of ELD.

4.3.3 Different processes inside the quantum well

To sum up, as the temperature increases, QW escape process dominates over shallow defect mediated contribution to steady state radiative recombination, consequently we see a decrease in the magnitude of VMEL and NC signals above a certain temperature $T_{Max.}$. Schematic of these processes is shown in figure 4.7.

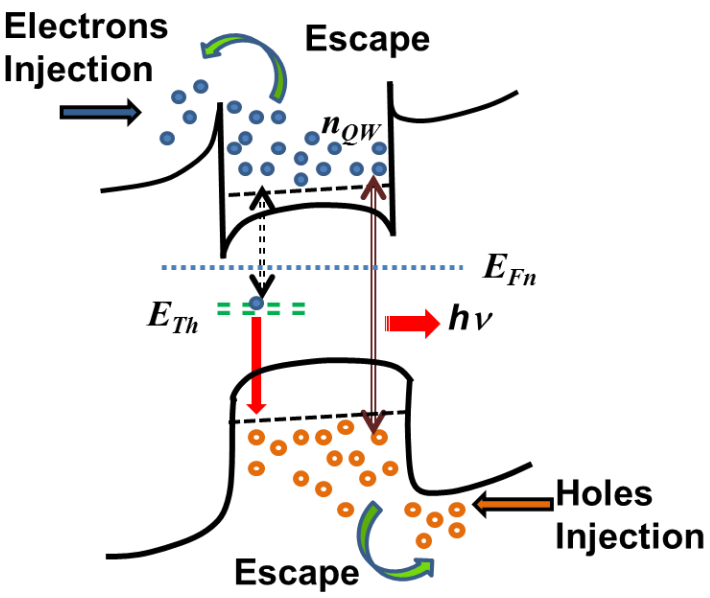

Figure 4.7: Schematic band diagram of the electronic processes occurring in QW which can be extended to multi QW structures as well. Electrons (holes) are injected from the n (p) neighborhood of the junction. These electrons (holes) can undergo radiative recombination or defect mediated recombination through some defect with activation energy E_{Th}. With increasing temperature, field assisted thermal escape of charge carriers starts to dominate, thereby reducing the number of charge carriers inside the well (n_{QW}). Straight arrows show the direction of carrier injection under a constant DC bias. Curved arrows show the field assisted dynamic escape of charge carriers drifting in the direction of the remnant inbuilt field of the junction. E_{Fn} shows the quasi Fermi level for electrons within QW for small forward bias. Quasi Fermi level for holes is not shown here for simplicity. In present devices, we experimentally measured the combined effect of these processes in the different multi QW structures.

Thermal activation of escape along with the deep defects is the cause of continuously decreasing CW light emission with increasing temperature. However, increase in modulated light emission with temperature for low temperature regime and occurrence of peak-like feature is due to the dynamics of processes which can only be reflected under modulation. This peak-like feature in VMEL at low temperatures indicates that under direct modulation, device efficiency is not maximum around room temperature which is closer to the working condition of the device. This temperature can be brought to the working temperature of the device by optimizing defects and quantum well parameters for the device. Effect of quantum well parameters can be determined by equations (4.2) and (4.3). However, different thermally activated processes like defect

dynamics along with carrier recombination happen simultaneously in an active device. Mutual effect of these processes can be specific to particular device structure. Hence careful study of various processes in actual working device, like we have presented, is required to improve its efficiency which may not have a generalized prescription. In such scenario, characterization techniques we have developed can provide significant information about the device dynamics which can be useful in device improvement.

4.4 Conclusions

We discussed the counterintuitive increase in the magnitude of VMEL from ELD when its temperature is raised from a low value till a certain value $T_{Max.}$ This deviates from the usual, monotonically decreasing nature of CW light emission with increasing temperature. This is caused by the increasing participation of shallow defect levels in radiative recombination with increasing temperature. Beyond T_{Max}, thermal escape of charge carriers from the quantum well starts to dominate and VMEL magnitude falls. This results in a temperature range around T_{Max} where modulated light emission is maximum. T_{Max} systematically shifts to higher temperature side with increasing forward bias and is relatively independent of the modulation frequency within the range of our measurements. Similar qualitative features are also observed in negative capacitance. This correlated behavior of optical and electronic processes is important to understand the device behavior during light emission or charge carrier injection. From the point of view of the applications, the temperature of maximum light emission must be brought to the operating temperature of the light emitting device for its efficient performance under direct modulation. Although here we presented results on AlGaInP based multi quantum well laser diodes below lasing threshold, we expect these results and analyses to be valid for a wider range of quantum well based light emitting devices.

The work presented in this chapter has been published in Applied Physics Letters, Vol. 102, p. 053508, 2013 and Physics of Semiconductor Devices: *Environmental Science and Engineering*, p. 795 (2014).

4.5 References

[1] K. Bansal and Shouvik Datta, *J. Appl. Phys.* **110**, 114509 (2011).

[2] K. Bansal, *Phys. Status Solidi C* **10**, 593 (2013).

[3] S. Kolev, B. Delacressonniere and J. Gautier, *IEEE Trans. Microw. Theory Tech*. **49**, 2425 (2001).

[4] S. Salahuddin and S. Datta, *Nano Lett*. **8**, 405 (2008).

[5] J. Shulman, Y. Y. Xue, S. Tsui, F. Chen and C. W. Chu, *Phys. Rev. B* **80**, 134202 (2009).

[6] M. Ershov, H. C. Liu, L. Li, M. Buchanan, Z. R. Wasilewske and A. K. Jonscher, *IEEE Trans. Electron. Devices* **45**, 2196 (1998).

[7] O. Vural, Y. Safak, A. Turut and S. Altindal, *J. Alloys Compd.* **513**, 107 (2012).

[8] W. Yang, D. Li, J. He, C. Wang and X. Hu, *Phys. Status Solidi C* **11**, 714 (2014).

[9] E. F. Schubert, *Light Emitting Diodes* (Cambridge University Press, 2nd Edition, 2006).

[10] In the context of photoluminescence efficiency, which is also CW emission within our frame work, some reports show non-monotonic features with temperature variation. For example: R. H. Bube, Phys. Rev. **81**, 633 (1951).

[11] W. Shockley, *B. S. T. J*. **28**, 435 (1949).

[12] R. B. Hammond, D. L. Smith and T. C. McGill, *Phys. Rev. Lett*. **35**, 1535 (1975).

[13] F. Barigelletti, D. Sandrini, M. Maestri, V. Balzani, A. v. Zelewsky, L. Chassot, P. Jolliet and U. Maeder, *Inorg. Chem*. **27**, 3644 (1988).

[14] R. Kane, H. Sell, *Revolution in Lamps: A Chronicle of 50 Years of Progress* (Fairmont Press, 2nd Edition, 2001).

[15] X. T. Zhang, Y. C. Liu, Z. Z. Zhi, J. Y. Zhang, Y. M. Lu, D. Z. Shen, W. Xu, X. W. Fan and X. G. Kong, *J. Luminescence* **99**, 149 (2002).

[16] O. Labeau, P. Tamarat and B. Lounis, *Phys. Rev. Lett.* **90**, 257404 (2003).

[17] J. Iveland, L. Martinelli, J. Peretti, J. S. Speck and C. Weisbuch, *Phys. Rev. Lett*. **110**, 177406 (2013).

[18] S. Weber, W. Limmer, K. Thonke, R. Sauer, K. Panzlaff, G. Bacher, H. P. Meier and P. Roentgen, *Phys. Rev. B* **52**, 14739 (1995).

[19] P. K. Bhattacharya, S. Subramanian and M. J. Ludowise, *J. Appl. Phys*. **50**, 3364 (1984).

[20] M. Krahl, D. Bimberg, R. K. Bauer, D. E. Mars and J. N. Miller, *J. Appl. Phys.* **67**, 434 (1990).

[21] H. Hillmer, A. Forchel, R. Sauer and C. W. Tu, *Phys. Rev. B* **42**, 3220 (1990).

[22] V. Srinivas, J. Hryniewicz, Y. J. Chen and C. E. C. Wood, *Phys. Rev. B* **46**, 10193 (1992).

[23] W. Z. shen, S. C. Shen, W. G. Tang, Y. Chang, Y. Zhao and A. Z. Li, *Appl. Phys. Lett*. **69**, 952 (1996).

[24] H. Schneider and K. v. Klitzing, *Phys. Rev. B* **38**, 6160 (1988).

[25] K. Fujiwara, N. Tsukada, T. Nakayama and A. Nakamura, *Phys. Rev. B* **40**, 1096 (1989).

[26] J. D. Lambkin, D. J. Dunstan, K. P. Homewood, L. K. Howard and M. T. Emeny, *Appl. Phys. Lett*. **57**, 1986 (1990)

[27] M. Gurioli, A. Vinattieri, M. Colocci, C. Deparis, J. Massies, G. Neu, A. Bosacchi and S. Franchi, *Phys. Rev. B* **44**, 3115 (1991).

[28] P. Michler, A. Hangleiter, M. Moser, M. Geiger and F. Scholz, *Phys. Rev*. *B* **46**, 7280 (1992).

[29] G. Bacher, C. Hartmann, H. Schweizer, T. Held, G. Mahler and H. Nickel, *Phys. Rev. B* **47**, 9545 (1993).

[30] J. R. Botha and A. W. R. Leitch, *Phys. Rev. B* **50**, 18147 (1994).

[31] A. M. Fox, D. A. B. Miller, J. E. Cunningham and W. Y. Jan, *IEEE J. Quantum Electron.* **27**, 2281 (1991).

[32] V. V. Nikolaev and E. A. Avrutin, *IEEE J. Quantum Electron*. **39**, 1653 (2003).

[33] J. Nelson, M. Paxman, K. W. J. Barnham, J. S. Roberts and C. Button, *IEEE J. Quantum Electron.* **29**, 1460 (1993).

[34] A. Frost, R. Pearson, *J. Phys. Chem.* ***65,*** 384 (1961).

[35] K. J. Laidler, *J. Chem. Educ.* **61**, 494 (1984).

[36] Shouvik Datta, B. M. Arora and S. Kumar, *Phys. Rev. B* **62**, 13604 (2000).

Chapter 5

Room Temperature Electrical Investigation of the Signatures of Excitons and Mott Transition

5.1 Introduction

We have discussed, in the preceding chapters, the connection between voltage modulated optical and electrical properties and mutually non-exclusive nature of radiative and non-radiative transitions[1-3] from multi quantum well based electroluminescent diodes (ELD). We clearly showed that slowly responding (~ ms) electronic defects can influence faster (~ps-ns) radiative recombinations in a non-trivial fashion which necessitates $1/\tau_{Effective} \neq 1/\tau_{Radiative} + 1/\tau_{Non\text{-}radiative}$ where $\tau_{Effective}$ is the effective time constant for modulated electroluminescence. Additionally, we reported an unusual non-monotonic behavior of voltage modulated electroluminescence with decreasing temperature[4, 5]. We also observed clear change in both conductance and capacitance of the ELD at the onset of lasing[1]. This connection between the electrical and the optical properties of ELD is remarkable and is through the involvement of charge carriers in these processes. Hence, one would expect that probing the impedance changes along with the onset of light emission should also reveal the process of light emission itself, directly or indirectly. In this work we will discuss the change in the steady state defect response due to the onset of light emission and identify the process originating light emission.

In the direct band gap quantum well system we are working with (as detailed in chapter 2, section 2.2), significant processes of light emission that can be from direct band to band transition involving the presence of free electron-hole plasma (EHP) in respective bands or it can be due to the transitions between excitonic states.

Excitons are formed due to the Coulombic attraction between negatively charged electrons and positively charged holes producing 'Positronium' like bound pairs when a material is either optically or electrically excited[6-10]. At low charge carrier densities, exciton as a bosonic quasi particle of two fermions (electron and hole), can either move freely or form localized complexes inside a solid. For III-V semiconductors like AlGaInP, binding energy of free excitons is reported to be only on the order of 5-10 meV[11]. Still quantum structures of III-V materials exhibit resonant excitonic light emission at room temperature[12-14] due to the effect of strong spatial quantum confinement. It is possible due to the stationary nature of resonant excitonic quantum states in semiconductor nanostructures. This suggests that despite having a very short life time, on the order of ps, under continuous excitation there will always be a stable population of resonant excitons in the quantum well at any given instance of time even at room temperatures. Furthermore, excitons are also expected to reveal exquisite condensed phases of matter like Bose Einstein Condensation (BEC) of excitons[15-21] and exciton-polaritons[22-26], BCS like states with excitonic pair formations in the momentum space[27-29] and electron–hole liquid[30] etc. at low enough temperatures. Many of these are also finding applications in novel devices like ultralow threshold exciton-polariton lasers[31-33].

A large majority of the studies related to excitonic phases almost exclusively use light as a medium of excitation and/or detection. Solely optical spectroscopies have been used to explore the presence of excitons and presence or absence of a sharp Mott transition[34,35] from neutral excitonic phase to metallic electron-hole plasma phase in semiconductor quantum wells[12-14] quantum wires[36, 37] and quantum dots[38]. Presence of excitonic phases is inferred from the properties of luminescence spectra, for example, shape of the spectra or change in spectral features with changing excitation density (current[32, 39, 40] or photons[41, 42]) or temperature[18, 19]. These techniques are however not very accurate due to the presence of various other factors which affect spectral line shapes as discussed in chapter 1, section 1.4.1. On the other hand, there are hardly any investigations on electrical signatures of the condensed matter physics of these excitonic phenomena or the transition of excitonic phase to EHP phase. It will be surprising if these delicate excitonic phases, more often than not explored by their optical traces only, do not

have any electrical counterparts. Also, for an active device like light emitting diodes it is more appropriate to study the electrical properties of device to probe its electronic transport process.

Therefore, in this work we probed and detected the existence of excitons in AlGaInP laser diodes by measuring steady state, small signal impedance response in frequency domain as the carrier injection is gradually increased. Instead of the standard temperature activation of a rate process, here, we monitor the bias activated rate processes at a certain temperature. We model this response with a phenomenological rate equation which explains the experimental data effectively. Observations illustrate that the bias activated differential capacitance response inverts its frequency dependence as the light emission starts and exhibits *'negative activation energy'*. We proposed that this phenomenon of negative activation energy can be attributed to the presence of a *'stable intermediate electronic bound state'* whose binding energy coincides with the standard binding energy of excitons in AlGaInP like III-V semiconductors. Since we identify the presence of excitonic state through frequency dependent differential capacitance response, our technique is useful even at frequencies which are low as compared to the excitonic resonance frequencies. Furthermore, we observed that the differential capacitance response gets suppressed with further increase in the bias marking the Mott transition of the excitonic state into free EHP state. Optical spectroscopy results also support our interpretations based on electrical signatures. Hence, this work presents a unique way to look at the multifaceted nature of the physics of excitons by looking at its electrical signatures alone.

5.2 Results and discussion

We show the onset of light emission and injection current (I_{dc}) as a function of applied bias (V_{dc}) in figure 5.1. We observe a significant light emission around 1.5 V when injection current is on the order of a few μA.

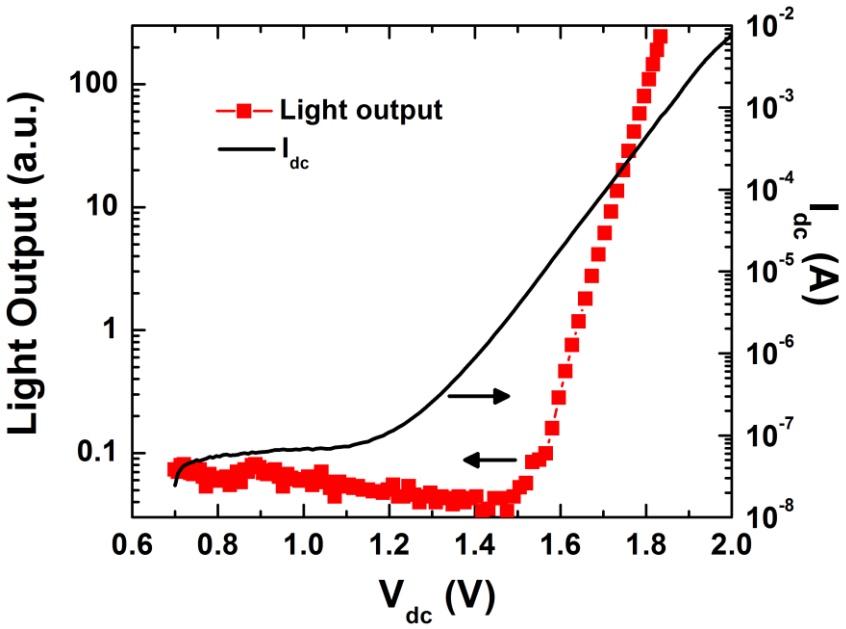

Figure 5.1: Light output (line with squares) and injection current (solid line) as a function of applied bias voltage V_{dc} (measured at room temperature). We observe the onset of significant light emission around 1.5 V. At this value, current is on the order of 2-3μA. Further increase in bias causes current to increase exponentially as expected from diode characteristics (as discussed earlier).

We are interested in exploring changes in the behavior of impedance response with the onset of light emission and its further growth as the V_{dc} is increased at maintained room temperature.

5.2.1 Frequency response of conductance (G) and capacitance (C) under charge carrier injection

In figure 5.2a and 5.2b we present the measured $G/2\pi f$ and C respectively as a function of modulation frequency (f) for different applied forward bias values (V_{dc}). Measurements were performed according to the circuit model discussed in chapter 2, section 2.2.2. We observe that $G/2\pi f$ goes through a maximum as the frequency changes. This behavior can be attributed to defect response[43]. This maximum is observed when quasi Fermi level overlaps with the defect activation energy. An inflection point is observed in capacitance when $G/2\pi f$ goes through a peak as is evident from figure 5.2b (this connection has been discussed in chapter 1, section 1.5).

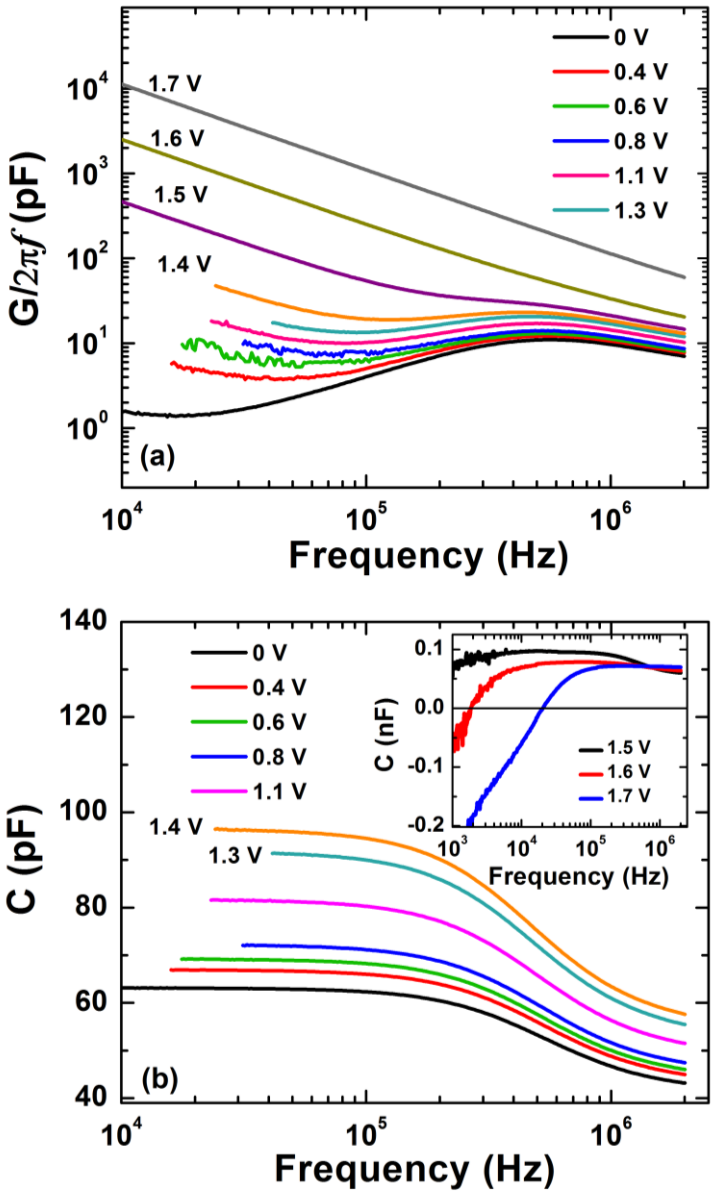

Figure 5.2: (a) Plots of G/2πf vs f show peak like features corresponding to the activation of conductance at a certain modulation frequency f due to defect response, as described in chapter 1, section 1.5. (b) Capacitance (C) shows matching inflection points corresponding to peaks in G/2πf. The inset of (b) depicts junction capacitance for high bias values and negative capacitance effect can be observed above 1.5V.

We observe that for low forward biases, measured capacitance decreases with increasing frequencies. Whereas, for biases above 1.5 V (when light emission starts), capacitance starts to decrease at lower frequencies and eventually turns negative (inset of figure 5.2b). This negative capacitance enhances at higher biases and lower frequencies and we had explained it in terms of dynamic competition between fast light emission

process and slowly responding defect channels[1, 2]. We also see a change in the behavior of $G/2\pi f$ above this bias value. Depending upon the applied bias, we observe that the peak in $G/2\pi f$ and corresponding inflection point in C shift in frequency domain. This is because quasi Fermi level changes with changing applied bias and hence affects the defect response. Since the defect response seems to be coupled with the light emission process, we would like to explore it in detail.

5.2.2 Frequency derivative of capacitance: bias activated response

To analyze the defect response and calculate the frequency of maximum response, we use the frequency derivative of capacitance. In this technique[44], one plots $f\mathrm{d}C/\mathrm{d}f$ with frequency to understand such defect response. It is easier to recognize such peak features and locate the frequency (f_{Max}) of the peak maximum. Defect density $N(E_{Th})$ is proportional to $f\mathrm{d}C/\mathrm{d}f$ and is given by a generalized equation[44-46]

$$N(E_{Th}) \approx -\left(f \frac{dC}{df} \right) \frac{U}{k_B T} \frac{1}{qw} \tag{5.1}$$

where U is the effective built-in-potential and is linearly related to applied bias V_{dc} such that $U = [\Phi_B - V_{dc}]$ and Φ_B is the built-in potential at zero bias, q is the electronic charge, w is the width of the junction. We discussed that when defect energy overlaps with the quasi Fermi level position, we observe a maximum in $G/2\pi f$ and due to this activation of conduction from defects, capacitance changes showing an inflection point and hence a peak in the capacitance derivative. The usual thermal activation energy is obtained from the slope of an Arrhenius plot of $\ln f_{Max}$ with $1/T$. In frequency scan, f_{Max} shifts towards lower frequency side with increasing 1/T (or decreasing temperature) following the defect rate equation (2.2) as discussed in chapter 2. However, in this work, we are particularly interested in exploring the frequency response of electrical impedance with and after the onset of light emission. Hence, in place of varying temperature we increase voltage bias V_{dc} to achieve light emission onset and track any change in the impedance response. We essentially keep the temperature constant in this experiment (296 ±0.1 K). However, from equation (5.1) one can guess that the roles of temperature and bias are mutually reversed for defect dynamics.

Figure 5.3a demonstrates this variation of fdC/df with frequency at smaller forward biases starting from zero.

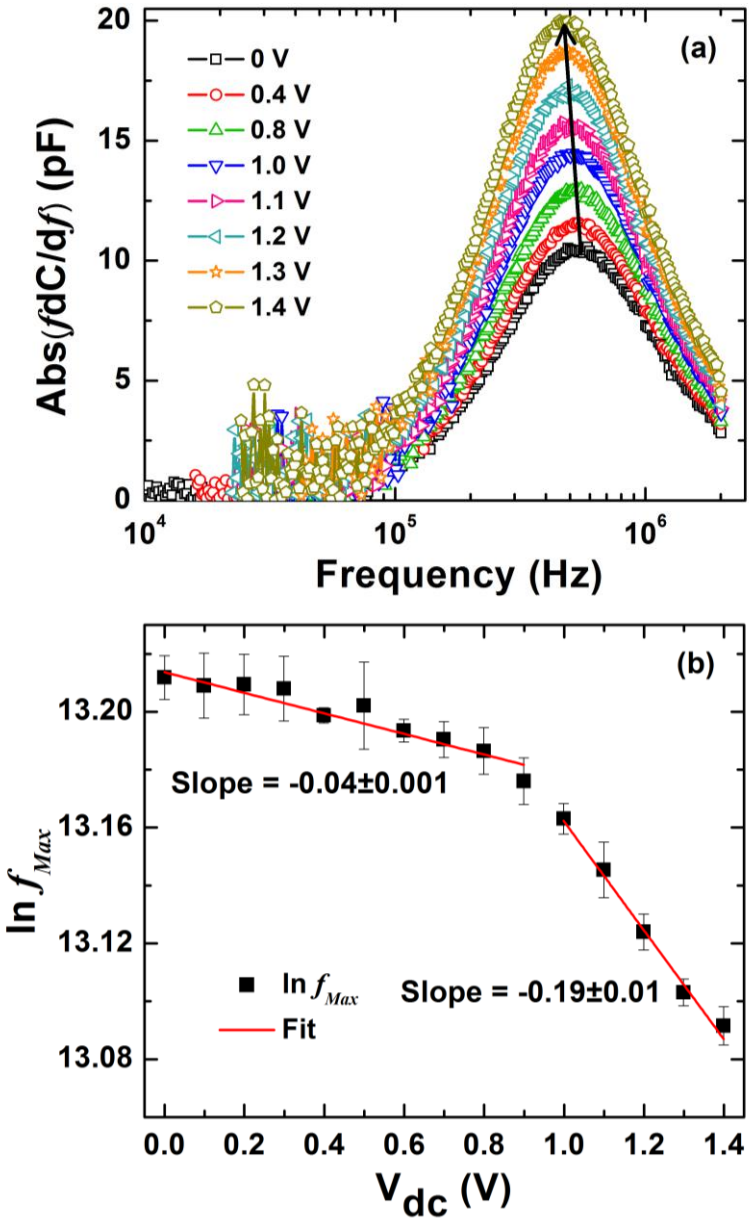

Figure 5.3: (a) Frequency derivative of capacitance peaking at certain frequency f_{Max} due to the activated defect response. As the bias increases, peak shifts towards lower frequency side and the peak amplitude increases. This bias dependence is qualitatively inverse of the usual temperature dependence of such defect response. (b) Linear behavior of ln f_{Max} with V_{dc} indicates that the 1/T ~ V_{dc} in the defects rate equation $R = \frac{1}{\tau} = \nu \exp\left(-\frac{E_{Th}}{k_B T}\right)$. *Change in the slope after 1 V is due to the onset of injection current.*

These f_{Max} values shift toward decreasing f when the forward bias (V_{dc}) slowly increases from zero value. We also see the anticipated increase in this fdC/df peak amplitude with increasing V_{dc} due to the increasing defect response[1]. Therefore, this observed phenomenological activation rate with increasing V_{dc} is qualitatively analogous to the usual variations[46] of fdC/df vs $1/T$ following the electronic transition rate $R = \frac{1}{\tau} = \nu \exp\left(-\frac{E_{Th}}{k_B T}\right)$, where a decrease in temperature decreases the peak position of frequency response (f_{Max}) but increases the overall amplitude of fdC/df peaks. We must emphasize that observations of similar dynamic behavior of small signal impedance response at these smaller forward biases are also reproduced in non-light emitting Silicon diodes (as will be discussed in chapter 6). With this understanding, we write a revised phenomenological rate equation for bias activated electronic transitions rate R' at one temperature as:

$$R' \approx \frac{1}{\tau} = \nu' \exp\left(-\frac{E_{Th}}{k_B} \eta V_{dc}\right) \tag{5.2}$$

where η is a proportionality factor in units of $V^{-1}K^{-1}$ to ensure correct dimensionality. Rewriting this equation gives,

$$\ln R' = \left(-\frac{E_{Th}}{k_B}\right) V_{dc} + \ln \nu' \tag{5.3}$$

hence, plotting $\ln(f_{max})$ with V_{dc} should give a straight line with slope (m) as:

$$m = \left(\frac{-E_a \eta}{k_B}\right). \tag{5.4}$$

We fit the measured fdC/df data as shown in figure 5.3a to obtain these peak frequencies (f_{Max}) at different V_{dc}. Subsequent $\ln(f_{Max})$ vs V_{dc} plot shown in the figure 5.3b indeed fits nicely to straight line in support of the above phenomenological rate equation (5.2). Initial slope is very small (-0.04) for very low biases just above zero and abruptly increases to -0.19 after bias ~1.0 V as shown in the figure 5.3b. This drastic slope change around 1 V is connected with changes in the carrier dynamics due to the

onset of significant injection as evidenced from the I-V plot shown in figure 5.1. The intercept values of the straight lines fitted in the figure 5.3b, 13.21 and 13.34 for < 1V and > 1V regions respectively, also show a change. This intercept is intrinsically related to the entropic changes (ΔS) associated with the injection process following[47] $R' = \frac{1}{\tau} = \nu' \exp\left(-\frac{\Delta F}{k_B T}\right) = \left[\nu_0 \exp\left(\frac{\Delta S}{k_B}\right)\right] \exp\left(-\frac{\Delta H}{k_B T}\right)$ where change in free energy is $\Delta F = \Delta H - T\Delta S;\ \Delta H \approx E_{Th}$, ΔH being change in enthalpy. Increase in the slope after the start of significant injection at ~1 V is connected with a corresponding increase in the intercept and thereby an enhanced Δ*S*. This increase in Δ*S* for V_{dc} > 1 V possibly happens due to the increased presence of free charge carriers as increased number of available microstates for the concerned electronic transition.

Most importantly, we have also measured the differential capacitive response in the bias regime (V_{dc} > 1.5 V) where we could also measure electroluminescence signal (figure 5.1). The matching data of *f*dC/d*f* vs f for various $V_{dc} \geq 1.5$ V are displayed in figure 5.4a. With increasing bias above 1.5 V, injected charge reservoir of the active junction depletes through radiative recombination. It also drastically reduces the above mentioned entropic change Δ*S* connected with the number of carriers (microstates) in the reservoir of injected charges at the active junction. Corresponding intercept value of ln(f_{max}) with V_{dc} plot shown in the figure 5.4b, found to be 10.13, also reduces considerably as compared to the intercept values of the plots shown in the figure 5.3b before the light emission.

Moreover, we note that the peak frequency for *f*dC/d*f* shifts towards higher modulation frequencies instead. Consequently, the resultant Arrhenius like plot of ln(f_{Max}) with V_{dc} shows a seemingly counterintuitive positive slope (~ 1.99) for a reasonably linear fit. Plugging this into the phenomenological rate equation (5.4) then indicates the presence of *'negative activation energy'* for the bias activated rate processes above V_{dc} > 1.5 V. Therefore, at these higher injection levels, we certainly observe an exact opposite dynamical behavior of bias activation than what was seen in case of lower injection levels (figure 5.3). We must also mention here that the seemingly Boltzmann like behavior of rate processes [e.g. equation (5.3)] may no longer apply at higher carrier densities and our

data tends to show (figure 5.4b) slight deviations from linearity at higher biases which is still well below[1] the typical lasing threshold (~2.2 V) of these devices.

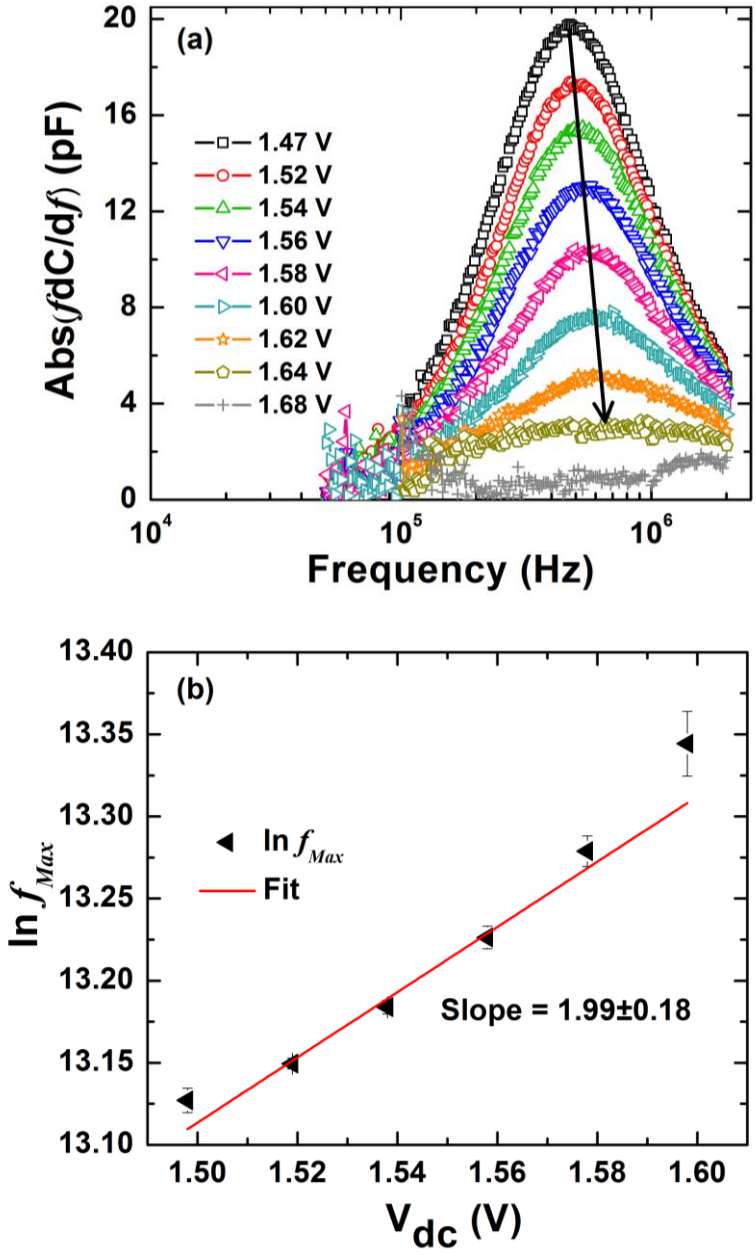

Figure 5.4: (a) Frequency derivative of capacitance after the onset of light emission. As the bias increases, peak shifts towards higher frequency side and the peak amplitude decreases. This derivative response completely vanishes around 1.7 V. This behavior is inverse of what has been observed before light emission as shown in the previous figure. (b) Positive slope of ln f_{Max} vs V_{dc} variation points towards the presence of a negative activation energy due to the presence of an intermediate bound state.

5.2.3 Understanding the observed negative activation energy: presence of intermediate excitonic bound state

To understand the origin of this negative activation energy, we now elaborate on the interpretation of activation energy (E_a) as per the usual understanding of transition state theories. In general, the activation energy is recognized as an energy barrier to a one-step transition process and actually determines the fraction of carriers which ultimately cross that free energy barrier. However, there are well known situations in physical chemistry where certain reaction rates decrease with increasing temperatures. Presence of a rate process with effective negative activation energy can be explained[48-50] by a certain type of transitions where a quintessential two-step configurational route has to evolve through another *'stable intermediate transition state'*. This happens in such a way that the low energy initial states make the transition to the final state at a much faster rate[48] than the high energy initial states. The net effective activation energy for the whole transition is given by Tolman's interpretation[48, 49, 51]

$$E_a = \langle E_{TS} \rangle - \langle E_R \rangle \tag{5.5}$$

where $\langle E_{TS} \rangle$ is the average energy of the stable intermediate transition state and $\langle E_R \rangle$ is the average energy of initial states which is typically proportional[48] to the energy of the thermal bath (~k_BT). Clearly, if the first term in equation (5.5) is lower than the second term then one can get a resultant activation energy which is negative. Since we observe such negative activation energy by measuring '*steady state'* electrical responses, we argue that in the present case this intermediate transition state represents a *'stable'* population.

It is possible that this stable intermediate transition state is associated with the formation of exciton like bound states with average binding energy $\langle E_{TS} \rangle$. To verify such excitonic presence at these injection levels we go back to equations (5.4) and (5.5). Combining these, we get

$$E_a = -m\frac{k_B}{\eta} = \langle E_{TS} \rangle - \langle E_R \rangle. \tag{5.6}$$

With decreasing temperature, $\langle E_R \rangle \sim k_B T$ should decrease and as a result the slope '*m*' given in equation (5.4) should also change with temperature. To verify this, we measured the *fdC/df* response just after the onset of light emission for different temperatures and present ln (f_{Max}) vs V_{dc} plots in figure 5.5. We indeed observe that the slope '*m*(T)' changes with changing temperatures.

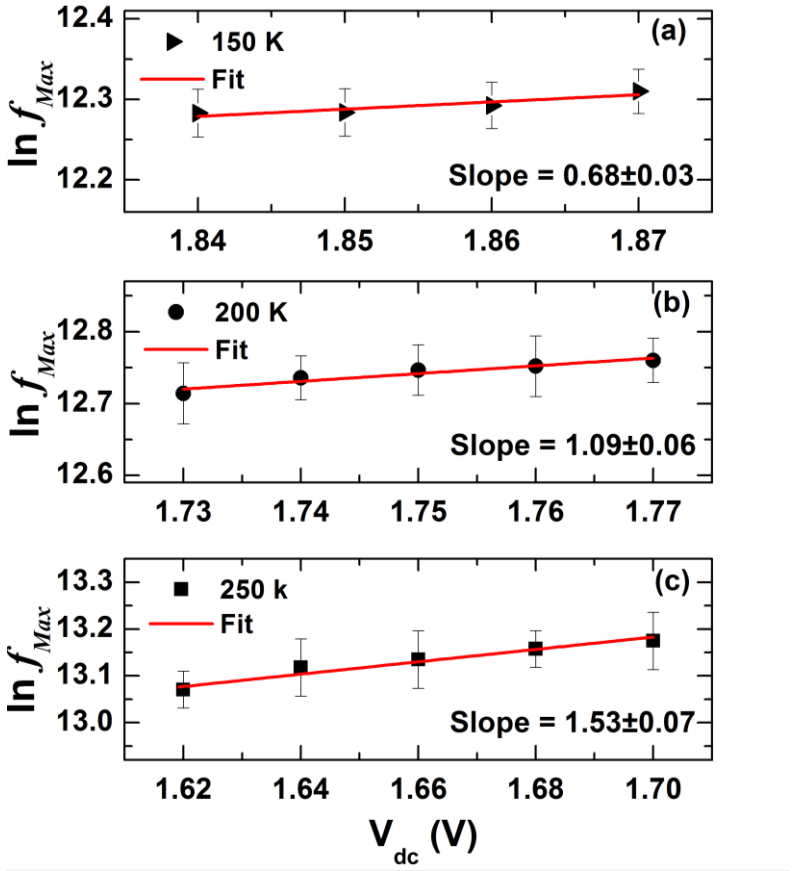

Figure 5.5: ln f_{Max} vs V_{dc} for different temperatures: (a) 150 K, (b) 200 K and (c) 250 K. Data fits nicely to the straight line as per the phenomenological equations (5.3) and (5.4). Slope of these fitted straight lines decreases with decreasing temperatures.

Not only do we see a decrease in slope, we also find that the frequency of peak response (f_{Max}) shifts to lower frequency side with decreasing temperature (as can be seen by observing ln f_{Max} values on y-axes of the plots). This is due to the thermal rate of defect response changes with changing temperature as discussed in chapters 1, 2 and 4.

To get a quantitative estimate of $\langle E_{TS} \rangle$, we replace $\langle E_R \rangle$ by energy ~k_BT of the thermal bath and by re-arranging terms we get:

$$m(T) = -\frac{\langle E_{TS} \rangle \eta}{k_B} + \eta T = b + nT \tag{5.7}$$

this suggests that a plot of slope *m(T)* vs *T* should be a straight line where '*b*' is the new intercept and '*n*' is the new slope. Figure 5.6 shows the variation of *m(T)* with temperature.

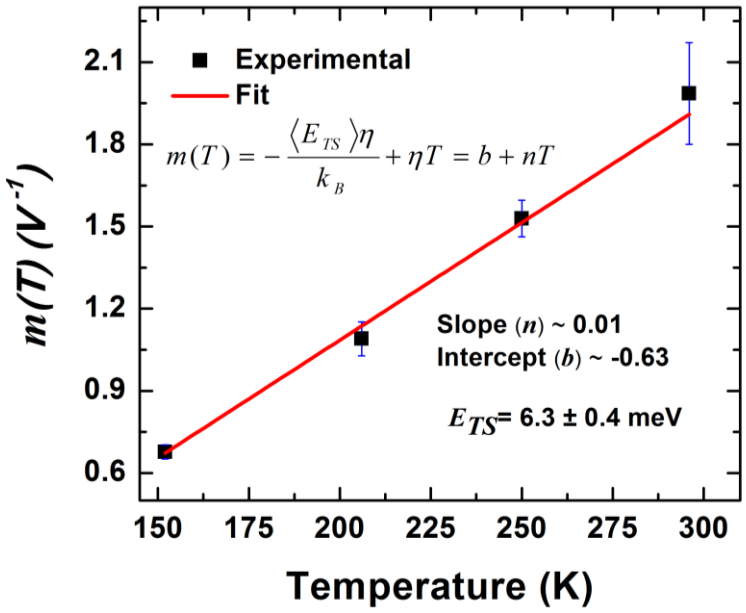

Figure 5.6: Temperature variation of slopes m(T) determined from ln f_{Max} vs V_{dc} plots. Estimated average energy of the intermediate transition state as per equation (5.7) is 6.3±0.4 meV. This coincides well with excitonic binding energy of such III-V materials[11].

By fitting a straight line to the data shown in figure 5.6, we obtain this value of η from the new slope '*n*' and then estimate $\langle E_{TS} \rangle$ from the intercept '*b*'. We also assume that both η and $\langle E_{TS} \rangle$ do not vary much with temperature in this range such that $\frac{\Delta \langle E_{TS} \rangle}{\langle E_{TS} \rangle} << 1$ even when the band gap of the material may change somewhat[52, 53]. Thus we estimate $\langle E_{TS} \rangle$ to be 6.3±0.4 meV, which closely matches with the binding energy of excitons in these materials[11]. Therefore, we recognize this effective *'negative activation energy'* in the

steady state frequency response of electrical impedance as a signature of the presence of a stable population of *'intermediate transition states'* which is *'excitonic bound state'*. For better understanding, we present a schematic configurational state diagram of the composite transition processes in figure 5.7.

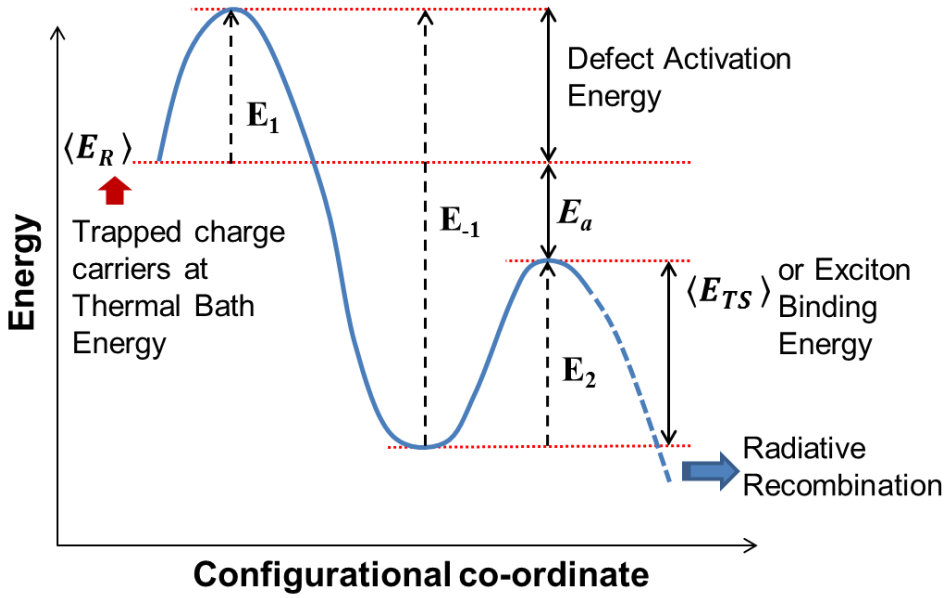

Figure 5.7: Schematic of the bias activated process of electroluminescence in the configurational diagram following the transition state theory[48-50] of activated response. Presence of a 'stable intermediate transition state' at an energy lower than the shallow defect levels (such that $E_{-1} > E_1+E_2$) leads to an effective overall transition having 'negative activation energy'.

Initially, charge carriers trapped in shallow defects are having average thermal energy $\langle E_R \rangle$ available to them at one temperature. In general, these carriers just have to cross the defect activation energy barrier E_1 and then directly take part in light emission. However, at higher injection levels, quasi Fermi levels move closer to band edges. Some of these carriers can now first populate this stable bound state, situated at energy $\langle E_{TS} \rangle$ lower than these shallow defect states and then make further transitions to produce light through radiative recombinations. This ensures that the condition of $E_{-1} > E_1 + E_2$ is satisfied[49] to have an effective negative activation energy for the overall transition process.

5.2.4 Optical signatures and suppression of bias activated response

To further confirm this assertion about electrical signatures of excitonic presence, we measured the standard electroluminescence (EL) spectra at different levels of carrier injections as a function of applied bias. Eventually, these excitons are screened out with increasing presence of charge carriers. Figure 5.8 presents the observed spectral features.

In figure 5.8a we plot integrated electroluminescence (EL) intensity as a function of injection current. It has been shown experimentally[39-42] as well as theoretically[54] that luminescence (photo or electro) L, follows a power law variation with excitation power P (photons or current) i.e. $L \sim P^k$. Value of the exponent can vary depending upon the properties of luminescence source mechanism. Generally, linear variation of L with P ($k = 1$) is associated with excitonic luminescence and quadratic dependence ($k = 2$) is associated with the luminescence from EHP[41]. For $V_{dc} > 1.7$ V ($I_{dc} > 0.2$ mA), integrated EL intensity vs injection current (I_{dc}) shows a power law with exponent ~1.7. This may indicate a mixture of both excitonic and EHP light emission at room temperature with a dominant presence of the latter. However for $V_{dc} < 1.7$ V, we see a sharp deviation from this power law which could be because of excitonic light emission. For a better confirmation of this fact we plot peak energy values and emission line width as a function of injection current in figure 5.8b. For lower biases there is no significant change in the EL peak energy and emission line width indicating excitonic light emission[11, 55].

On the other hand, above the applied bias of 1.7 V, EL peak energy starts to red shift and line width also increases drastically. Such sudden broadening of EL peak with increasing injection levels usually marks the onset of considerable exciton-exciton and exciton-charge carrier scattering. All these evidences certainly point towards a significant presence of band-gap renormalization effect[37] due to ensuing Mott transition[34, 35] of excitonic state to a dominant EHP state at such high injection levels.

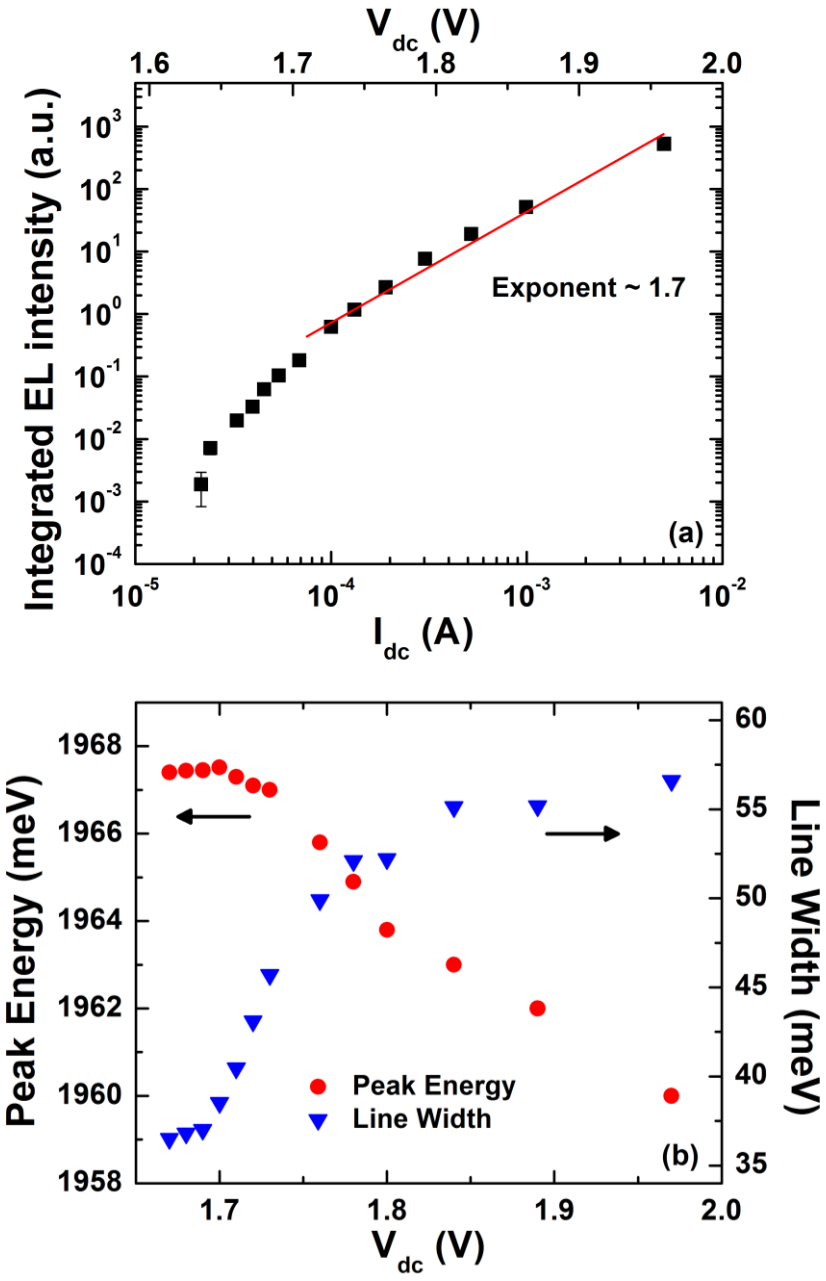

Figure 5.8: A log-log plot of integrated EL intensity with injected current showing power law behavior for higher current biases (with exponent ~1.7). This indicates the enhanced presence of EHP luminescence above ~1.7 V (~ I_{dc} = 0.2 mA). For low biases, deviation from this power law is observed due to excitonic light emission. This is further corroborated in (b) which shows corresponding transitions of EL peak positions and line width with applied bias. For low biases (< 1.7 V), peak position remains constant indicating excitonic presence in light emission. Above 1.7 V, EL peaks start to red shift due to band gap renormalization effects and line width starts to increase drastically. This is where we expect exciton-EHP Mott transition to occur and EHP recombination to dominate over the excitonic light emission.

To put it in the context of our electrical results, we also see in figure 5.4a that peaks in *fdC/df* tend to fade away just below this bias of ~1.7 V. Apparent disappearance of this steady state electrical signature of a stable intermediate transition state depicting negative activation energy, which is in all probability excitonic in nature, can be contemplated as an electrical signature of the onset of Mott transition. We must also mention that although there are observations which fit into power law behavior of integrated luminescence intensity with the increase in excitation density and also lie in between regimes claiming the presence of both the mechanisms, there are reports[41, 52, 53] with differences in exponent values for this power law. $k > 2$ has also been reported[39]. In short, there still are debates on the nature of luminescence from semiconductor quantum structures[41] and there is no unique tool to differentiate the source mechanisms around a Mott transition by optical means alone. However, plots in figure 5.8 showing the presence of a Mott transition at biases above 1.7 V matches well with the suppression of the electrical signature of excitonic response just below 1.7 V as evident from figure 5.4a. Therefore, this steady state all-electrical technique based on measuring the frequency dependent dynamic impedance response can be a useful additional tool to study the light emission physics in general.

5.3 Conclusions

We have probed the underlying electronic mechanisms of light emission in AlGaInP based multi-quantum well laser diodes electrically at room temperature. The frequency domain, steady state, small signal, electrical impedance response of electronic rate processes activated with dc bias across these semiconductor laser diode junctions reveals an intricate picture of carrier dynamics. We utilized frequency derivative of capacitance to study such bias activated response and used a phenomenological rate equation to understand these rate limited processes. The dynamical behavior of such electrical response inverts its trend after significant light emission and points to the presence of a negative activation energy process. We explain that the occurrence of such ‘negative activation energy’ is possibly due to the formation of a stable, intermediate

exciton like bound state in this essential multi-step transition rate. Spectral features of the electroluminescence and calculated average energy of this intermediate state matches well with the binding energy of excitons in this III-V material. Further increase in charge injection suppresses this differential capacitive response of excitonic presence indicating the Mott transition by electrical means. This contention is again fully supplemented by optical spectroscopies showing a clear band gap renormalization effect at the transition from excitonic to free electron hole plasma state. Our work, therefore, presents a novel all-electrical approach to probe condensed matter physics of light emitting semiconductor media and may also be extended to characterize the presence of exotic excitonic phases.

The work presented in this chapter is under review for publication arXiv:1312.7259 [cond-mat.mes-hall].

5.4 References

[1] K. Bansal and S. Datta, *J. Appl. Phys.* **110,** 114509 (2011).

[2] K. Bansal, *Phys. Status Solidi C.* **10,** 593-596 (2013).

[3] K. Bansal and S. Datta, *Physics of Semiconductor Devices* (Springer International Publishing p795 2014).

[4] K. Bansal and S. Datta, *MRS Proceedings* **1635**, mrsf13-1635-t07-05 (2014).

[5] K. Bansal and S. Datta, *Appl. Phys. Lett.* **102,** 053508 (2013).

[6] I. Pelant and J. Valenta, *Luminescence Spectroscopy of Semiconductors* (Oxford University Press, New York, 2012).

[7] C. F. Klingshirn, *Semiconductor Optics* (Springer, 3rd Edition, 2006).

[8] R. J. Elliott, *Phys. Rev.* **108,** 1384 (1957).

[9] R. S. Knox and N. Inchauspe, *Phys. Rev.* **116,** 1093 (1959).

[10] G. D. Scholes and G. Rumbles, *Nature Mater.* **5,** 683 (2006).

[11] M. Noriyasu and K. Fujiwara, *Appl. Phys. Lett.* **97,** 031103 (2010).

[12] K. Fujiwara, N. Tsukada and T. Nakayama, *Appl. Phys. Lett*. **53,** 675 (1988).

[13] P. Dawson, G. Duggan, H. I. Ralph and K. Woodbridge, *Phys. Rev. B* **28,** 7381 (1983).

[14] I. Galbraith, R. Chari, S. Pellegrini, P. J. Phillips, C. J. Dent, A. F. G. van der Meer et al. *Phys. Rev. B* **71,** 073302 (2005).

[15] L. V. Keldysh and Y. V. Kopaev, *Sov. Phys. Solid State* **6,** 2219 (1965).

[16] L. V. Butov, A. C. Gossard and D. S. Chemla, *Nature* **418,** 751 (2002).

[17] J. P. Eisenstein and A. H. MacDonald, *Nature* **432,** 691 (2004).

[18] L. V. Butov, C. W. Lai, A. L. Ivanov, A. C. Gossard and D. S. Chemla, *Nature* **417,** 47 (2002).

[19] K. Yoshioka, E. Chae and M. Kuwata-Gonokami, *Nat. Commun*. **2,** 328 (2011).

[20] D. Snoke and G. M. Kavoulakis, arXiv:1212.4705 [cond-mat.quant-gas].

[21] A. A. High, J. R. Leonard, A. T. Hammack, M. M. Fogler, L. V. Butov, A. V. Kavokin, K. L. Campman and A. C. Gossard, *Nature* **483,** 584 (2012).

[22] H. Deng, H. Haug, Y. Yamamoto, *Rev. Mod. Phys.* **82,** 1489 (2010).

[23] J. Kasprzak, M. Richard, S. Kundermann, A. Baas, P. Jeambrun, J. M. J. Keeling et al. *Nature* **443,** 409 (2006).

[24] F. Manni, Y. Leger, Y. G. Rubo, R. Andre and B. Deveaud, *Nat. Commun*. **4,** 2590 (2013).

[25] C. W. Lai, N. Y. Kim, S. Utsunomiya, G. Roumpos, H. Deng, M. D. Fraser, T. Byrnes, P. Recher, N. Kumada, T. Fujisawa and Y. Yamamoto *Nature* **450,** 529 (2007).

[26] S. Utsunomiya, L. Tian, G. Roumpos, C. W. Lai, N. Kumada, T. Fujisawa, M. Kuwata-Gonokami, A. Loffler, S. Hofling, A. Forchel and Y. Yamamoto, *Nature Physics* **4,** 700 (2008).

[27] F. P. Laussy, A. V. Kavokin and I. A. Shelykh, *Phys. Rev. Lett.* **104,** 106402 (2010).

[28] T. Ogawa, Y. Tomio and K. Asano, *J. Phys.: Condens. Matter* **19,** 295205 (2007).

[29] D. Kremp, D. Semkat and K. Henneberger, *J. Phys: Conference Series* **220,** 012004 (2010).

[30] E. Hanamura and H. Haug, *Phys. Rep.* **33,** 209 (1977).

[31] H. Deng, G. Weihs, C. Santori, J. Bloch and Y. Yamamoto, *Science* **298,** 199 (2002).

[32] H. Deng, G. Weihs, D. Snoke, J. Bloch and Y. Yamamoto, *Proc. Natl. Acad. Sci. U.S.A.* **100,** 15318 (2003).

[33] S. I. Tsintzos, P. G. Savvidis, G. Deligeorgis, Z. Hatzopoulos and N. T. Pelekanos, *Appl. Phys. Lett.* **94,** 071109 (2009).

[34] N. F. Mott, *Rev. Mod. Phys.* **40,** 677 (1968).

[35] D. Jerome, T. M. Rice and W. Kohn, *Phys. Rev.***158,** 462 (1967).

[36] Z. K. Tang, G. K. L. Wong, P. Yu, M. Kawasaki, A. Ohtomo, H. Koinuma and Y. Segawa, *Appl. Phys. Lett.* **72,** 3270 (1998).

[37] S. D. Sarma, and D. W. Wang, *Phys. Rev. Lett.* **84,** 2010 (2000).

[38] T. Takagahara and K. Takeda, *Phys. Rev. B* **46,** 15578 (1992).

[39] K. X. Chen, Y. A. Xi, F. W. Mont, J. K. Kim, E. F. Schubert, W. Liu, X. Li and J. A. Smart, *J. Appl. Phys*. **101**, 113102 (2007).

[40] M. Noriyasu and K. Fujiwara, *Appl. Phys. Lett*. **97**, 031103 (2010).

[41] G. T. Dang, H. Kanbe and M. Taniwaki, *J. Appl. Phys.* **106**, 093523 (2009).

[42] K. Fujiwara, N. Tsukada and T. Nakayama, *Appl. Phys. Lett*. **53**, 675 (1998).

[43] E. O' Connor, S. Monaghan, R. D. Long, A. O'Mahony, I. M. Povey et al. *Appl. Phys. Lett.* **94,** 102902 (2009).

[44] T. Walter, R. Herberholz, C. Müller, and H. W. Schock, *J. Appl. Phys.* **80,** 4411 (1996).

[45] Pablo P. Boix, Germà Garcia-Belmonte, Udane Muñecas, Marios Neophytou, Christoph Waldauf, and Roberto Pacios, *Appl. Phys. Lett*. **95**, 233302 (2009).

[46] J. V. Li, and D. H. Levi, *J. Appl. Phys.* **109,** 083701 (2011).

[47] S. Datta, J. D. Cohen, Y. Xu, A. H. Mahan and H. M. Branz, *J. Non-Cryst. Sol*. **354**, 2126 (2008).

[48] M. Mozurkewich and S. W. Benson, *J. Phys. Chem.* **88,** 6429 (1984).

[49] J. L. Muench, J. Kruuv and J. R. Lepock, *Cryobiology* **33,** 253 (1996).

[50] J. R. Alvarez-Idaboy, N. Mora-Diez, and A. Vivier-Bunge, *J. Am. Chem. Soc.* **122,** 3715 (2000).

[51] R. D. Levine and R. B. Bernstein, *Molecular Reaction Dynamics* (Oxford University Press, New York, 1974, p. 250).

[52] K. P. O'Donnell and X. Chen, *Appl. Phys. Lett*. **58,** 2924 (1991).

[53] S. Datta, B. M. Arora and S. Kumar, *Phys. Rev B* **62**, 13604 (2000).

[54] T. Schmidt, K. Lischka and W. Zulehner, *Phys. Rev. B* **45**, 8989 (1992).

[55] E. F. Schubert and W. T. Tsang, Phys. Rev. B **34**, 2991 (1986).

Chapter 6

Generalized Frequency Dependence of Negative Capacitance and Bias Activated Response

6.1 Introduction

We have discussed how defect response couples with radiative recombination process in frequency[1-3] and temperature[4, 5] domain to produce impedance changes with the light emission onset in quantum well based electroluminescent diodes (ELDs). We have also monitored bias activated defect response to explore the light emission mechanism in these devices[6]. We observed how the effect of bias can be plugged in to explain the defect response in place of temperature following our phenomenological rate equation of bias activated process.

In the context of negative capacitance (NC), we pointed out in chapter 3 that our understanding based on the mutual competition of two different time scale processes (radiative recombination and defect response) provides a most generalized description of NC that can accommodate many of the reported results and explanations. Our description goes well in agreement with the most cited works of the field by Hess et al.[7] who presented the improved analytical expression for junction current to include the possibility of negative capacitance and Jonscher et al.[8, 9] who developed the generalized expression for diode admittance in terms of transient current behavior. Most of the studies in the context of NC, including electroluminescent and non-luminescent diodes report occurrence and enhancement of NC for lower modulation frequencies[10]. We also observed NC effect for low modulation frequencies in case of quantum well based ELDs.

In this chapter we present the capacitance response of functionally different junction diodes under high injection levels or forward bias. We will demonstrate that quantum dot based ELDs show NC effect at low modulation frequencies like quantum well based ELDs. Interestingly, in case of non-luminescent Si-based diodes we will show that NC behavior is observed for higher frequencies while low frequencies show the usual positive capacitance response. Observation of drastically different frequency dependence of NC in two diodes with different functionalities can only be explained by the consideration of mutually competing different time scale processes involving available charge carrier density, as we proposed[1, 2]. To probe these processes, we will discuss the bias activated capacitance derivative response from the devices. We will show that in case of Si diodes also, bias activated capacitance derivative follows our phenomenological equation (5.2).

Hence, we will present the results giving a generalized completeness to the work and techniques we have presented so far. We recognize that although the higher injection levels are always required to give rise to inductive like reactance or negative capacitance effect; to understand the frequency characteristics of such response, one has to go into the details of the dynamical processes happening inside the device and their mutual interplay. Presence and absence of a fast radiative recombination channel competing with slower defect related response, involving charge carriers, can affect the frequency dependent reactance component of diodes.

6.2 Experimental methods

In addition to the AlGaInP based multi quantum well laser (QWL) diodes described in chapter 2, we have used a variety of different diodes for this work. We used InGaAs based quantum dot laser diodes grown by molecular beam epitaxy (kindly provided by Prof. M. Henini, University of Nottingham, Nottingham, UK). Details of sample structure and growth parameters can be found in the reference 11. We also used commercially available Si based diodes 1N 4001, 1N 4007 and SFH-213 p-i-n photodiode.

6.3 Results and discussion

Figure 6.1a and 6.1b show the variation of measured capacitance and voltage modulated electroluminescence (VMEL) respectively for quantum dot laser (QDL) diode.

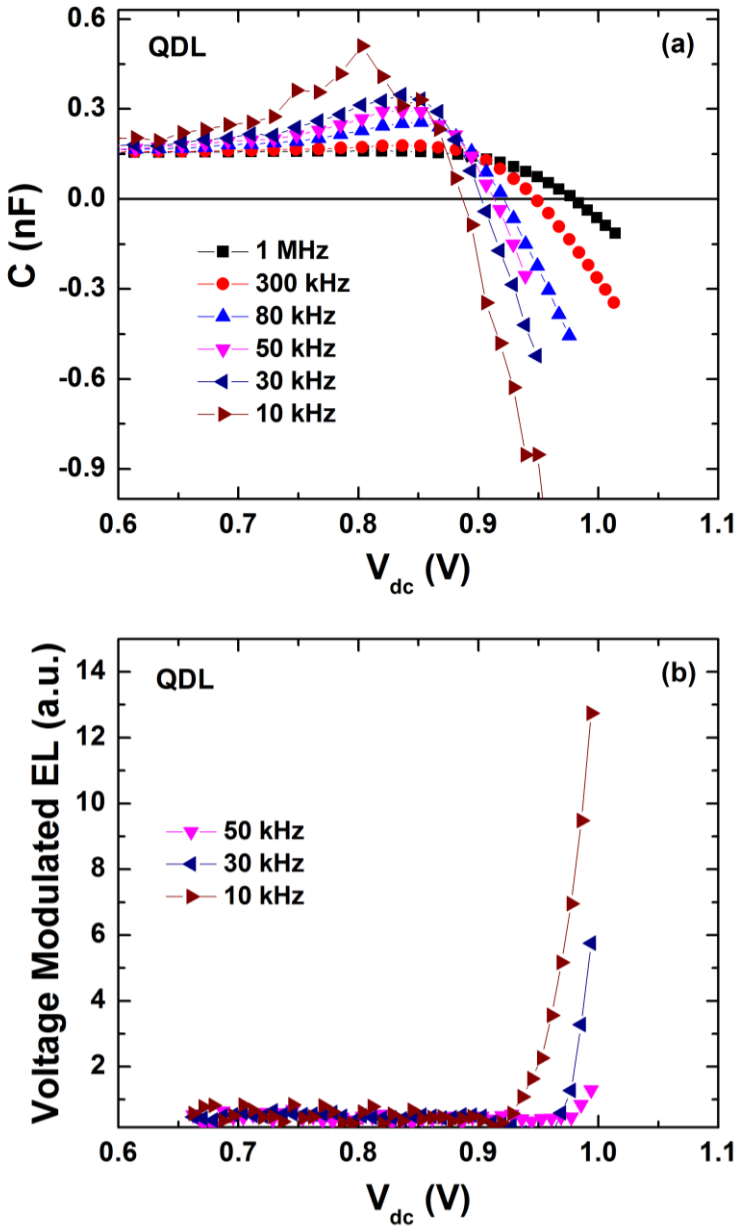

Figure 6.1: (a) Capacitance and (b) voltage modulated electroluminescence signal for InGaAs quantum dot laser diodes[11] grown by molecular beam epitaxy. As the bias increases, capacitance becomes negative. Simultaneously we observe the onset of modulated light emission between the V_{dc} range of 0.9 V to 1 V. With decreasing applied modulation frequencies, onset of both NC and VMEL shifts to lower biases and their magnitude increases.

We observe that as the bias increases, we start to see the onset of NC and modulated light emission. These onset biases shift to lower values as the frequency of the applied modulation is lowered. Also, the magnitude of both NC and VMEL increases with decreasing modulation frequencies. The occurrence of negative capacitance, its frequency dependence and correlation with the modulated emission can be explained by considering the role of sub-band gap defect levels in charge recombination dynamics as discussed in chapter 2, section 2.3.2 and described further in the following section.

6.3.1 Different dynamical dependence of negative capacitance on applied modulation frequency for different sets of diodes

Figure 6.2a shows the variation in measured small signal capacitance (C) with forward bias for QWL at different modulation frequencies. As the bias increases, capacitance becomes negative. In log scale, given frequency response curve terminates at a point where it becomes negative (this is a different presentation of the results discussed in chapter 2). With lower applied modulation frequency, the onset of negative capacitance occurs at lower forward biases. On the other hand, frequency dependence of negative capacitance is completely reversed in case of Si diode (1N 4001) as shown in figure 6.2b. As the frequency decreases, we observe negative capacitance onset shifting towards higher applied injection levels. We also measured such negative capacitances in other Si based diodes (p-i-n photo diode SFH 213 and 1N 4007), all of which gave qualitatively similar frequency dependence.

In our earlier studies[1, 2], to explain the occurrence of negative capacitance in light emitting diode structures, we considered the mutual competitive dynamics of sub-band gap defect levels and radiative recombination of available charge reservoir at high injection levels. Depending upon the applied modulation frequency and temperature of the device, defects within a certain energy depth E_{Th} can respond[1] to the applied signal and contribute to the measured impedance (shaded region in figure 2.8, chapter 2). Therefore, one can write the standard expression relating E_{Th}, thermal rate of charge carriers trapping and de-trapping from defect states (τ) and modulation frequency (f) as: $f \approx 1/\tau = \nu \exp\left(-E_{Th}/k_B T\right)$. When applied modulation is comparable to $1/\tau$, defect

responds to applied sinusoidal modulation which ultimately affects the measured impedance of the active junction.

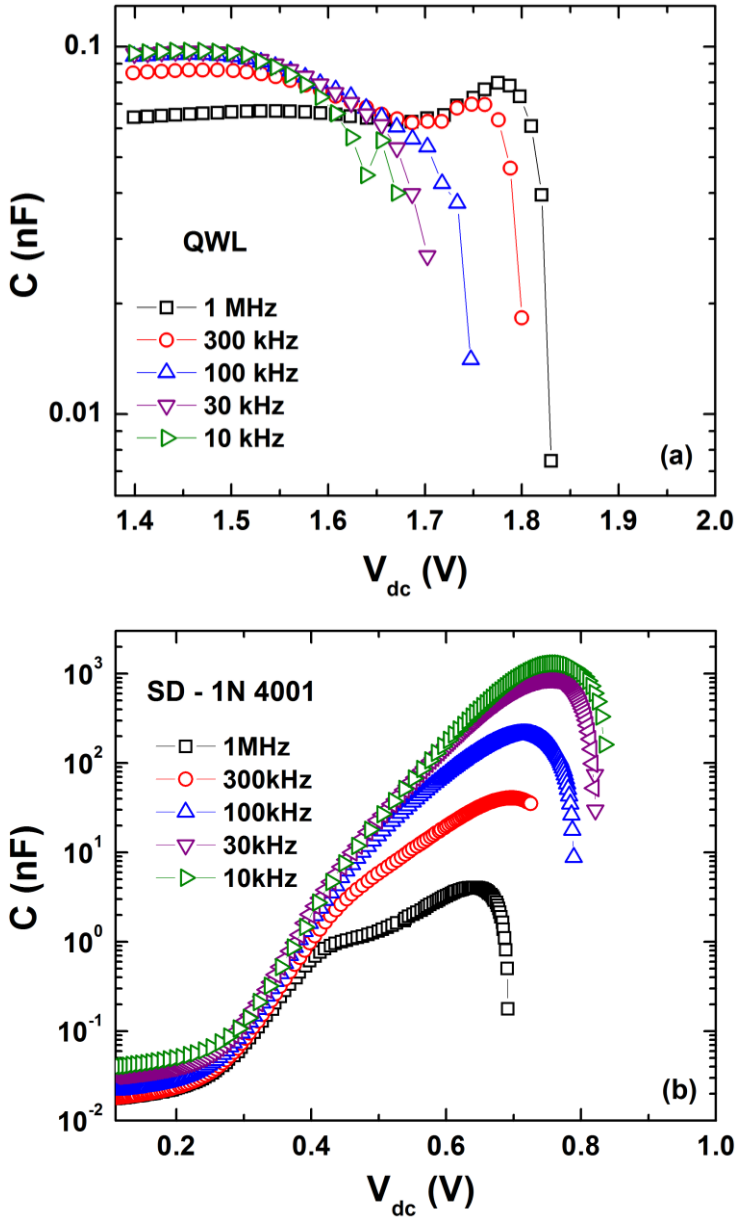

Figure 6.2: Variation of capacitance with bias under different applied modulation frequencies for (a) quantum well laser diode DL 3148-025 (QWL) and (b) Si diode (SD - 1N 4001). The point where a particular data plot terminates is the starting of negative capacitance. In Si diodes high frequency gives negative capacitance for lower biases which is reverse of what is seen in QWL. We also observed similar behavior in other Si based diodes including 1N 4007 and SFH 213 photodiode.

Onset of light emission in ELDs interrupts the total number of charge carriers available at the junction which includes the contribution from defect levels ($n_{Trapped}$). Radiative recombination process consumes charge carriers coming out of the defect states irreversibly and faster than they are replenished. As a result, at the end of the sinusoidal modulation cycle, equilibrium defect population is not recovered. This can cause a transient change in the quasi Fermi level (which tracks the charge carrier population) position and in the carrier reservoir at the junction which induces a compensatory lagging behind current to establish the equilibrium. Consequently, we observe an 'inductive like' reactance, experimentally measured as negative capacitance. The more the contribution from defect levels ($n_{Trapped}$), the more compensation would be required to achieve such equilibrium. Then it is easy to understand from the rate equation (2.2, chapter 2) that with decreasing frequency energy depth (E_{Th}) increases. This increases $n_{Trapped}$ and hence the magnitude of compensatory 'inductive like' current which ultimately increases the magnitude of negative capacitance at decreasing modulation frequencies as has been observed in the past[1, 2]

Similar explanation, based on competing different time scale processes, can be extended to understand the impedance response of Si-based diodes too. However, in case of non-luminescent Si-based diodes, such fast (~ps) radiative recombination is absent. Still the occurrence of negative capacitance points towards the presence of different mutually competing rate limited electronic processes with different time scales.

To further examine the dynamic dependence of negative capacitance on frequency, in figure 6.3, we plot and compare the bias values at which negative capacitance starts to occur (V_{NC}) at a particular modulation frequency for two different sets of diodes. In case of ELDs, as shown in figure 6.3a, V_{NC} increases monotonically with increasing applied frequency. This behavior remains qualitatively the same for quantum well laser diodes (QWL) and quantum dot laser diodes (QDL). This is also in agreement with the work by Feng et al. [12].

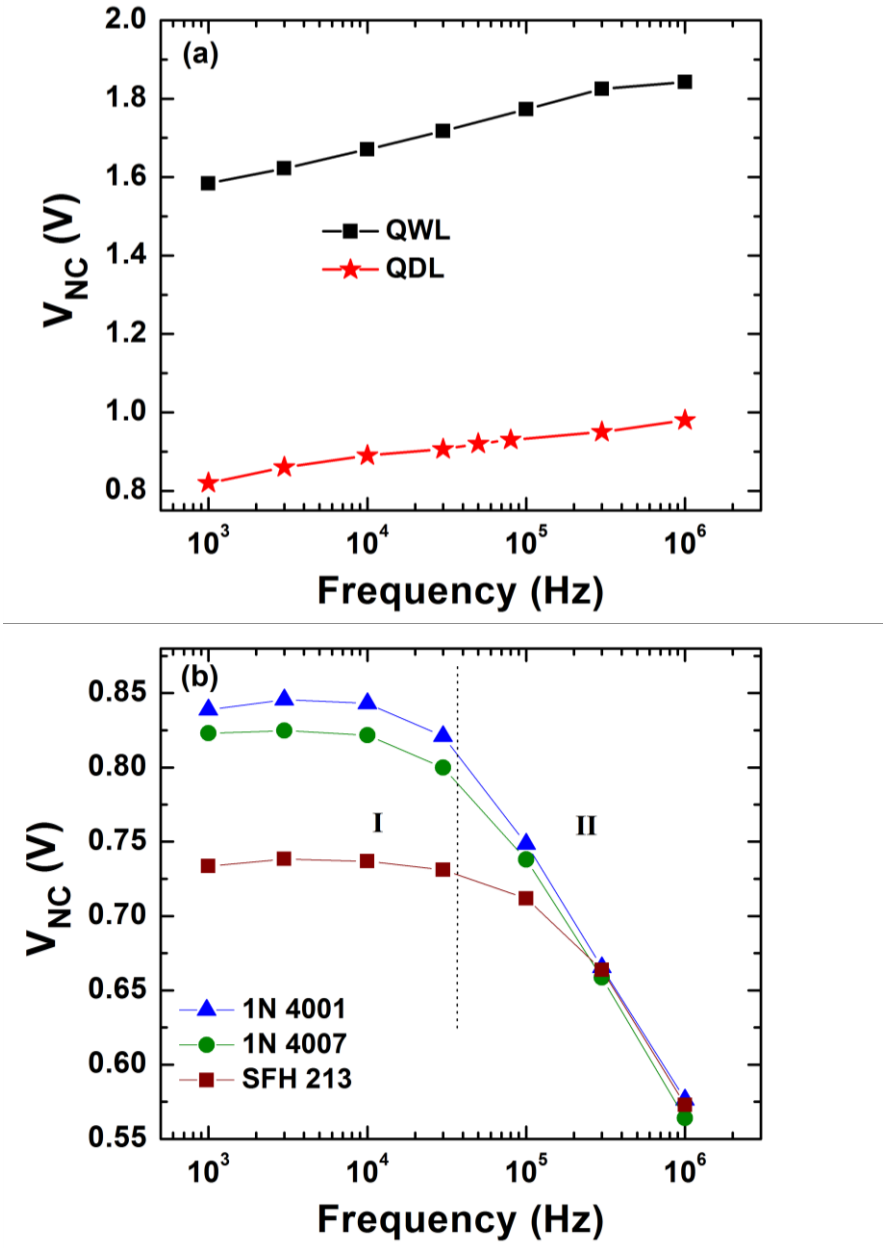

Figure 6.3: Variation of the bias at which negative capacitance is observed (V_{NC}) for different applied modulation frequencies for (a) quantum well laser diodes (QWL) and quantum dot laser diodes (QDL) and (b) Si based diodes. For laser diodes, V_{NC} increases monotonically with increasing frequencies. For Si diodes, V_{NC} first stays somewhat constant (region I) and then decreases with increasing frequencies (region II).

It is important to note that the defect contribution can only be activated if it exists below the quasi Fermi level in the band gap[1]. As we increase the frequency, we decrease the depth E_{Th}, and hence contribution from relatively deeper defects is lost. To overcome this, quasi Fermi level has to move towards the band edge to increase the effective defect

contribution, which can be achieved by increasing applied bias (at a constant temperature). Once the defect contribution is significant to compete with the radiative recombination process, we start observing NC. This is why we see that as the modulation frequency increases, V_{NC} increases in ELDs[1].

On the other hand, in figure 6.3b we observe that for all the Si based 'non-luminescent' devices used, V_{NC} does not follow monotonic behavior with increasing *f*. There, two different regions can be visualized depending upon the variation of V_{NC} with frequency. In region I, V_{NC} is relatively independent of applied modulation frequencies for lower frequency ranges below ~5 x 10^4 Hz and remains nearly constant. In region II, above ~5 x 10^4 Hz, V_{NC} decreases with increasing frequencies which is the exact opposite of what is observed in case of electroluminescent diodes.

6.3.2 Frequency dependent impedance response

To understand the frequency variation of defect response we need to see the impedance response as a function of modulation frequency. Figure 6.4 shows the variation of $G/2\pi f$ (where G is conductance) and capacitance (C) for Si-diode 1N-4001. This is analogous to the plots shown in figure 5.2 (chapter 5) for QWL.

As we discussed in chapter 5 in connection with defect response, usually, a peak in $G/2\pi f$ is observed with frequency or temperature variation. This peak corresponds to a position of maximum response from the defects or the position where quasi Fermi level crosses the respective defect energy level[13]. A corresponding inflection point is always observed in capacitance (C) due to their mutual connection through Kramer-Kronig relations[14]. The observed defect response peak in this case, as shown in figure 6.4a, is comparatively broader than that in case of QWL (figure 5.2a). In capacitance, we observe two inflection points in different frequency ranges as compared to a single inflection point observed in case of QWL (figure 5.2b). In this case also, we observe negative capacitance values for high biases but for higher modulation frequencies. When modulation frequency approaches 2 MHz (the highest value in our experimental parameter range), capacitance values seem to converge to a smaller value.

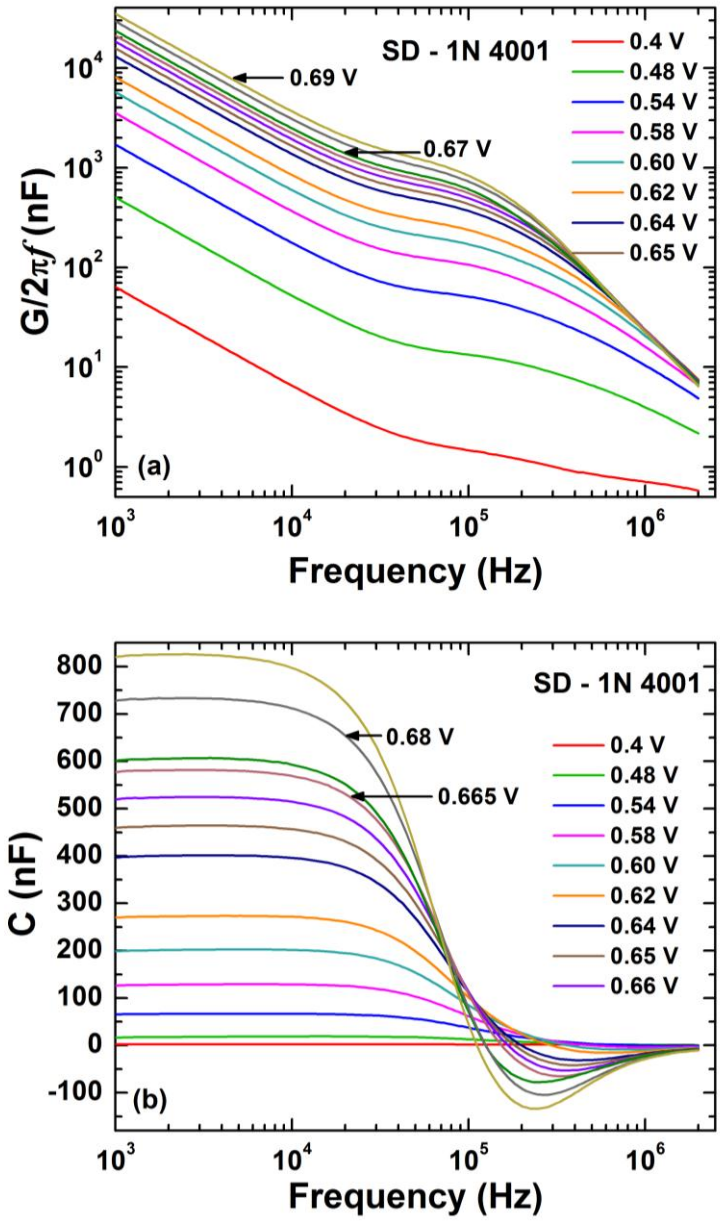

Figure 6.4: (a) Plots of G/2πf vs f show peak like features. Peak observed in this case are broader as compared to the peaks observed in case of quantum well laser shown in chapter 5, figure 5.2a. (b) Capacitance (C) shows two inflection points in two different frequency regimes. Here also we observe negative capacitance but for higher modulation frequencies. We note that as the modulation frequency reaches 2 MHz, capacitance seems to converge to a low value.

To probe the variation of defect response with applied bias variation, we used capacitance derivative technique[13, 15, 16] as discussed in chapter 5. Like in the case of QWL diodes[6], we look at the bias activated dynamic rate processes at room temperature

to probe the device response under carrier injection. Experiments showed that[6] the dependences of rate process on T and V_{dc} are mutually inverse and we wrote it as $1/T=\eta V_{dc}$ where η is a proportionality constant for correct dimensionality. This equation can then be modified to the form $f_{Max} \approx \nu \exp\left(-E_{Th}\eta V_{dc}/k_B T\right)$. We do expect a different dynamics of these processes due to the different frequency dependence of the capacitance response in this case.

Figure 6.5a shows variation of fdC/df for a wide range of applied modulation frequencies for Si diode 1N 4001. We see two prominent peaks in the fdC/df vs f plot showing the presence of two defect channels with different time scales and strengths. However, in case of ELDs, we only observed a single peak in such response showing the dominance of single defect channel (as shown in figure 5.3a, chapter 5). For simplicity, we name low and high frequency range peaks as peak 1 and peak 2 respectively. As the bias increases, f_{Max} for both the peaks shifts to the respective lower frequency sides. The variation of lnf_{Max} with applied bias is plotted in figure 6.5b. Such linear variation of ln f_{Max} with V_{dc} validates our conceived equation as mentioned above (also equation (5.2) in chapter 5). Values of the slopes are found to be -4.3±0.1 for lower frequency response and -13.0±0.3 for higher frequency response. This difference may be related to the entropic contribution to free energy barrier for a particular electronic defect[17]. Unlike ELDs[6], Si-based diode does not show any sign change of slopes in lnf_{Max} vs V_{dc} plot which was related to the presence of excitons during light emission. This again emphasizes the point that qualitatively different internal dynamics of ELDs and Si based diodes is responsible for the observed difference in the frequency dependence of negative capacitance response.

In these bias activated processes, it is important to note that as the modulation frequency reaches between ~5x10^4 to 10^6 Hz, peak 2 starts to respond significantly only above 0.45 V, however, the slower defect response (peak 1) starts appearing at much lower biases. Density of defects responding at such frequencies is directly proportional to the derivative fdC/df[13, 16] and hence the area under the peaks corresponds to the density of defects within the energy range spanned by the corresponding range of modulation frequency.

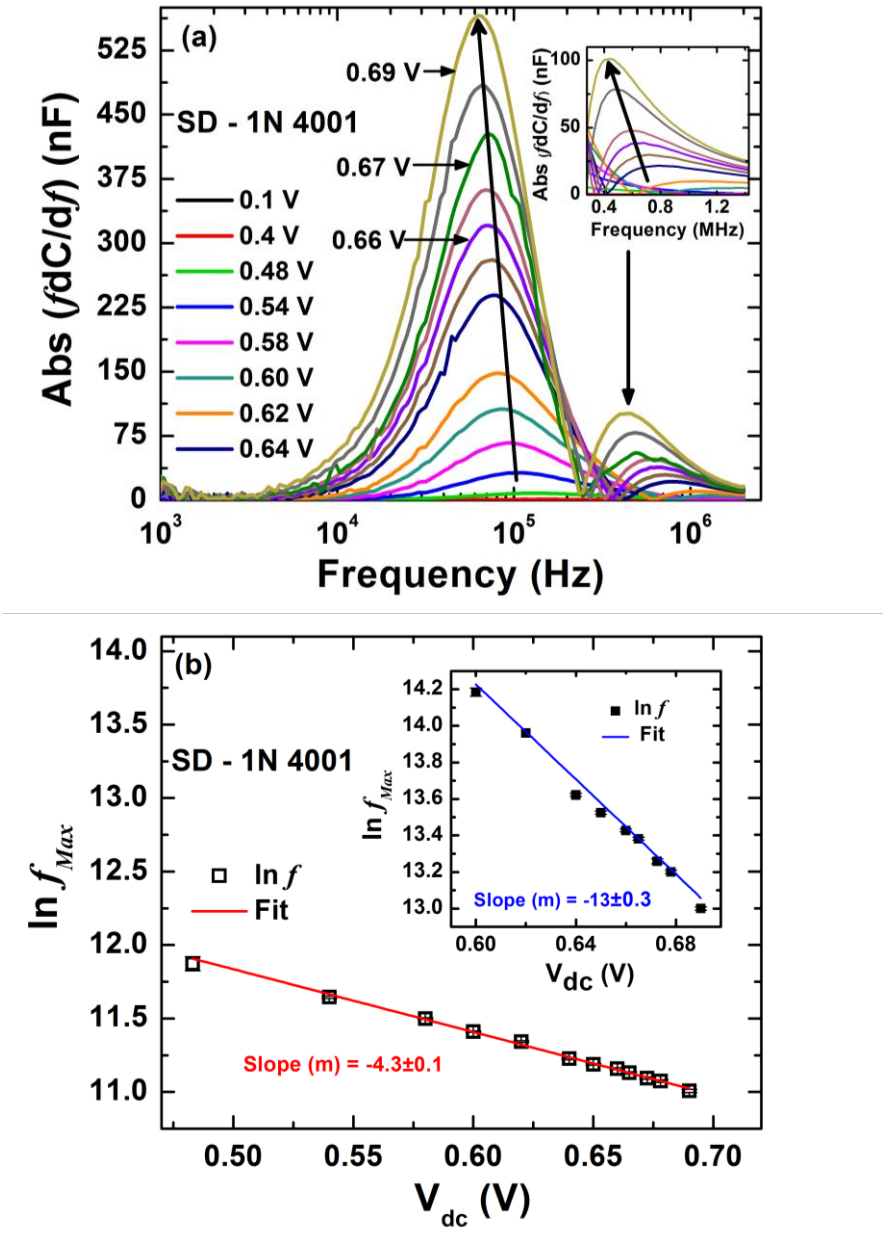

Figure 6.5: (a) Absolute value of fdC/df showing two peaks at different frequency positions for Si diode. We call lower and higher frequency range peaks, peak 1 and peak 2 respectively. Variation of peak position towards lower frequencies with increasing applied bias can be more clearly observed. (b) Peak frequency values are used to plot lnf_{Max} with applied bias (V_{dc}) for peak 1 and in inset for peak 2. Peak frequency decreases with increasing bias.

In figure 6.6, we see that the area acquired by the right half of peak 1 (which overlaps with peak 2) increases in correlation with the area acquired by peak 2. Net defect density of peak 1 is much larger as compared to peak 2. However, at large forward

biases, rate of increase in peak 2 is faster than that in peak 1. This can be viewed from the plot in the inset of figure 6.6, where values are normalized with respect to the highest area value for respective peaks. We ascribe this observed correlation as an evidence for competition of two rate limited processes governing voltage onset of respective negative capacitance.

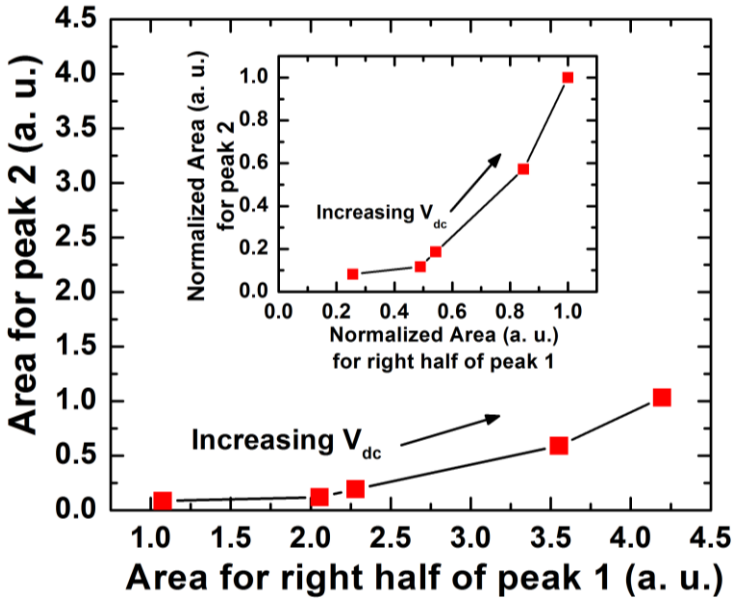

Figure 6.6: Shows that the area acquired by the right half of peak 1 and peak 2 increases with increasing bias in a correlated fashion. Lines joining the data points are for visual clarity only. In the inset we plot the normalized area showing that with increasing bias, peak 2 acquires a faster rate of increase in area.

In Si diodes, two differently sized defect responses (bigger peak 1 and smaller peak 2) overlap (within similar frequency/energy ranges) and compete with each other for the overall impedance of the junction. At modulation frequency > $5x10^4$ Hz, steady state situation is not recovered at the end of the sinusoidal modulation because the presence of a dominant but slower defect channel interrupts the dynamics of relatively smaller but faster defect response. This results in a mismatch of charge trapping and emission from these two defect channels over a complete modulation cycle. Subsequently, population from these defects can undergo a transient change, giving rise to a compensatory lagging behind current and hence the negative capacitance[1, 2] in the measured steady state response of the active junction. In this region II of figure 6.3b, the contribution from

relatively faster defect channels is reduced with decreasing frequency. This demands further increase in applied bias to generate significant contribution from shallower and faster channels which compete with slower channels to produce any negative capacitance. As a result, V_{NC} increases with decreasing frequencies. However, this is qualitatively opposite to the case of ELDs[1] where fast and dominant radiative recombination irreversibly depletes the charge carrier reservoir and competes with much slower and smaller steady state response from defect states.

As we decrease the frequency below ~$5x10^4$ Hz, we modulate the defects which only have the slower component of thermal rate of carrier exchange with the band edge. However, until a significant amount of bias is applied, that can activate the shallower defects/ faster channels, we do not observe any NC effect. For high enough forward biases, contribution of faster channels again competes with the slower defect response and NC is observed (figure 6.3b, region I). Since the activation of this high frequency defect response (peak 2) with increasing bias does not depend on slower modulation frequencies, we observe that V_{NC} in region I of figure 6.3b also does not vary much with changing modulation frequencies. It is important to mention here that in some of the Si-based devices, frequency dependence of NC, qualitatively similar to that of ELDs has been reported[18, 19]. We speculate that this could be due to the interplay of different time scale processes in a manner similar to ELDs.

As we reach the very high frequency range (around 2 MHz, which is also the limit of our experimental setup), capacitance approaches a small positive value as shown in figure 6.4b. This can be due to the absence of any competing defect response in this frequency range. In this case, capacitance value will be governed by the geometric capacitance of the junction.

6.4 Conclusions

We observed different frequency dependent dynamics of impedance response in electroluminescent diodes and non-luminescent Si-based diodes under charge carrier

injection. In both sets of devices we see negative capacitance response with increasing bias however, frequency dependence is mutually inverted. In electroluminescent diodes negative capacitance effect increases with lower applied frequencies whereas in Si-based diode it is observed for higher applied frequencies. We studied bias activated differential capacitance response to understand the observed difference in capacitance behavior. The phenomenological rate equation we developed for such response agrees well with the experimental results in case of Si diodes too. We explained that the reason behind the observed negative capacitance effect is the involvement of different radiative and non-radiative channels in the time dependent dynamics of the devices. In electroluminescent diodes, faster radiative recombination competes with slower and weaker defect response. In Si diodes, two overlapping defect channels of varied strength and time scales compete and cause negative capacitance. This study can help us to better understand the electronic processes giving rise to negative capacitance like response in junction diodes. These understandings can easily lead to new device functionalities. To further identify the nature of a particular electronic defect and thereby optimize the device application, one can extend this study by carefully looking into the necessary details of a typical device structure.

The work presented in this chapter has been published in Applied Physics Letters, Vol. 105, p. 123503, 2014.

6.5 References

[1] K. Bansal and S. Datta, *J. Appl. Phys*. **110**, 114509 (2011).

[2] K. Bansal, *Phys. Status Solid (C)* **10**, 593 (2013).

[3] K. Bansal and S. Datta, *MRS Proceedings* **1635**, mrsf13-1635-t07-05 (2014).

[4] K. Bansal and S .Datta, *Appl. Phys. Lett*. **102**, 053508 (2013).

[5] K. Bansal and S. Datta, *Physics of Semiconductor Devices: Environmental Science and Engineering, (Springer Publishing,* p795 (2014).

[6] K. Bansal and S. Datta, arXiv:1312.7259 [cond-mat.mes-hall].

[7] S. E. Laux and K. Hess, *IEEE Trans. Electron. Devices* **46**, 396 (1999).

[8] A. K. Jonscher, *J. Chem. Soc., Faraday Trans. II* **82**, 75 (1986).

[9] M. Ershov, H. C. Liu, L. Li, M. Buchanan, Z. R. Wasilewske and A. K. Jonscher, *IEEE Trans. Electron. Devices* **45**, 2196 (1998).

[10] See references 12-49 in chapter 3.

[11] A. Polimeni, M. Henini, A. Patane, L. Eaves, P. C. Main and G. Hill, *Appl. Phys. Lett.* **73**, 1415 (1998).

[12] L. F. Feng, Y. Li, D. Li, X. D. Hu, W. Yang, C. D. Wang and Q. Y. Xing, *Appl. Phys. Lett*. **101**, 233506 (2012).

[13] T. Walter, R. Herberholz, C. Müller, and H. W. Schock, *J. Appl. Phys*. **80,** 4411 (1996).

[14]G. L. Miller, D. V. Lang and L. C. Kimerling, *Ann. Rev. Mater. Sci*. **7**, 377 (1977).

[15]P. Boix, G. Garcia-Belmonte, U. Muñecas, M. Neophytou, C. Waldauf, and R.Pacios, *Appl. Phys. Lett.* **95**, 233302 (2009).

[16]J. V. Li and D. H. Levi, *J. Appl. Phys.* **109,** 083701 (2011).

[17] S. Datta, J. D. Cohen, Y. Xu, A. H. Mahan and H. M. Branz, *J. Non-Cryst. Sol*. **354**, 2126 (2008).

[18] M. Anutgan and I. Atilgan, *Appl. Phys. Lett*. **102,** 153504 (2013).

[19] F. Lemmi and N. M. Johnson, *Appl. Phys. Lett.***74**, 251 (1999).

Chapter 7

Summary and Conclusions

In this thesis we presented the studies on the properties of electroluminescent diodes (AlGaInP based multi quantum well structures) under charge carrier injection. We probed optical and electrical properties along with their mutual connection by mainly using impedance spectroscopy and modulated electroluminescence spectroscopy for relatively low modulation frequencies. We proposed that under charge carrier injection, these diodes may not follow the conventional theory of junction diodes based on depletion approximation and electrostatic description. Observed negative capacitance (NC) under high charge carrier injection and low modulation frequencies validated our proposition. NC was found to be related with the voltage modulated electroluminescence, with both the quantities showing simultaneous onset and similar frequency dependence.

We gave a basic and generalized explanation for the phenomenon of NC and its correlation with modulated electroluminescence by considering the role of sub-band gap defect states in fast radiative recombination process. Our explanation in this case necessitates the presence of a mutually coupled dynamics of slow defect response (non-radiaive process) and fast radiative recombination. These processes are considered mutually exclusive in general. We presented a model to explain the frequency variation of these correlated electrical and optical modulation properties. Based on the model, we argue that the high frequency performance of electroluminescent diodes (ELDs) can get hampered by such slowly responding defects. Hence our characterization methods can be helpful in improving the efficiency of ELDs under high frequency direct modulation used in applications like optical communication.

We also presented voltage modulated electroluminescence spectra of these devices for the first time which reveals the nature of modulation in the condition of high forward bias. We found that standard theory of modulated reflectance for depleted junctions need not be true in our case. This opens up a direction for further experimental investigations and theoretical analysis.

We further studied the behavior of current transients after a small forward bias voltage pulse in connection with NC. We presented analytical expressions to describe the negative and positive capacitance behavior based on current transient properties. We also demonstrated experimentally that monotonically increasing current transients indicate the presence of negative capacitance for a wide range of applied modulation frequencies. Non-monotonic transients can also represent negative capacitance behavior in a particular range of frequencies. However, monotonically decreasing current transients indicate positive capacitance regime.

We also presented, for the first time, the temperature variation of negative capacitance and modulated electroluminescence for these diodes. Expectedly CW light emission from these diodes decreases monotonically with increasing temperature. Unlike this, counter intuitively, modulated light emission first rises and then starts to fall when the temperature is increased from a very low value (~60 K). This gives a peak in the modulated light emission within a certain temperature range depending on the applied forward bias. We recommended that the temperature of maximum light emission must be brought to operating temperature of ELDs for their efficient performance under direct modulation. This can be achieved either by careful choice of materials and/or by clever device engineering. In agreement to the model we developed, we observed that negative capacitance also shows similar behavior like modulated light emission under temperature variation. We explained that the participation of sub-band gap defect levels in radiative recombination dynamics causes the counter intuitive increase in measured modulation properties with increasing temperature for low temperature range. However after a certain range of temperatures, thermal escape of charge carriers from quantum well starts to affect these modulated properties and we observe a decrease in both modulated light emission and negative capacitance.

The quantitative analysis of these physical processes requires further rigorous theoretical framework which may go beyond the electrostatic description of p-n junction based on Poisson's equation. Further experimental attention is required on the interdependence of optical and electronic properties of ELDs. This certainly opens up a huge scope for future work from both basic and applied perspectives.

We extended our understanding of correlated electrical and optical properties arising due to the participation of defect levels in radiative recombination to probe the light emission process itself. We studied bias activated, small signal frequency derivative capacitance response at room temperature. We developed a phenomenological rate equation to understand the dynamics dependence of this response on applied modulation frequency. Interestingly, this dependence reverses its behavior after the onset of light emission indicating an intriguing presence of effective 'negative activation energy'. We explained that the occurrence of this effective negative activation energy is due to the presence of a 'stable, intermediate transition state' in the process. Calculated average energy of this state was found to be same as the excitonic binding energy of these III-V materials. Hence we identify the presence of negative activation energy as the electrical signature of excitonic state. Further increase in charge injection suppresses the signature of excitonic bound state, indicating a Mott transition. This is additionally vindicated by optical measurements showing the transition from excitonic to free electron hole plasma state in support of our electrical signatures.

In general, optical spectroscopies are exclusively used to study excitons and their complexes in various materials. These systems are of great interest to explore basic quantum physics and develop new low threshold lasers. Therefore our work presents a new, steady state, all-electrical approach to probe condensed matter physics of light emitting semiconductor media in general and may find its application in characterizing the more complex and exotic excitonic phases at low temperatures.

We also applied similar experimental techniques and analyses to other light emitting devices (e.g. InGaAs based quantum dot lasers) and functionally different devices based on Silicon which are intrinsically inefficient for light emission. We showed that our understanding of negative capacitance can be used to explain its different

frequency dependence in case of Si based diodes as compared to ELDs. We also showed that bias activated defect response follows our phenomenological rate equation in case of these diodes.

In brief, we can make the following conclusions based on the work presented in this thesis:

- Under high charge carrier injection, electroluminescent diodes show negative capacitance behavior and deviate from the textbook description of junction diodes based on electrostatics and depletion approximation.
- Negative capacitance tracks the onset of modulated electroluminescence and both follow similar frequency dependence.
- Mutual competition of sub-band gap defect levels with radiative recombination process is responsible for observed correlation between optical and electrical properties. This necessitates the mutual non-exclusivity of radiative and non-radiative (defect response) processes in this case.
- Negative capacitance signatures can be seen in the behavior of current transient after a forward bias voltage pulse.
- Mutual dynamics of defect response and thermal escape of charge carriers from the inbuilt quantum well structures causes counterintuitive temperature dependence of modulated light emission.
- We predict that for better efficiency of devices under high frequency direct modulation, low frequency defect response as well as quantum well parameters need to be optimized.
- We identified the presence of excitonic bound state through the presence of negative activation energy in bias activated differential capacitance response. Suppression of this signature at high bias indicates Mott transition of excitonic state to free electron-hole plasma state.
- Techniques and analyses presented here can be used in a generalized way for different sets of junction based semiconductor structures.

7.1 Future directions

We have pointed out that a rigorous theoretical framework, which may need a treatment beyond the electrostatic description, is required to describe the behavior of a diode, in general, under charge carrier injection. A detailed study of the correlation between optical and electrical properties of electroluminescent diodes can lead to further understanding of light emission processes in different material systems including quantum confined system. It is required, therefore, to pursue more research in this direction which is often overlooked due to the other very apparent aspects of device physics driven by technology requirements. Here, we will point out a few directions which can be pursued in continuation of this work. Some of them are already being actively explored in our lab.

A. Dielectric response of electroluminescent diodes under high frequency (GHz) modulation

In the work presented in this thesis, applied modulation is very slow as compared to the fast radiative recombination happening at the heart of the device dynamics. Though this reveals interesting physics of defect response, it would be interesting to probe these devices under very high modulation ~GHz. This can directly affect the radiative recombination process itself with similar time scales. We have already received the grant to pursue this work in the lab and instrumentation required for high frequency measurements is in progress.

B. Change in the dielectric properties of electroluminescent diodes at and after lasing threshold

Onset of lasing, in terms of the presence of coherent light emission, can lead to the change in the dielectric behavior of these diodes. We have also presented the change observed in capacitance as well as conductance at lasing threshold (chapter 2, figure 2.6). As a signature of lasing, junction voltage has been reported to jump to a saturation value due to the existence of quasi Fermi levels in respective bands (population inversion like condition). In some cases junction voltage has been found to show a drop due to the

subsequent pinning of the quasi Fermi levels in respective bands after lasing threshold [e. g. Li et al. *Appl. Phys. Lett.***102**, 123501 (2013)]. However, modulation properties are rarely studied with lasing threshold which can reveal interesting physics.

C. Sub-Kelvin temperature studies of excitonic physics

We have observed the electrical signatures of excitons and their Mott transition to free electron-hole plasma state. It could be very informative to probe various condensed phases of excitons like excitonic Bose-Einstein condensation (BEC), exciton-polariton BEC, Bardeen-Copper-Schrieffer (BCS) like states at low temperatures. What are the electrical signatures of such phases, what are the electronic processes leading to these condensed states, how these complexes affect or take part in light emission are some of the questions which can be pursued.

D. Probing plasmonic materials under electrical perturbation and modulation

Plasmonic materials, having a large number of free electrons can be considered a system similar to a diode under high charge carrier injection. Application of electrical perturbation and/ or modulation (like we have used in our work) can be useful to probe plasmon propagation and any losses attached with the process in these materials. In this context, it has been demonstrated that plasmons can be excited electrically [Bharadwaj et al. *Phys. Rev. Lett*. **106**, 226802 (2011)], effect of electrical perturbation on plasmon propagation has also been reported with very preliminary results [Song et al. *Nanotechnology* **24**, 095201 (2013)]. Intuitively, change in the dielectric properties of the material locally or instantaneously by the application of modulation will affect plasmon physics and its propagation in the material which can lead to interesting physical phenomena or device applications. In our lab we have designed and developed systems to pursue this work. Study on the plasmon propagation under external voltage in Ag nanowires is being carried out in collaboration with Dr. G. V. Pavan Kumar and his group.

Other potential extensions to the work presented could be probing the polarization state of the emitted light before and after lasing threshold to probe the lasing process and establishment of coherence in diode structures. High frequency response from the device

can be probed at lower temperature which can reveal interesting physics. In short, the work can be extended in various directions to probe the physics of junction based devices under charge injection and material systems with similar properties.